FEDERAL UNIVERSITY OF PARANÁ

JORGE FELIPE EURIQUES

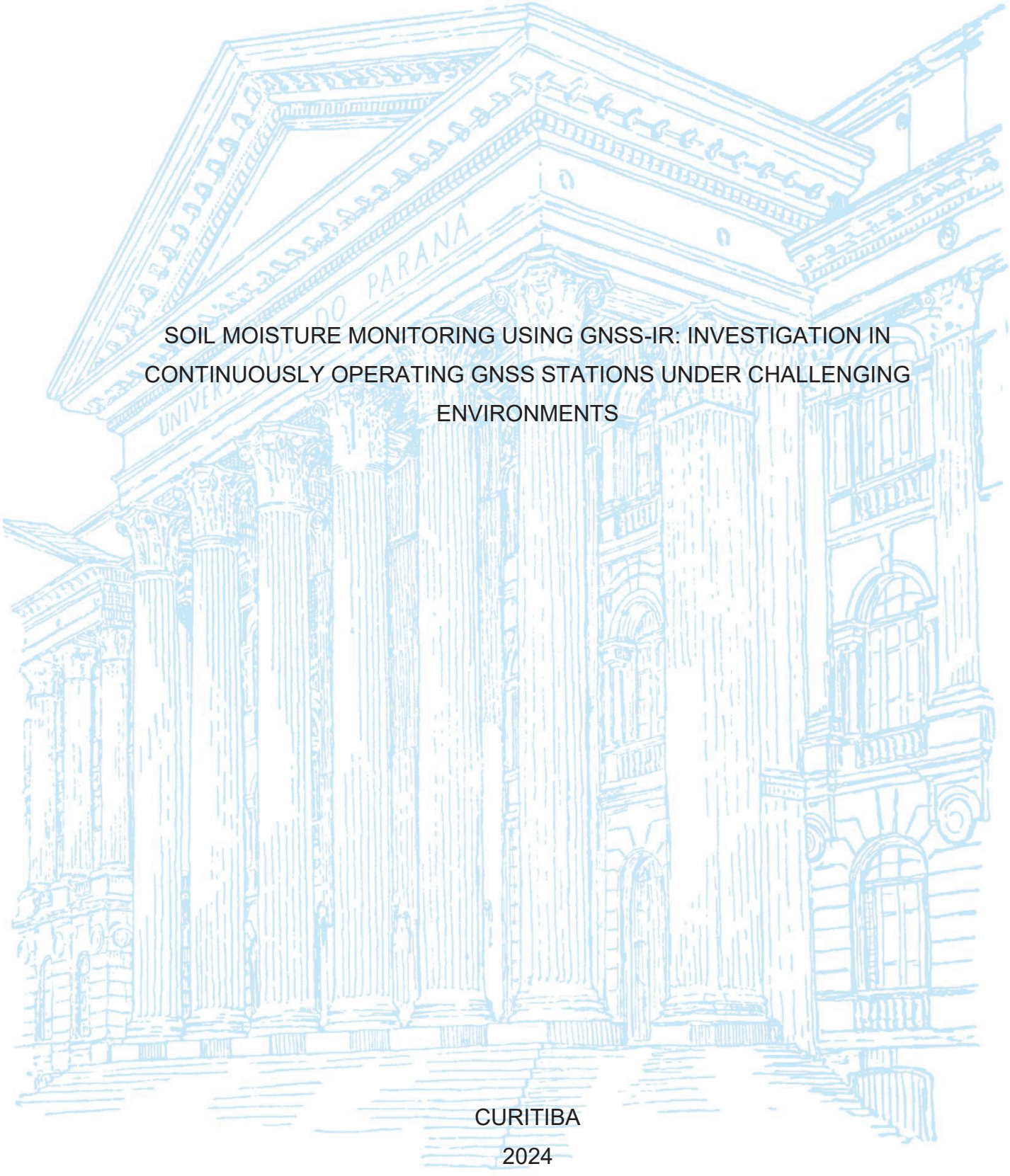

SOIL MOISTURE MONITORING USING GNSS-IR: INVESTIGATION IN CONTINUOUSLY OPERATING GNSS STATIONS UNDER CHALLENGING ENVIRONMENTS

CURITIBA

2024

JORGE FELIPE EURIQUES

SOIL MOISTURE MONITORING USING GNSS-IR: INVESTIGATION IN CONTINUOUSLY OPERATING GNSS STATIONS UNDER CHALLENGING ENVIRONMENTS

Tese de Doutorado apresentada ao Programa de Pós-Graduação em Ciências Geodésicas, Setor de Ciências da Terra, Universidade Federal do Paraná, como requisito parcial à obtenção do título de Doutor em Ciências Geodésicas.

Orientador: Professor Luis Augusto Koenig Veiga
Coorientador: Professor Felipe Geremia-Nievinski

CURITIBA

2024

DADOS INTERNACIONAIS DE CATALOGAÇÃO NA PUBLICAÇÃO (CIP)
UNIVERSIDADE FEDERAL DO PARANÁ
SISTEMA DE BIBLIOTECAS – BIBLIOTECA CIÊNCIA E TECNOLOGIA

Euriques, Jorge Felipe
Soil moisture monitoring using GNSS-IR: investigation in continuously operating GNSS stations under challenging environments. / Jorge Felipe Euriques. – Curitiba, 2024.
1 recurso on-line : PDF.

Tese (Doutorado) - Universidade Federal do Paraná, Setor de Ciências da Terra, Programa de Pós-Graduação em Ciências Geodésicas.

Orientador: Professor Luis Augusto Koenig Veiga
Coorientador: Professor Felipe Geremia-Nievinski

1. Monitoramento ambiental – Sensoriamento remoto. 2. Ciclo Hidrológico. I. Universidade Federal do Paraná. II. Programa de Pós-Graduação em Ciências Geodésicas. III. Veiga, Luis Augusto Koenig. IV. Geremia-Nievinsk, Felipe. V. Título.

Bibliotecária: Roseny Rivelini Morciani CRB-9/1585

TERMO DE APROVAÇÃO

Os membros da Banca Examinadora designada pelo Colegiado do Programa de Pós-Graduação CIÊNCIAS GEODÉSICAS da Universidade Federal do Paraná foram convocados para realizar a arguição da tese de Doutorado de **JORGE FELIPE EURIQUES**, intitulada: **SOIL MOISTURE MONITORING USING GNSS-IR: INVESTIGATION IN CONTINUOUSLY OPERATING GNSS STATIONS UNDER CHALLENGING ENVIRONMENTS**, sob orientação do Prof. Dr. LUÍS AUGUSTO KOENIG VEIGA, que após terem inquirido o aluno e realizada a avaliação do trabalho, são de parecer pela sua APROVAÇÃO no rito de defesa.

A outorga do título de doutor está sujeita à homologação pelo colegiado, ao atendimento de todas as indicações e correções solicitadas pela banca e ao pleno atendimento das demandas regimentais do Programa de Pós-Graduação.

CURITIBA, 19 de Novembro de 2024.

Assinatura Eletrônica
08/04/2025 15:59:25.0
LUÍS AUGUSTO KOENIG VEIGA
Presidente da Banca Examinadora

Assinatura Eletrônica
08/04/2025 13:56:10.0
WAGNER CARRUPT MACHADO
Avaliador Externo (UNIVERSIDADE FEDERAL DE UBERLÂNDIA)

Assinatura Eletrônica
17/04/2025 10:17:16.0
PAULO SERGIO DE OLIVEIRA JUNIOR
Avaliador Interno (UNIVERSIDADE FEDERAL DO PARANÁ)

Assinatura Eletrônica
08/04/2025 15:39:28.0
ALESSANDRA SVONKA PALMEIRO
Avaliador Externo (UNIVERSIDADE FEDERAL RURAL DO RIO DE JANEIRO)

Documento assinado eletronicamente de acordo com o disposto na legislação federal Decreto 8539 de 08 de outubro de 2015.
Gerado e autenticado pelo SIGA-UFPR, com a seguinte identificação única: 441068
Para autenticar este documento/assinatura, acesse https://siga.ufpr.br/siga/visitante/autenticacaoassinaturas.jsp e insira o codigo 441068

Dedico este trabalho a todos que estiveram comigo e contribuíram para sua realização, oferecendo apoio e incentivo ao longo desta jornada.

ACKNOWLEDGMENTS

A gratidão está associada a um estado de espírito. Com a finalização deste trabalho, sinto-me genuinamente grato ao lembrar de todo o incentivo que recebi ao longo dessa jornada. Seria muito difícil fazer um agradecimento nominal, pois corro o risco de esquecer alguém, portanto, expresso aqui minha gratidão de forma ampla e sincera.

Agradeço primeiramente à minha família pelo amor incondicional e pelo companheirismo. O suporte de vocês torna os meus sonhos realidade. Neste grupo, incluo também amigos que são verdadeiros irmãos, que estiveram ao meu lado nos momentos mais desafiadores e sempre me apoiaram com palavras de incentivo e gestos de carinho.

Aos meus amigos de forma geral, expresso minha mais profunda gratidão por terem me acompanhado nessa luta. No fim das contas, comprovei que amizade verdadeira é aquela que o tempo e a distância não desfazem. Nos momentos mais difíceis, sempre pude contar com vocês. Obrigado por não desistirem de mim, mesmo diante da minha ausência e das ambiguidades que cercaram o tema ‘doutorado’ em nossas conversas: ora recorrente e inevitavelmente associado a qualquer outro assunto, ora proibido para não comprometer a minha paz de espírito.

Agradeço à Universidade Federal Rural do Rio de Janeiro, onde tenho a honra de trabalhar como docente desde 2022 — uma profissão que sempre almejei e que foi minha maior motivação para a realização deste doutorado. Agradeço aos amigos e colegas do Departamento de Engenharia que me acolheram em um ambiente amistoso, respeitoso, e de companheirismo, com os quais aprendo diariamente. Um agradecimento especial aos alunos do curso de Engenharia de Agrimensura e Cartográfica que me proporcionaram muito incentivo ao longo dessa jornada. Não posso deixar de mencionar meus amigos queridos da FAPUR, do CTUR, minhas amigas da cantina, bem como todos os demais amigos que conheci após ter me mudado para o Rio de Janeiro.

Agradeço à minha querida Universidade Federal do Paraná, da qual tenho muito orgulho. Sou profundamente grato ao meu orientador, Prof. Luis Koenig Veiga, por ter estendido a mão no momento em que eu mais precisei. Prof. Luis é um exemplo de profissional e ser humano. Agradeço aos professores do Programa de Pós-Graduação em Ciências Geodésicas, especialmente ao Professor Paulo Oliveira, bem

como agradeço aos meus amigos e colegas discentes do PPGCG. Agradeço aos demais professores do Departamento de Geomática, onde atuei como professor substituto. Agradeço sobretudo à professora Claudia Krueger que foi minha orientadora e teve um papel fundamental para que eu chegasse até aqui.

Agradeço imensamente ao meu coorientador, Prof. Felipe Geremia-Nievinski, da Universidade Federal do Rio Grande do Sul. Em 2018, ainda no mestrado, assisti a uma palestra do Prof. Felipe sobre Refletometria GNSS durante um evento científico. Fiquei tão interessado que resolvi mudar o tema de pesquisa. Foi um grande desafio concluir a pesquisa em apenas um ano, mas tive contribuições constantes e essenciais do Prof. Felipe. Posteriormente, já no doutorado, continuei a pesquisa sobre o tema, e os desafios se tornaram ainda maiores: passei a trabalhar com diferentes áreas de estudo e de maneira independente; enfrentamos uma pandemia; comecei a trabalhar como professor; entre outros. Desta forma, agradeço a todas as oportunidades e desafios.

Agradeço ao Prof. Luiz Fernando Sapucci, do Instituto Nacional de Pesquisas Espaciais; ao Prof. Sajad Tabibi, da *Université du Luxembourg*; ao Prof. Wagner Carrupt, da Universidade Federal de Uberlândia, e ao Prof. David K. Adams, da *Universidad Nacional Autónoma de México*, pelo compartilhamento de conhecimento, pela troca de experiências e pelos trabalhos em conjunto que tanto têm agregado ao meu aprendizado.

Aos membros da banca examinadora, Prof. Wagner; Profa. Alessandra Palmeiro; e Prof. Paulo Oliveira. Agradeço pela leitura atenta, pelas sugestões construtivas e pelo tempo dedicado à análise deste trabalho, o que foi feito em tempo recorde. Suas contribuições foram fundamentais para o aprimoramento da minha pesquisa.

Por fim, agradeço à CAPES pelo suporte financeiro, que tornou possível a realização deste estudo e viabilizou minha dedicação no início desta pesquisa.

A todos que, de alguma forma, contribuíram para que eu chegasse até aqui, meu mais sincero obrigado, seriam muitas pessoas pra indicar, afinal, “Eu não ando só” como diz a música. Vencemos!

RESUMO

O monitoramento da umidade do solo é essencial para aplicações ambientais, agrícolas e geotécnicas, influenciando a gestão de recursos hídricos e a previsão de desastres. Métodos tradicionais, como sondas e sensoriamento remoto, apresentam limitações quanto à resolução espacial, temporal e aos custos envolvidos. A Refletometria Interferométrica GNSS (GNSS-IR) surge como uma alternativa promissora, explorando o efeito do multicaminho, fenômeno decorrente da recepção simultânea de sinais diretos, utilizados no posicionamento, e de sinais refletidos nas superfícies ao redor da estação GNSS. A Razão Sinal-Ruído, registrada por receptores GNSS convencionais, é a observável que melhor evidencia esse efeito e é empregada na GNSS-IR para estimar propriedades das superfícies refletoras, incluindo a umidade do solo. Nesse contexto, a técnica se destaca pelo aproveitamento da infraestrutura consolidada do GNSS, permitindo medições contínuas, com cobertura global, *footprint* intermediário e possibilidade de uso combinado para posicionamento e sensoriamento. Contudo, sua aplicação apresenta limitações, principalmente por requerer uma linha de visada direta entre a superfície de reflexão e a antena, além de ser influenciada pela topografia e cobertura do solo. O escopo desta pesquisa é a aplicação da técnica GNSS-IR no monitoramento da umidade do solo a partir de diferentes estações, incluindo locais ideais e adversos. Três estudos de caso são apresentados. O primeiro estudo foi realizado em São Paulo, Brasil, em um ambiente ideal, caracterizado por vegetação rasteira, topografia plana e poucas obstruções, condições que favorecem a validação da técnica. O segundo caso investiga duas estações GNSS no Arizona, EUA, localizadas em áreas com características não ideais devido à presença de vegetação e relevo irregular. Esse cenário permitiu identificar limitações da técnica e desenvolver estratégias metodológicas para minimizar a influência dessas adversidades por meio de adaptações nas configurações do processamento refletométrico. O terceiro estudo concentra-se na implementação da GNSS-IR em uma estação da Rede Brasileira de Monitoramento Contínuo dos Sistemas GNSS, no Paraná, Brasil. Para isso, foi desenvolvido um algoritmo voltado à automatização da preparação dos dados de entrada. Os resultados demonstram que a técnica GNSS-IR fornece estimativas consistentes de umidade do solo, especialmente em locais com baixa interferência de vegetação e relevo. No estudo de caso 1, obteve-se correlação superior a 0,70 em relação a uma sonda de raios cósmicos. No estudo de caso 2, comprovou-se que ajustes nas configurações de processamento podem otimizar os resultados em até 54%. As configurações devem ser definidas especificamente para cada estação a fim de garantir precisão nas estimativas, destacando-se a seleção do intervalo de ângulos de elevação dos satélites, a máscara de azimute e a parametrização da média móvel. Conclui-se que a GNSS-IR possui grande potencial para o monitoramento oportunístico da umidade do solo, além de complementar e validar outros métodos de sensoriamento, contribuindo para o monitoramento global dessa variável. A metodologia mostrou-se aplicável mesmo em estações não ideais, embora os resultados ainda sejam influenciados por adversidades ambientais. Trata-se de uma técnica em desenvolvimento, que exige investigações adicionais, como o aprimoramento dos coeficientes de calibração teóricos e a minimização dos efeitos da vegetação. Esta tese contribui para o avanço da metodologia e estabelece diretrizes para futuras pesquisas na área.

Palavras-chave: Sensoriamento Remoto Geodésico. Ciclo Hidrológico. Multicaminho. Monitoramento ambiental. SNR

ABSTRACT

Soil moisture monitoring is essential for environmental, agricultural, and geotechnical applications, influencing water resource management and disaster forecasting. Traditional methods, such as in situ probes and remote sensing, have limitations like spatial and temporal resolution, and cost. GNSS Interferometric Reflectometry (GNSS-IR) emerges as a promising alternative, leveraging the multipath effect, resulting from the simultaneous reception of direct signals, used for positioning, and signals reflected from surfaces around the GNSS station. The Signal-to-Noise Ratio (SNR), recorded by conventional GNSS receivers, is the observable that best reveals this effect and is used in GNSS-IR to estimate properties of the reflecting surfaces, including soil moisture. In this context, the technique stands out for utilizing the well-established GNSS infrastructure, enabling continuous measurements with global coverage, an intermediate footprint, and the possibility of combined use for positioning and sensing. However, its application has limitations, mainly due to the need for a direct line of sight between the reflecting surface and the antenna, and its sensitivity to topography and land cover. The scope of this research is the application of GNSS-IR in soil moisture monitoring using different GNSS stations, including both ideal and challenging environments. Three case studies are presented. The first study was conducted in São Paulo, Brazil, in an ideal environment characterized by low vegetation, flat topography, and few obstructions—conditions that favor the validation of the technique. The second case investigates two GNSS stations in Arizona, USA, located in areas with non-ideal characteristics due to vegetation and irregular terrain. This scenario allowed the identification of limitations in the technique and the development of methodological strategies to minimize the influence of these adversities through adaptations in reflectometric processing configurations. The third study focuses on the implementation of GNSS-IR in a station of the Brazilian Network for Continuous GNSS Monitoring (RBMC) in Paraná, Brazil. For this purpose, an algorithm was developed to automate the preparation of input data. The results demonstrate that the GNSS-IR technique provides consistent soil moisture estimates, especially in locations with low vegetation and terrain interference. In Case Study 1, a correlation above 0.70 was obtained compared to a cosmic-ray neutron probe. In Case Study 2, it was proven that adjustments in processing configurations can optimize results by up to 54%. The configurations must be specifically defined for each station to ensure accuracy in the estimates, with emphasis on selecting the range of satellite elevation angles, azimuth mask, and moving average settings. It is concluded that GNSS-IR has great potential for opportunistic soil moisture monitoring, in addition to complementing and validating other sensing methods, contributing to global monitoring of this variable. The methodology proved applicable even in non-ideal stations, although the results are still influenced by environmental adversities. This is a developing technique that requires further investigations, such as improving theoretical calibration coefficients and minimizing vegetation effects. This thesis contributes to the advancement of the methodology and establishes guidelines for future research in the field.

Keywords: Geodetic Remote Sensing. Hydrological Cycle. Multipath. Environmental Monitoring. SNR

ABBREVIATIONS AND ACRONYMS

AIGEO	- *Anuário do Instituto de Geociências*
ANA	- *Agência Nacional das Águas*
CAPES	- *Coordenação de Aperfeiçoamento de Pessoal de Nível Superior*
CEMADEN	- *Centro Nacional de Monitoramento e Alerta de Desastres Naturais*
CNPq	- *Conselho Nacional de Desenvolvimento Científico e Tecnológico*
COSMOS	- Cosmic-ray Soil Moisture Observing System
GNSS	- Global Naviation Satellite System
GNSS-R	- GNSS Reflectometry
GNSS-IR	- GNSS Interferometric Reflectometry
GPS	- Global Positioning System
IBGE	- *Instituto Brasileiro de Geografia e Estatística*
INMET	- *Instituto Nacional de Meteorologia*
INPE	- *Instituto Nacional de Pesquisas Espaciais*
RBMC	- *Rede Brasileira de Monitoramento Contínuo dos Sistemas GNSS*
RINEX	- Receiver Independent Exchange Format
SNR	- Signal-to-Noise Ratio
SMAP	- Soil Moisture Active Passive
TDR	- Time-Domain Reflectometry
UFPR	- *Universidade Federal do Paraná*

TABLE OF CONTENTS

1 INTRODUCTION

The Earth is a dynamic planet, subject to various natural processes that influence its system. However, over the past 150 years, human activities have caused unprecedented transformations, impacting the climate and natural resources (Simon et al., 2006). Population growth and the intensive exploitation of natural resources have led to significant environmental changes, such as global warming, alterations in the hydrological cycle, and extreme climatic events (Awange & Kiema, 2013).

Soil moisture is a crucial parameter in this context, as it is directly related to the hydrological cycle and plays a fundamental role in water resource management, agriculture, geotechnical processes, and soil-atmosphere interactions (Babaeian et al., 2019). However, conventional soil moisture monitoring techniques, such as in situ probes and remote sensing, present limitations regarding spatial coverage, temporal resolution, and operational costs.

In this scenario, GNSS Reflectometry (GNSS-R) emerges as a promising alternative that exploits the multipath effect of the GNSS signals to estimate properties of the reflecting surface, including soil moisture. Although all GNSS observables are affected by multipath, the signal-to-noise ratio (SNR) is the observable that best reveals this effect. It is commonly recorded by conventional GNSS equipment designed for GNSS positioning (Larson et al., 2010). The category of GNSS-R performed using the SNR recorded by conventional stations is called GNSS Interferometric Reflectometry - GNSS-IR (Li et al., 2022). This technique enables the use of the established GNSS infrastructure, allowing continuous and extensive measurements without requiring additional equipment (Euriques et al., 2021).

Since all GNSS equipment is subject to multipath, recording the SNR allows the use of data from continuous GNSS stations, such as the stations of the Brazilian Continuous Monitoring Network of GNSS systems (RBMC), established and maintained by the Brazilian Institute of Geography and Statistics (IBGE). This includes acquiring historical series to obtain time series of soil moisture. However, certain assumptions are required, as the area surrounding the antenna should be predominantly bare soil or low vegetation and preferably located in a flat and horizontal area (Geremia-Nievinski; Hobiger, 2019).

However, the application of GNSS-IR presents challenges, such as the need for a direct line of sight between the reflecting surface and the GNSS antenna, as well

as the influence of environmental factors such as vegetation and topography. To investigate these limitations and advance the methodological development, this research presents three distinct case studies covering both ideal and adverse conditions for soil moisture monitoring using GNSS-IR.

1.1 RATIONALE FOR STUDY

In recent decades, soil moisture monitoring has become a global demand, driven by the challenges posed by climate change, the need for efficient water resource management, and a commitment to sustainable development.

Although it is an essential parameter for reducing uncertainties in hydrological and environmental models, soil moisture is often overlooked due to the limitations of conventional methods. However, it is an important variable in predicting disasters, helping to minimize the effects of extreme events, such as floods and wildfires, and assisting in delineating risk areas.

In other activities, such as agriculture, soil moisture monitoring is essential at a local scale. It enables the efficient use of water and energy resources applied to irrigation, which impacts agricultural productivity, operational costs, and environmental preservation (Babaeian et al., 2019).

Conventional soil moisture monitoring methods are costly and limited in spatial and temporal coverage, making their application on a large scale challenging (Di Bello, 2005; Edokossi et al., 2020). The GNSS-IR technique is a promising alternative solution as it can have intermediate coverage compared to traditional methods. It allows for soil moisture monitoring based on the SNR continuously recorded by GNSS receivers, without the need for adaptations to the equipment, enabling combined use for positioning and GNSS-IR.

There is potential to leverage data from active GNSS stations, such as the RBMC, for the development of soil moisture monitoring methodologies, provided that the station meets the requirements of the technique. This process would enable the monitoring of this variable throughout the national territory, contributing to numerous sectors and also allowing for the complementing or validation of other methods, such as products derived from remote sensing. Another highlight would be the reduced cost, as the raw GNSS tracking data is obtained for free from IBGE repositories.

However, GNSS-IR applied to soil moisture estimation remains under development due to the complexities associated with determining compositional variables of the soil. Therefore, further scientific investigations are needed to validate its effectiveness under different environmental conditions and GNSS antenna installation scenarios.

This thesis includes case studies that justify addressing these challenges progressively: the first case study focuses on ideal installation conditions to establish a methodological baseline; the second explores non-ideal scenarios, allowing for the evaluation of limitations and adjustments under adverse conditions, such as dense vegetation and irregular topography; finally, the third case study was conducted at an RBMC station, demonstrating the feasibility of applying GNSS-IR in an active station with an automated GNSS data acquisition and processing system. Each case study contributed complementarily to the validation and enhancement of the GNSS-IR technique in different scenarios.

1.2 HYPOTHESIS

Considering the potential and challenges of estimating soil moisture using the GNSS-IR technique, if scientific investigations confirm its feasibility under different installation conditions, land cover, and topographic settings, then it will be possible to establish a methodology for opportunistic soil moisture monitoring at active GNSS stations, such as those of the RBMC. This would allow validating its use in both ideal and non-ideal conditions.

1.3 RESEARCH OBJECTIVES

1.3.1 General objective

This thesis aimed to investigate the application of the GNSS-IR technique for soil moisture estimation in continuously operating GNSS stations, including both ideal and adverse environmental conditions, contributing to the methodological enhancement of the technique.

1.3.2 Specific Objectives

The objectives of this research were:

a) assess the impact of different GNSS station installation conditions on soil moisture estimation via GNSS-IR, considering variables such as topography, land cover, and surrounding characteristics;
b) investigate processing configurations of the reflectometric algorithm, including GNSS signal selection, range of elevation angles, azimuthal masks, and the moving average;
c) identify and mitigate limitations of the GNSS-IR technique in soil moisture estimation considering adverse environmental conditions;
d) Define a methodology to automate soil moisture monitoring at RBMC stations.

1.4 THESIS CONTENT

This research is based on an experimental design involving three case studies, with a comparative analysis between ideal and adverse conditions. This thesis is organized into three sections. Section 1 encompasses this initial section, which includes the Introduction. Section 2 is subdivided into chapters presenting propositions and case study results formatted as papers.

Chapter 1: Conceptual Review. Subsection 2.1, presents a literature review by the article *“Soil Moisture Estimation with GNSS Reflectometry: A Conceptual Review”* by Euriques et al. (2021), published in the *Revista Brasileira de Cartografia* (ISSN 1808-0936). This publication offers the state-of-the-art GNSS-IR for soil moisture estimation, providing the theoretical foundation upon which this research is built.

The review synthesizes findings from multiple studies, highlighting the reliability and acknowledgment, methodological challenges, the key advantages, and limitations of GNSS-IR for soil moisture estimation, such as sensitivity to vegetation cover, surface topography, and dependence on theoretical calibration parameters. By establishing this theoretical framework, Chapter 1 lays the groundwork for the experimental investigations developed in the subsequent chapters. The insights

gained guide the methodological decisions throughout the thesis and support the refinement of the data processing techniques explored in this research.

Note that, as GNSS Reflectometry is still an emerging field, the authors of this paper adopted the more generalized term “GNSS-R”, the most commonly used designation at the time. However, this thesis follows the more recent trend in international literature, which favors the term GNSS-IR when referring specifically to GNSS reflectometry conducted using conventional GNSS antennas and SNR.

Chapter 2: Ideal conditions Study. Subsection 2.2, the article 'Field-Wide Non-Contact Soil Moisture Sensing: Comparison between GNSS Interferometric Reflectometry and Cosmic-Ray Neutron Probe', submitted for peer review in a scientific journal, is provided. This chapter focuses on the first case study, which investigates soil moisture estimation under ideal conditions in São Paulo, Brazil. This chapter presents the estimations of soil moisture by an optimal installation environment. The selected site features flat terrain, low vegetation, and minimal obstructions, creating an ideal setting for validating the methodology. The results were compared with data obtained from a probe of the Cosmic-ray Soil Moisture Observing System (COSMOS) and a rain gauge, yielding a correlation coefficient of 0.73 when using the RS2P signal.

This study plays a crucial role in establishing baseline performance metrics for GNSS-IR. The results obtained in this chapter serve as a reference point for comparison with more challenging environments analyzed in subsequent chapters. Furthermore, the findings help refine the processing configurations, such as the range of satellite elevation angles and azimuth masks, which are later adapted to non-ideal conditions. By demonstrating the effectiveness of GNSS-IR in a controlled setting, Chapter 2 reinforces the feasibility of using this technique for soil moisture monitoring and provides essential insights for optimizing its application in diverse environmental scenarios.

Chapter 3: Challenging Environments Study. Subsection 2.3, presents a manuscript that has not yet been submitted, resulting from an investigation carried out within the scope of the project: The Atmospheric Hydrological Cycle and Deep Convective Activity: Observations from the North American Monsoon GPS Hydrometeorological Network (2017) and follow-on Campaigns. This project aimed to estimate hydrological cycle variables to investigate land-atmosphere interactions, such as convective activities, using GNSS data from ground-based stations in Arizona, USA.

The study focuses on two GNSS stations in locations with different terrain characteristics, allowing a comparative assessment of how adverse conditions impact the technique's performance by analyzing the challenges posed by vegetation, complex topography, and environmental variability. Soil moisture was estimated around two GNSS stations, Lucky Hills and Kendall. The GS2L (GPS L2) and RS2P (GLONASS L2) signals yielded the best results, considering a range of satellite elevation angles between 15 and 30 degrees above the antenna horizon. It was observed that the results were influenced by moving average configurations, which were applied to smooth fluctuations in the data over time.

This research is crucial for identifying the limitations of GNSS-IR and testing processing adaptations to mitigate environmental effects. The results demonstrate that adjusting reflectometric processing configurations, such as elevation angle selection and signal filtering, can improve accuracy by up to 54%. By examining GNSS-IR's performance in challenging conditions, Chapter 3 contributes to the refinement of the methodology, ensuring its applicability in diverse monitoring scenarios and enhancing the robustness of soil moisture estimations.

Chapter 4: GNSS-IR in Active GNSS Stations**.** Subsection 2.4, presents the article titled 'Soil Moisture Estimation by GNSS-IR from Active Stations: Case Study – RBMC/IBGE, UFPR Station,' published in the *Anuário do Instituto de Geociências (AIGEO)*. This paper focuses on developing an automated methodology for soil moisture estimation in GNSS stations of the RBMC. Further investigations were conducted, including topographic mapping of the surrounding area to optimize the selection range of satellite elevation angles. To achieve this, a script was developed for downloading, converting, and standardizing SNR data, enabling its application to any RBMC station. The study demonstrates the feasibility of GNSS-IR in two existing geodetic stations, making opportunistic soil moisture monitoring more accessible and scalable.

Section 3 presents the conclusions and recommendations for future work. Appendix 1 includes a map related to the continuation of the research for other RBMC stations.

2 CHAPTERS

2.1 CHAPTER 1: PAPER 1 – CONCEPTUAL REVIEW

This chapter presents the paper "Soil Moisture Estimation with GNSS Reflectometry: A Conceptual Review", published in the *Revista Brasileira de Cartografia*. The study provides a theoretical foundation on GNSS Reflectometry (GNSS-R) applied to soil moisture estimation, discussing its principles, advantages, and limitations compared to conventional methods.

Reference: Euriques, J. F.; Krueger, C. P.; Machado, W. C.; Sapucci, L. F.; Geremia-Nievinski, F. (2021). Soil Moisture Estimation with GNSS Reflectometry: A Conceptual Review. Rev Bras Cartogr 73(2):413–434. DOI: 10.14393/rbcv73n2-55033

2.1.1 Soil Moisture Estimation With GNSS Reflectometry: A Conceptual Review

Jorge Felipe Euriques 1, Claudia Pereira Krueger 2, Wagner Carrupt Machado 3, Luiz Fernando Sapucci 4, Felipe Geremia-Nievinski 5

1 Universidade Federal do Paraná, Departamento de Geomática, Programa de Pós-Graduação em Ciências Geodésicas, Curitiba, Brasil. jorge.euriques@gmail.com
ORCID: https://orcid.org/0000-0001-9234-7551

2 Universidade Federal do Paraná, Departamento de Geomática, Programa de Pós-Graduação em Ciências Geodésicas, Curitiba, Brasil. cpkrueger64@gmail.com
ORCID: https://orcid.org/0000-0002-4839-1317

3 Universidade Federal de Uberlândia, Centro de Ciências Exatas e Tecnologia, Monte Carmelo, Brasil. wagnercarrupt@ufu.br
ORCID: https://orcid.org/0000-0003-3112-7808

4 Instituto Nacional de Pesquisas Espaciais, Centro de Previsão de Tempo e Estudos Climáticos, Programa de Pós-Graduação em Meteorologia, Cachoeira Paulista, Brasil. luiz.sapucci@inpe.br
ORCID: https://orcid.org/0000-0001-8420-8033

5 Universidade Federal do Rio Grande do Sul, Departamento de Geodésia, Programa de Pós-Graduação em Sensoriamento Remoto, Porto Alegre, Brasil. felipe.nievinski@ufrgs.br.
ORCID: https://orcid.org/0000-0002-3325-1987

ABSTRACT

Soil moisture monitoring enables efficient management and use of water resources, having great importance for several purposes, such as: monitoring of risk areas; delimitation of areas susceptible to flooding; geotechnical activities; and in agriculture development. GNSS Reflectometry (GNSS-R) is a scientific and technological development that allows one to perform proximal or remote sensing, depending on the antenna height concerning the surface, by means of navigation satellites. This method exploits GNSS signals indirectly reaching a receiver antenna after they are reflected on the surrounding surfaces. In this method, direct and indirect GNSS signals that reach the receiving antenna are exploited, after reflection on the surfaces existing around the antenna. The combination of these two signals causes the multipath effect, which affects GNSS observable and deteriorates positioning. On the other hand, when interacting with these reflecting surfaces one can estimate their properties. One of the main advantages of GNSS-R, when compared with the conventional methods, is the intermediate coverage area, as well as, the use of the well-defined structure of GNSS systems that guarantee appropriate temporal resolution. The scope of this paper is to present a conceptual review of GNSS-R applied to soil moisture monitoring.

Keywords: GNSS-R. Multipath. Soil Moisture. SNR.

1 INTRODUCTION

Soil moisture can be defined as the water content stored in the unsaturated soil zone, also termed the vadose zone (HILLEL, 1998). The vadose zone contains the root zone of the plants and extends from the land surface to the groundwater table of the first unconfined aquifer, where all soil pores are filled with water (ARORA et al., 2019).

Soil moisture content is inhomogeneously distributed vertically (over depth) and horizontally (over land) (SENEVIRATNE et al., 2010). This quantity is commonly expressed for a given portion of soil at a given matric potential in gravimetric or volumetric units (TULLER; OR, 2004). Gravimetric soil moisture (g/g) is the ratio between the mass of the water within a soil sample and the dry mass of the soil sample.

Volumetric soil moisture is the ratio between the volume of water contained in a given volume of a soil sample (cm^3/cm^3) (BABAEIAN et al., 2019).

Soil moisture is linked to processes that are characterized at various scales. At large scales it is a key component of the water and biogeochemical cycles, as well as influencing the flow and exchange of energy between the Earth's physical surface and the atmosphere (ENTEKHABI et al., 2010; ROBINSON et al., 2008). Within the scope of the water cycle, quantifying soil moisture allows inputting models for the delimitation of aquifer recharge areas and flood areas (OCHSNER et al., 2013). The water stored on land is a relevant agent in mass displacements, thus soil moisture is an important parameter in systems for monitoring areas susceptible to natural hazards; in geotechnical activities; and in the planning and control of engineering works. Locally, soil moisture has critical importance in agriculture, for example, because it is essential for the healthy development of plants. Monitoring soil moisture allows optimizing the use of water and energy resources in irrigation mechanisms (PEREIRA, 2001). In this way, its management contributes to the increase in production and, concomitantly, the preservation of the environment.

Global Navigation Satellite System Reflectometry (GNSS-R) has been successfully used in soil moisture estimation (TABLE 1), emerging as an alternative to conventional methods (Section 2). This method allows the realization of remote or proximal sensing exploring the reflections of the radio waves transmitted by GNSS satellites. It makes it possible to extract information on the properties of the reflecting surfaces (TEUNISSEN; MONTENBRUCK, 2017), such as soil moisture. GNSS-R has certain advantages over other methods, including global coverage; low cost; independence from climatic conditions; the possibility of obtaining information almost in real-time; and the short revisit time of GNSS satellites (EDOKOSSI et al., 2020). In the present paper, a conceptual review of the GNSS-R method for estimating soil moisture is presented.

2 CONVENTIONAL METHODS

There exist several methods to measure or estimate soil moisture, directly or indirectly (SENEVIRATNE et al., 2010). In the gravimetric method, soil moisture content is directly measured. In the laboratory, soil moisture content can be derived weighting an *in situ* soil sample before and after drying. The original volume of water

in the soil sample is calculated by dividing the water mass by its density (HANSON, 2009). The gravimetric method is the most accurate method and the only direct method. It represents the reference measurements for calibrating equipment used in indirect methods (MENDES, 2006). However, it provides punctual measurements, which may not be representative of the larger surrounding area at a local scale. Besides, it is laborious and destructive, due to the need to collect soil samples (ZHANG et al., 2014). Therefore, it may not be suitable for continuous monitoring.

In all other methods, soil moisture is indirectly estimated from measurement of physical properties of the soil. In these cases, measurements can be made by *in situ* probes or by remote or proximal sensing (BABAEIAN et al., 2019). Probes are autonomous and allow ample data recording, allowing continuous monitoring. The main property explored by these types of equipment is the dielectric permittivity of the soil. The two most common techniques among probes that measure electric permittivity of the soil are based on the

Time Domain Reflectometry[1] (TDR) and Frequency Domain Reflectometry (FDR), also termed capacitance probes (SENEVIRATNE et al., 2010). In TDR probes, permittivity is determined by evaluating the variation in the propagation time of an electromagnetic pulse. In turn, in FDR probes, permittivity is estimated by assessing the frequency variation of an electromagnetic pulse (LIMA, SILVA and KOIDE, 2012). These probes are accurate, but limited in terms of range, which is a few centimeters around the sensor. The capacitance probes have limitations related to soil composition, mainly due to the content of salinity and iron oxides (DELTA-T DEVICES LTD, 2001).

Furthermore, one can evaluate the moderation of fast neutrons, which is linked to the presence of hydrogen atoms. Neutron probes can be active or passive. The active probes have their radiation source, mainly from Americium and Beryl, to give rise to fast neutrons (PEREIRA, 2001). They have the disadvantage of biological risks to the equipment operator and the environment due to the emission of ionizing radiation. Passive probes explore radiation from extraterrestrial sources that originate from galactic cosmic rays. When these rays reach the atmosphere, they give rise to a

---

1 Note the conceptual distinction between these conventional methods of indirect measurement of soil moisture Time Domain Reflometry (TDR) and Frequency Domain Reflometry (FDR), and the GNSS-R geodetic method, which is based on GNSS transmissions.

cascade of neutrons with high energy. These neutrons continue to propagate downward reaching the soil, when a second cascade of neutrons arises. These neutrons are moderated by hydrogen atoms contained in water that characterizes the soil moisture (DESILETS; ZREDA; FERRÉ, 2010). The probes of the COsmic-ray Soil Moisture Observing System (COSMOS) network exploit this property (ZREDA et al., 2012). They have a range of hundreds of meters, are accurate, and allow ample and autonomous data recording; however, they can be expensive. On the other hand, through orbital and aerial remote sensing, global or regional coverage can be reached, respectively, but with generalized information (VEY et al., 2016).

The spatial resolution obtained with orbital sensors is approximately 100 m for active sensors (radars) and 10 km for passive sensors (radiometers) (EDOKOSSI et al., 2020). Also, the temporal resolution, which is related to the satellite revisiting the same location, is low. These characteristics limit its use in applications such as agriculture. Electromagnetic waves of different spectrum bands from visible to microwaves can be used in remote sensing through active and passive sensors. Some examples of satellite missions for monitoring soil moisture are the European Space Agency's Soil Moisture and Ocean Salinity satellite (SMOS) of (KERR et al., 2001) and National Aeronautics and Space Administration's Soil Moisture Active Passive (SMAP)(ENTEKHABI et al., 2010). Both employ radio waves with active and passive sensors. Other missions in this theme include: Special Sensor Microwave/Imager (DE RIDDER, 2003), Tropical Rainfall Measuring Mission (GAO et al., 2006), Advanced Microwave Scanning Radiometer – Earth Observing System (XIE; MENENT; JIA, 2019), and gravimetric missions such as the Gravity Recovery and Climate Experiment (SWENSON et al., 2008).

3 GNSS REFLECTOMETRY

Several studies have demonstrated that soil moisture can be estimated by GNSS-R (Section 4). In addition to the results obtained by these researchers demonstrating the efficiency of GNSS-R in this purpose, some advantages can be highlighted: 1) intermediate coverage area, between conventional methods (*in situ* probes and remote sensing) – approximately 50 meters radius for a 2-m tall GNSS antenna (TABIBI et al., 2017); 2) adequate spatial and temporal resolution guaranteed by the existing GNSS structure, which has global coverage, continuous transmission

of signals by dozens of satellites, independently to weather conditions (SEEBER, 2003); 3) possibility of using GNSS stations simultaneously for positioning and reflectometry (LARSON; NIEVINSKI, 2013).

GNSS satellites transmit electromagnetic waves of the radio or microwave type with frequency in the range of 1 to 2 GHz, in the L band (TEUNISSEN; MONTENBRUCK, 2017). Coincidentally, these frequencies are close to the frequencies used in SMOS and SMAP orbital missions. When such waves reflect on surfaces around a GNSS antenna, they can reach this antenna indirectly (FIGURE 1) delayed due to the additional distance traveled (LEICK, 1995). The combination between direct and reflected waves gives rise to the multipath effect, which is one of the main sources of errors that affect GNSS positioning, depending on the quality of the antenna (TEUNISSEN; MONTENBRUCK, 2017).

After the interaction with the ground surface, radio waves have their characteristics changed (amplitude, phase, polarization, and frequency). This makes it possible to estimate attributes about those reflection surfaces (ROUSSEL et al., 2016). This is the principle of remote sensing, including GNSS-R that exploites the GNSS observables affected by reflections. In this way, multipath enables GNSS-R, despited being detrimental to GNSS positioning, thus expanding the range of applications of this technology.

FIGURE 1 – SIMULTANEOUS RECEPTION OF DIRECT AND INDIRECT WAVES FROM REFLECTIONS ON THE SURFACES SURROUNDING A GNSS ANTENNA.

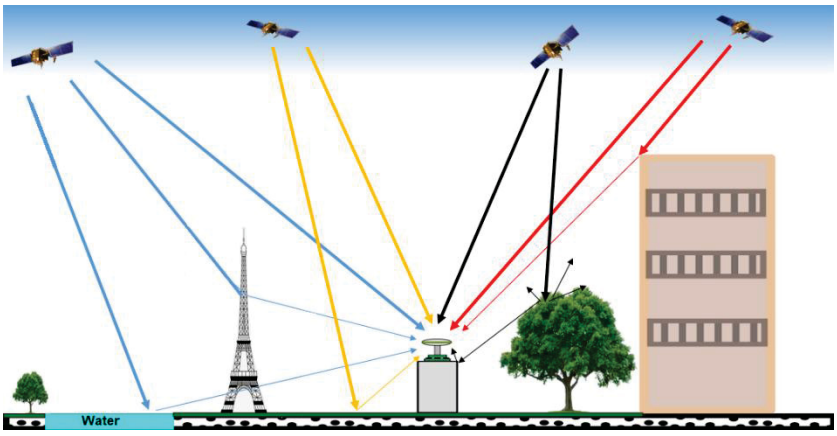

SOURCE: EURIQUES (2019).

GNSS-R can be considered as a multi-static radar since the antenna receives multiple transmissions from several satellites (JIA; PEI, 2018). This configuration contrasts with monostatic radars, where receivers and transmitters are on the same platform, as in the case of nadir-pointing satellite altimeters. Although the concept of GNSS Reflectometry was initially proposed by Martin-Neira (1993), most of the related research comes from the last decade. Applications involve the determination of geometric attributes and the composition of reflective surfaces. Altimetry is considered in the first type and consists of determining the vertical distance between the GNSS antenna and the reflection surface as in snow depth monitoring (ZHOU et al., 2019), water level variations (STRANDBERG; HOBIGER; HAAS, 2017), and some types of vegetation growth (ZHANG et al., 2017). The application type dealing with surface composition includes soil moisture estimation (TABIBI et al., 2015).

Multipath affects all observables, so GNSS-R can be performed, in principle, through pseudorange, Doppler, carrier phase, or Signal-to-Noise Ratio (SNR) data. According to Nievinski and Larson (2014a) and Larson et al. (2010), SNR consists of the power of the carrier phase (in watts) normalized by the noise power or its spectral density (watts or watts per hertz), often expressed in a logarithmic scale, in decibels (dB) or decibel-hertz (dB-Hz). This observable is recorded continuously by GNSS receivers throughout the tracking, considering each satellite individually (BILICH; LARSON, 2007).

With the orbital movement of satellites, the propagation delay and the phase difference between direct and reflected signals varies, creating constructive and destructive interference patterns between the two superimposed waves, in turn resulting in oscillations (FIGURE 2) in the SNR time series (TABIBI et al., 2015). SNR is the GNSS observable that best reveals the multipath effect, as it is invariable to the common effects between the direct and indirect paths, even with single frequency receivers, such as errors related to orbits, most of the atmospheric delays and synchronization errors, which would affect the other GNSS observables (LARSON et al., 2008a). In comparison, carrier phase and pseudorange observables require combinations of two or three carrier frequencies to isolate the multipath effect. In any case, it is possible to perform reflectometric determinations from conventional GNSS receivers, developed for positioning, without changes to the equipment or installation of the receiving antenna (LARSON et al., 2010). In this context, data from existing GNSS stations can be used, such as from the Brazilian Network for Continuous

Monitoring of GNSS (RBMC), the continuous monitoring network from the Geocentric Reference System for the Americas (SIRGAS), or from the International GNSS Service (IGS).

Different names can be found in the literature about the category of GNSS-R that exploits conventional ground instruments, developed for positioning and adapted to reflectometry: GNSS Multipath Reflectometry (GNSS-MR) by Nievinski et al. (2016); GNSS Interference Pattern Technique (GNSS-IPT) by Rodriguez-Alvarez et al. (2011a); GNSS Interferometric Reflectometry (GNSS-IR) by Larson (2016); SNR-based GNSS reflectometry by Löfgren and Haas (2014). GNSS-MR can be performed with any GNSS observable, while GNSS-IPT/IR is normally restricted to the use of the SNR-type observable.

Access to SNR can be done in two different ways:

a) observation file in Receiver Independent Exchange (RINEX) format, which allows different types of SNR for each carrier frequency (GURTNER; ESTEY, 2015). Since version 3, SNR values are provided for each modulation at the same frequency (e.g., civil and military);

b) National Marine Electronics Association (NMEA) 0183 format, which is the specification related to data standardization for communication between electronic equipment (MARTÍN et al., 2020). This specification includes the transmission of SNR data via the GPS Satellites in View message ($GPGSV).

FIGURE 2 shows an SNR interferogram for different modulations, considering the ascending arc of a satellite in the GPS constellation. Note that not all signals have the same quality concerning the multipath signature. In general, modern GPS modulations, such as L2C and L5, correspond better to theoretical models, while legacy modulations, such as C/A and P(Y) exhibit more distortions (TABIBI et al., 2017).

FIGURE 2 –SNR (DB) BY DIFFERENT MODULATIONS FOR AN ASCENDING ARC OF A GPS SATELLITE CONSIDERING ELEVATION ANGLES BETWEEN 5 AND 45 DEGREES.

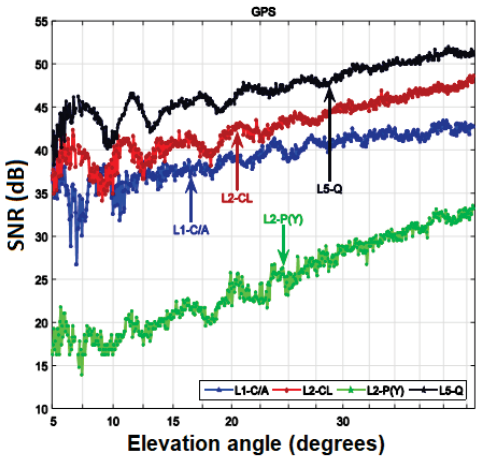

SOURCE: Adapted from Tabibi et al. (2017).

3.1 GNSS-R FOOTPRINT

The coverage area involved in GNSS-R is defined mainly as a function of the height (*H*) of the antenna above the surface. In this sense, the range is local, when GNSS stations are mounted a few meters above the ground (LARSON et al., 2008a); regional, when the receiving antenna is fixed on airborne platforms such as conventional and remotely piloted aircraft (RODRIGUEZ-ALVAREZ et al., 2013); or global, when the sensor is fixed on orbital platforms (GLEASON et al., 2005).

The coverage area for stations installed on the ground can be approximated by the Fresnel zones. Each one of the Fresnel zones is an ellipse defined in terms of the elevation angle (e) and azimuth (*a*) over the horizon of the antenna (FIGURE 3) (JIN; QIAN; KUTOGLU, 2016). In this calculation, the height of the antenna and the wavelength (λ) of GNSS carrier wave must also be considered. Following Larson and Nievinski (2013) and assuming a flat and horizontal surface, the formulation for the first Fresnel zone can be expressed in terms of its semi-major (*a*) and semi-minor axes (*b*) as well as the horizontal distance to the center (*D*):

$$a = \frac{b}{\sin e} \tag{1}$$

$$b = \sqrt{\frac{2dH}{\sin e} + \frac{d^2}{\sin^2 e}} \tag{2}$$

$$D = \frac{H}{\tan e} + \frac{d}{\sin e \tan e} \tag{3}$$

where $d = 0.5\lambda^{-1}$. The major semi-axis is positioned along the satellite's azimuth.

FIGURE 3 shows the Fresnel zones of a GNSS station with an antenna height of 1.8 meters. On the left, the Fresnel zone of a satellite with 90 ° azimuth is shown. The ellipses for different elevation angles are shown; the higher the elevation angle (closer to the zenith), the smaller and closer to the antenna is the ellipse. On the right, there is the set of Fresnel zones for a station assumed in the Southern Hemisphere. Note the absence of zones in the vicinity of the South direction, which occurs due to the inclination of the orbital plane of satellites (LARSON, 2016). When the GNSS station is located in the Northern Hemisphere, this gap occurs in the northern direction.

FIGURE 3 – FRESNEL ZONES OF A SIMULATED GNSS STATION CONSIDERING SATELLITE ELEVATION ANGLES BETWEEN 7 E 25 DEGREES FROM THE ANTENNA HORIZON

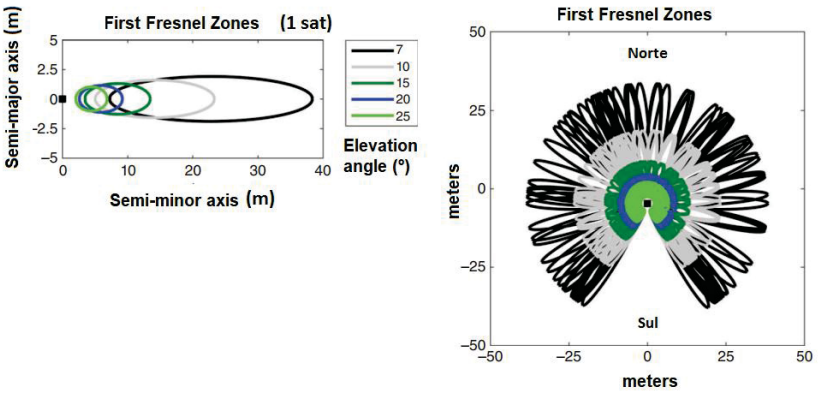

SOURCE: Adapted from Larson (2016).

3.2 RECEPTION OF REFLECTED SIGNALS

Indirect signals (reflected waves) are received by the antenna mainly from its lower hemisphere. The GNSS antennas are designed to aim at the rejection or mitigation of the reflected waves. In this context, it is common to use a metal plate integrated into the antenna element, named ground plane, or the use of a special

antenna attachment made of concentric metal rings named choke rings (MONICO, 2008). Specific configurations were developed to increase the reception of these reflected waves (JIA; PEI, 2018):

a) Two antennas: one of them oriented in a conventional way, towards zenith, aiming to receive direct waves, and another antenna oriented to nadir, or close to it, to capture the reflected waves. This was the first configuration proposed for GNSS-R (MARTIN-NEIRA, 1993). This configuration is not compatible with GNSS-MR/IPT/IR, because conventional GNSS receivers are unable to track the two waves separately. See FIGURE 4a;
b) Single vertical antenna: This is the case with only one antenna oriented towards zenith (conventional orientation to GNSS positioning). It simultaneously receives direct and reflected waves (FIGURE 4b.) This configuration allows the shared use of the GNSS station for positioning and reflectometry (LARSON et al., 2008a);
c) Single tilted antenna: analogous to the previous case, however with the antenna pointed at the horizon, or close to it (FIGURE 4c) (RODRIGUEZ-ALVAREZ, 2009). It has the advantage of amplifying the reception of waves reflected in the target azimuth; as a disadvantage, it impairs reception in the opposite azimuth.

FIGURE 4 – ANTENNA SYSTEM SCHEMES IN GNSS-R.

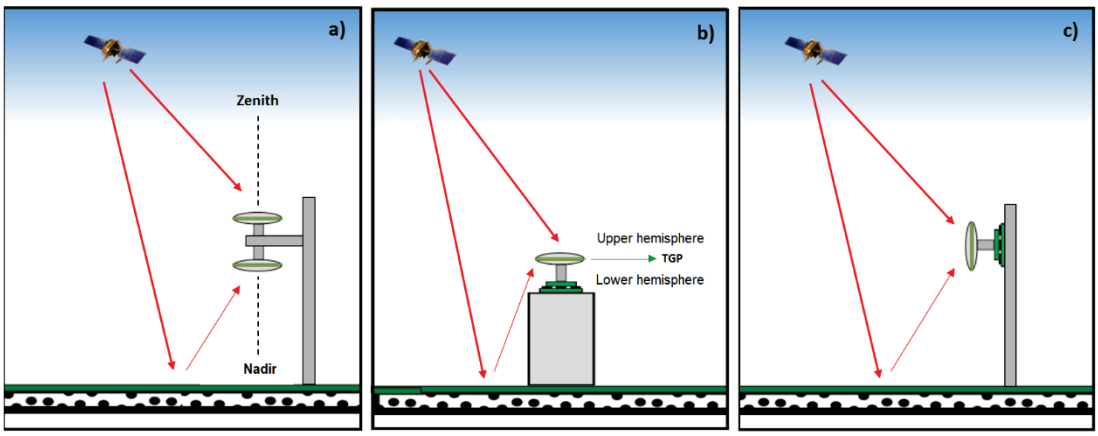

SOURCE: The authors (2021).

3.3 SNR MODELING

IThe modeling of SNR for reflectometry purposes is carried out through the combination of a physical model, related to the theoretical simulation of the multipath (NIEVINSKI; LARSON 2014b), and an inverse model, by which unknown parameters are estimated through GNSS measurements (NIEVINSKI; LARSON, 2014c).

3.3.1 Physical Model: Theoretical Simulation

The scattering of electromagnetic waves occurs in three ways: diffraction, specular (coherent reflection), and diffuse (incoherent reflection) (ZAVOROTNY et al., 2015). These conditions occur mainly due to the characteristics of the reflecting surfaces. Specular reflections are the ones that most interfere with direct waves since only coherent waves are subject to superposition. Coherent observations maintain a stable phase relationship between direct reflected waves (NIEVINSKI; MONICO, 2016). In contrast, incoherent observations have a random phase and do not maintain a predictable relationship between these waves.

The GNSS satellite transmissions are Right-Hand Circularly Polarised (RHCP) (WU; JIN, 2019). When reflecting on surfaces, two components can be generated, RHCP and Left-Hand Circularly Polarised (LHCP) (KATZBERG et al., 2006). The proportion between these components depends on the direction of incidence of the direct wave and the dielectric properties of the reflecting surface. The electric field of the reflected wave ($\overline{E_r}$), in volts per meter, is a complex vector, therefore with magnitude and phase given according to Eq. (4) (NIEVINSKI; LARSON, 2014a):

$$\overline{E_r} = S \cdot I \cdot \bar{\bar{R}} \cdot \overline{E_d} \tag{4}$$

where $\overline{E_d}$ is the direct field. The magnitude S represents a loss of coherent power due to the surface roughness, $S = \exp\left(-2\pi^2\lambda^{-2}\sigma_h^2 \sin^2 e\right)$, which is a real value and less than 1; σ_h is the surface height standard deviation (in meters). The scalar $I = \exp\left(2\pi\lambda^{-1}\tau_i\sqrt{-1}\right)$ is a complex value, usually unitary, which involves the phase difference resulting from the propagation delay (τ_i, in meters) between reflected and direct waves. For a flat and horizontal surface, τ_i (Eq. 5) can be estimated as a function

of the satellite's elevation angle and antenna height (GEORGIADOU; KLEUSBERG, 1988):

$$\tau_i = 2H\sin(e) \tag{5}$$

In Eq. (5), H is the vertical distance between the antenna phase center and the reflecting surface (TABIBI et al., 2015); it is not exactly the geometric height of the antenna above the ground surface, as it depends on the penetration depth of the electromagnetic wave.

The reflection matrix $\bar{\bar{R}}$ (Eq. 6), represents the effect of the surface composition on the reflected electromagnetic wave (NIEVINSKI; LARSON, 2014a):

$$\bar{\bar{R}} = \begin{bmatrix} R^S & R^X \\ R^X & R^S \end{bmatrix} \tag{6}$$

This matrix is determined by the combination of the circularly polarized scalar reflection coefficients (complex values): R^S (Eq. 8) for the same-sense polarizing value and R^X (Eq. 9) the cross-sense polarizing value (NIEVINSKI; LARSON, 2014a).

Although the direct electric field has only RHCP component (E_d^R) due to negligible LHCP component ($E_d^L \approx 0$), the reflected field can have both non-zero components (E_r^R, E_r^L). In the case of GNSS, Eq. (4) can be simplified as Eq. (7):

$$\overline{E_r} = [E_r^R, \quad E_r^L]^T = S \cdot I[R^S, \quad R^X]^T E_d^R \tag{7}$$

The circularly polarized scalar reflection coefficients are defined based on the linearly polarized reflection coefficients that follow from the Fresnel equations (NIEVINSKI; LARSON, 2014a):

$$R^S = \frac{R^H + R^V}{2} \tag{8}$$

$$R^X = \frac{R^H - R^V}{2} \tag{9}$$

These coefficients are complex values that depend on the angle of incidence of the wave. In general, the same-sense polarized reflection tends to zero for normal incidence (perpendicular to the surface), while cross-sense polarized reflection tends to zero for near-grazing incidence. In the case of GNSS, this means that high satellites tend to have LHCP reflections, and low satellites tend to have RHCP reflections. Therefore, for satellites close to the zenith, the reception of reflection signals would be better with an antenna with LHCP polarization.

In Eq. 8 and Eq. 9, the coefficients on the right side of the equalities are the linear vertical (R^V) and linear horizontal (R^H) reflection coefficients (NIEVINSKI; LARSON, 2014a):

$$R^V = \frac{(\cos\theta - \sqrt{\varepsilon - \sin^2\theta})}{(\cos\theta + \sqrt{\varepsilon - \sin^2\theta})} \tag{10}$$

$$R^H = \frac{(\varepsilon \cdot \cos\theta - \sqrt{\varepsilon - \sin^2\theta})}{(\varepsilon \cdot \cos\theta + \sqrt{\varepsilon - \sin^2\theta})} \tag{11}$$

where $\theta = 90° - e$ (assuming flat surface). The complex dielectric constant ($\varepsilon = \varepsilon' + \sqrt{-1}\varepsilon''$) of the medium is a complex number with real (ε') and imaginary (ε'') components that are related to the medium conductivity (EDOKOSSI et al., 2020). In the case of soil, the values of those components vary with moisture according to empirically calibrated curves (FIGURE 5), which link relative permittivity (adimensional) and moisture for different types of soil (HALLIKAINEN et al., 1985).

The indirect electric field exists only in the free space between transmitting satellite and receiving antenna (TABIBI et al., 2015). Consequently, it is necessary to calculate the electrical voltage (volts) of the direct (V_d) and reflected waves (V_r) induced in the electrical connection between antenna and receiver. This is done by multiplying the electric field vector by the antenna effective length ($\bar{L}$), a complex vector in meters:

$$V_d = E_d^R \cdot L_d^R \tag{12}$$

$$V_r = L_r^R \cdot E_r^R + L_r^L \cdot E_r^L = S \cdot I \cdot X \cdot E_d^R \tag{13}$$

Note that there are components for both polarizations (RHCP ou LHCP), denoted by superscript letters. The subscript denotes the direction of the reception (direct or reflected signal) e.g., L_d^R is the antenna response for a direct RHCP wave. The magnitude and argument of each $\bar{L}$ the component comes, respectively, from the gain pattern and the phase center variations of the antenna, both previously calibrated. The factor $X = L_r^R R^S + L_r^L R^X$ represents the interaction between the antenna responses (L) and the reflecting surface response (R) (TABIBI et al., 2015). Therefore, it is linked to the soil moisture of the reflected surface.

FIGURE 5 – COMPLEX COMPONENTS OF SOIL PERMITTIVITY FOR DIFFERENT TYPES OF SOIL AT A 1.4 GHZ FREQUENCY.

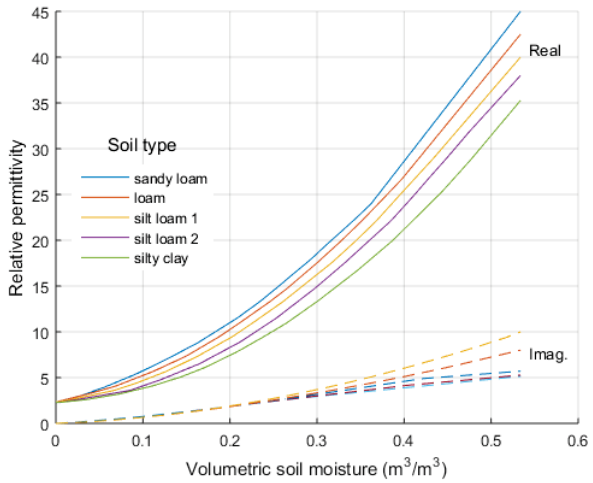

SOURCE: Adapted from Hallikainen et al. (1985).

Finally, the composite voltage, resulting from the superimposition of direct and reflected waves, can be obtained: $V = V_d + V_r$. This sum occurs on the complex plane, separately for the real and imaginary components. The corresponding power $P = V^2$, in watts, is given by:

$$P = P_d + P_r + 2\sqrt{P_d}\sqrt{P_r}\cos\phi_i \tag{14}$$

P is related to the powers of the direct signal ($P_d = |V_d|^2$) and the reflected signal ($P_r = |V_r|^2$). It also includes a trigonometric term dictated by the interferometric phase (ϕ_i), the difference between the phases of the two voltages: $\phi_i = \phi_r - \phi_d = \arg(V_r) -$

$\arg(V_d)$ (NIEVINSKI; LARSON, 2014a). The interferometric phase is dominated by the propagation delay (τ_i) stemming from the additional path of the reflected signal (TABIBI et al., 2015), which is given by Eq. (15):

$$\phi_i \cong 2\pi\lambda^{-1}\tau_i + \phi_X = 2\pi\lambda^{-1}2H\text{sin}(e) + \phi_X \quad (15)$$

This equation includes the compositional phase $\phi_X = \arg(X)$, resulting from the combination of the properties of the reflecting surface and the GNSS antenna (NIEVINSKI; LARSON, 2014a). This is the phase component that depends on soil moisture. It varies with the satellite's elevation angle as the reflected wave changes polarization. FIGURE 6a shows the relationship between these quantities in two theoretical scenarios: the first is completely dry soil (blue); the second with soil moisture equals 50% (red). Following Liu and Larson (2018), the variations in the compositional phase cause a bias in the geometric height, designating a compositional height bias $H_X = \partial\phi_X/\partial k_z$, given by the rate of change in ϕ_X with respect to vertical wavenumber, $k_z = 4\pi\lambda^{-1}\text{sen}\,(e)$. FIGURE 6b shows the simulated height bias as a function of elevation angle in the two soil moisture scenarios.

FIGURE 6 – COMPOSITIONAL PHASE (ϕ_X) ON THE LEFT PANEL AND COMPOSITIONAL HEIGHT BIAS ON THE RIGHT, AS A FUNCTION OF THE SATELLITE ELEVATION ANGLE IN TWO SCENARIOS CONCERNING SOIL MOISTURE (0 E 50%).

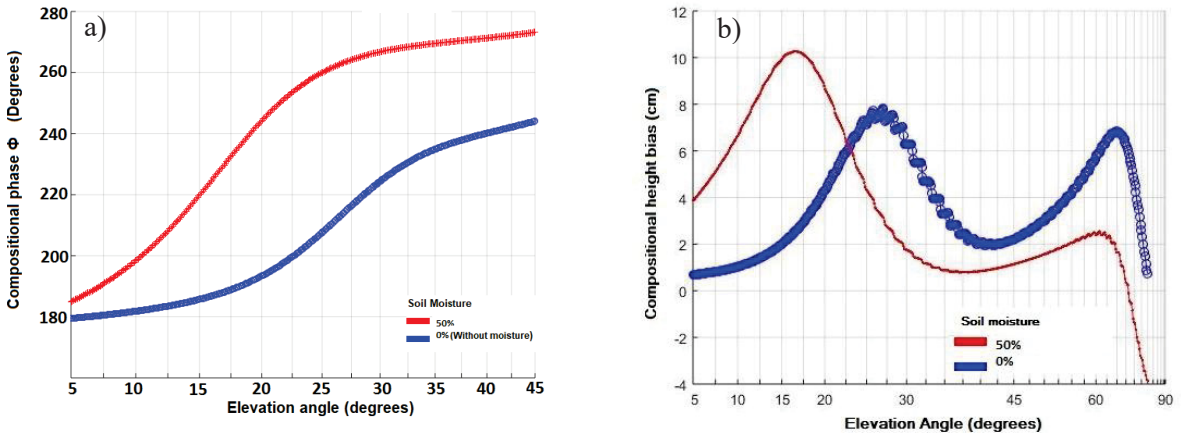

SOURCE: The authors (2021).

FIGURE 7 – SNR (DB) SIMULATED FOR TWO SCENARIOS: WITHOUT SOIL MOISTURE (BLUE); SOIL MOISTURE 50% (RED).

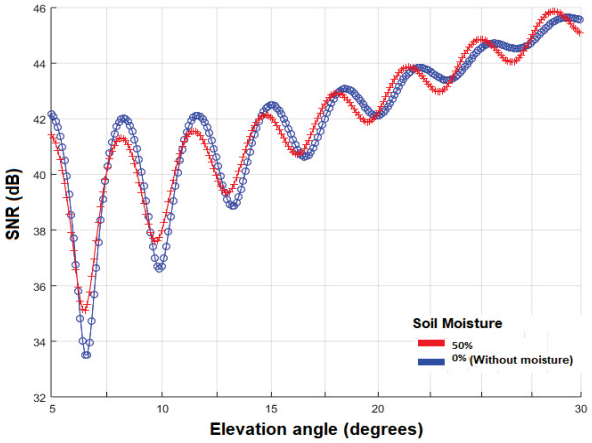

SOURCE: The authors (2021).

According to Nievinski and Monico (2016), when the input signal is received, its power (P) is normalized by the noise power (P_n) and recorded by the receiver. P_n is an arbitrary constant in the context of $SNR = P/P_n$, in watts per watts. The observed ratio can be modeled as the sum of two components, $SNR = tSNR + dSNR$: a trend ($tSNR$) and a detrended ($dSNR$) interference fringes term (TABIBI et al., 2017). The trend $tSNR = P_n^{-1}(P_d + P_r)$, stems mainly from the antenna gain pattern and has a polynomial form. The complementary component $dSNR = 2P_n^{-1}\sqrt{P_d}\sqrt{P_r}\cos\phi_i$, resulting from the in-phase and out-of-phase alignment of direct and reflected waves, has a sinusoidal form (NIEVINSKI; LARSON, 2014c).

3.3.2 Empirical model: sinusoidal fit

The physical model (section 3.3.1) can be approximated by the empirical model of Eq. 16. In this equation, k_z is adopted as an independent variable, because it is the basis of the propagation delay $\phi_i = k_z H + \phi_X$, assuming a flat, horizontal surface (ZAVOROTNY et al., 2010).

$$\begin{aligned} tSNR &\approx (c_0 + c_1 k_z + c_2 k_z^2 + \cdots) \\ dSNR &\approx A_m \cdot \cos(H_m k_z + \phi_m) \end{aligned} \tag{16}$$

The parameter H_m is related to the multipath oscillation frequency. The sum $\sum c_i k_z^i$, is a polynomial that approximates the trend; and the sinusoid approximates the dSNR complement. The amplitude A_m (Eq. 17), the initial phase ϕ_m (Eq. 18) and the effective height H_m (Eq. 19), are given following by Nievinski and Larson (2014c):

$$A_m \approx E\{2P_n^{-1}\sqrt{P_d}\sqrt{P_r}\} \tag{17}$$

$$\phi_m \approx E\{\phi_X - k_z H_m\} \tag{18}$$

$$H_m \approx H + E\{H_X\} \tag{19}$$

These empirical parameters (A_m, ϕ_m and H_m) are constants defined from the expectation $E\{\cdot\}$ of the variables resulting from the rigorous formulation of the theoretical model. The compositional height bias H_X ends up assimilated in the effective height $H_m = H + H_X$ (FIGURE 6b) (NIEVINSKI; LARSON, 2014a). In turn, the empirical phase ϕ_m is the average of the residual compositional phase, $\phi_X - k_z H_m$.

The parameters A_m, ϕ_m e H_m, observed in SNR observations, vary depending on factors such as carrier wavelength, free-space propagation medium, and the equipment, besides the influence of the reflected signal. Each of these empirical parameters responds better to a given application. The empirical height H_m has been applied for altimetric applications as sea level monitoring and snow depth. In turn, the empirical amplitude A_m has been applied in vegetation growth monitoring (SMALL et al., 2016) and sea waves, because such phenomena affect the surface roughness. The empirical phase ϕ_m parameter has been employed on soil moisture estimations (CHEW et al., 2014).

3.3.3 Inverse model: statistical model

The physical and empirical models can be ideally combined using previously available information, such as the antenna model and the type of soil, estimating as unknowns only the effects that vary with time, such as soil moisture. This strategy was developed and applied initially for the measurement of snow depth (NIEVINSKI; LARSON, 2014c, 2014d). Afterward, it was adapted for use in determining soil

moisture (TABIBI et al., 2015). The inversion is a statistical model through which the unknown parameters are determined from the GNSS observations. These measured observations are compared internally with the observations simulated by the forward physical model (NIEVINSKI; LARSON, 2014b). Hence, the simulated observations are fitted to the measurements, involving in this process a nonlinear least-squares adjustment of the unknown parameters (NIEVINSKI; LARSON, 2014c). As a result, we have the estimated parameters and their precision: amplitude, phase, antenna height, and polynomial coefficients of the trend.

3.3.4 Post-processing: physical-statistical combination

After inversion, several post-processing measures are required. Through this module, the inversion parameters are subjected to statistical inferences, quality control, and optimization of results (NIEVINSKI; LARSON, 2014d). FIGURE 8 shows simulated SNR observables and measured observations, as well as the residuals associated with the difference between these observables.

In the case of soil moisture, the phase parameters (phase shift and the respective phase rate) have their precision degraded, as they are very correlated. As soil moisture content affects the penetration depth of electromagnetic waves into the soil, this creates variations in the effective height of the antenna (LARSON, 2016). Thus, a strategy to improve the estimation of the phase parameters is to define an average value for this height and introduce it as a constraint in post-processing (EURIQUES, 2019).

It is also necessary to combine the independent estimates of the various satellites into an average value for the station. Finally, a calibration curve, using a first or second-degree polynomial, establishes the relationship between the parameters of the interferometric phase with the soil moisture values. FIGURE 9 exemplifies the relationship between phase values (vertical axis) and soil moisture (horizontal axis). In this figure, the phase values were estimated from the reflected waves of the GPS satellite PRN 29 at a given station, whereas soil moisture values were determined by the average of 5 TDR probes located close to this station (LARSON et al., 2008b).

FIGURE 8 – SIMULATED AND MEASURE SNR SIGNATURE AND ITS RESIDUES FOR AN ASCENDING ARC FOR THE PRN02 SATELLITE.

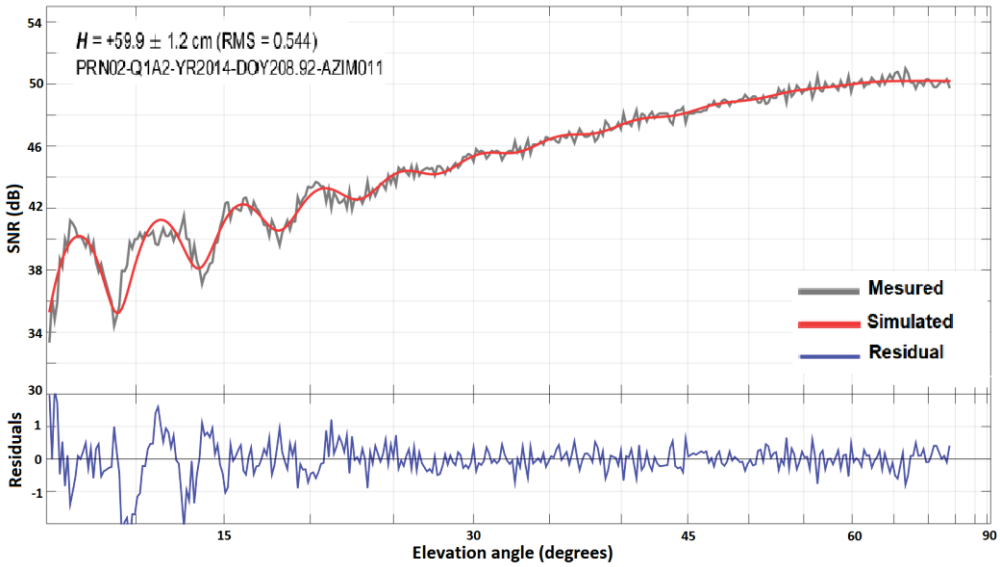

SOURCE: The authors (2021).

FIGURE 9 – RELATIONSHIP BETWEEN REFLECTOMETRIC PHASE AND SOIL MOISTURE.

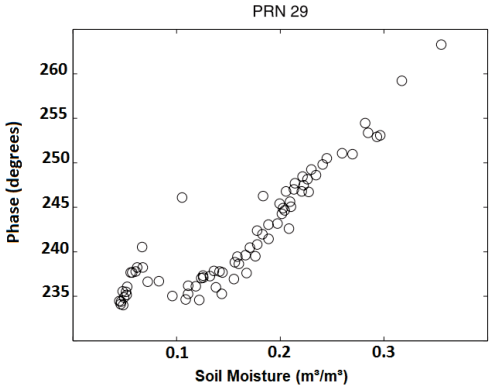

SOURCE: Adapted from Larson et al. (2008b).

The calibration curve between soil moisture and the phase-shift is based on linear regression in the form $a \cdot \phi_m + b$, whose slope is often reported in the literature as $a = 1{,}48\ \mathrm{cm^3 cm^{-3} {}^{\circ -1}}$ (CHEW et al., 2015) or its reciprocal, $a^{-1} = 65\ ^{\circ}/(\mathrm{cm^3/cm^3})$ (VEY et al., 2016) These values were determined from physical simulations considering specific antenna models. The intercept or constant coefficient of the regression (b) is associated with residual soil moisture, which represents the minimum value present in the soil. It is normally assumed $b = 0{,}05\ \mathrm{m^3 m^3}$ (VEY et al., 2016). Following Chew et al. (2015), the coefficient b can also be obtained through the interpolation of soil texture maps.

3.4 METHOD LIMITATIONS

The two coefficients of phase calibration for soil moisture are dependent on the site location and the GNSS antenna model; therefore, they are uncertain for locations without additional data from conventional methods or that have had an antenna exchange. This is probably the largest limitation of using the GNSS-R method to soil moisture monitoring. Other limitations must be considered such as the effects of topography, vegetation, surface roughness, and soil temperature because they affect the determinations.

Ground vegetation may obstruct the incidence and reflection of radio waves on the ground (ZHANG et al., 2017). Besides, as explained, vegetation influences the roughness of the reflection surface, which can affect the coherence of the signals and the amplitude and phase determinations. Furthermore, the location of the GNSS station and the characteristics of the surroundings should have unobstructed visibility to the ground on the reflection area, avoiding objects like fences, which is a basic condition for carrying out GNSS-R.

Another limitation, not only for GNSS-R but also for other remote sensing methods that use microwaves (L, C, and X bands), concerns the power of penetration of these electromagnetic waves into the ground, which in the case of GNSS frequencies is mainly limited to a depth of about 5 cm (EDOKOSSI et al., 2020). Thus, considering that the soil moisture varies along with a vertical profile in the soil when making statistical comparisons between different methods, one should consider these possible differences between the reference depths of each method.

4 RELATED STUDIES

In this section, we highlight the main works in which soil moisture was estimated through GNSS-R using SNR from ground stations. TABLE 1 lists information such as: authorship; antenna height about the ground (meters); duration (days); GNSS system: being GPS (G), GLONASS (R), BeiDou (B), or Galileo (E); GNSS modulation; soil cover; method of validating the reflectometric determinations; as well as the correlation (in percentage).

Other types of GNSS-R, such as from aerial and orbital platforms, are not discussed. Further details can be found, for example, in: Jin, Cardellach and Xie (2014); Masters, Axelrad and Katzberg (2004); Chew and Small (2018); and Eroglu et al. (2019).

Larson et al. (2008a) were the pioneers in this theme. They have detected correlations between the time series of reflected signal amplitudes, obtained by SNR via RINEX, and soil moisture obtained by the Noah Land Surface Model. This model allows evaluating the evolution of moisture using meteorological parameters as input data. GPS data recorded at the TASH station, located in Tashkent, Uzbekistan, were used. The surroundings of this station are covered by low vegetation (grass). The effects of vegetation on the modeling of reflective signals were not considered. To determine the amplitude series, the frequency L2 was used in a range of 15° to 30° in terms of the elevation angles of the satellites. Additionally, it was found that the two series had similar performances in precipitation events. Larson et al. (2008b), employed L2C modulation (6 satellites of Block IIR-M), with elevation angle range 10° to 30°, for a station located in Marshall - United States. The series of phases generated was converted empirically into a series of soil moisture. The results were validated through the series compiled from 10 in situ probes (TDR) calibrated by the gravimetric method. A correlation of 85% was obtained between these series. This research was expanded in Larson et al. (2010), with elevation angles between 5° and 25°, recorded at the NCAR station (Marshall), which is part of the active Earthscope Plate Boundary Observatory (PBO) network. The variation of the effective reflector height, or the penetration depth of waves into the ground varied according to the soil moisture content. They found that the parameter with the highest correlation with the moisture content close to the soil surface is the phase shift, which obtained a 90% correlation with FTD probes calibrated by the gravimetric method.

Rodriguez-Alvarez et al. (2009) presented the GNSS-IPT technique performed from specific equipment developed for reflectometry where the GPS hardware, in L1 frequency, was connected to a vertical linear polarization antenna. In this case, the antenna was oriented towards the horizon (FIGURE 4c), and the range of elevation angles between 7° e 50°. Unlike the previous cases, the SNR metric in this research was the notch, which represents the elevation angle where the minimum amplitude of the multipath oscillation occurs. The maximum soil moisture RMS error about the FDR probes was 3,1%. In later researches, Rodriguez-Alvarez et al. (2011a, and 2011b)

assessed the influence of different types of land cover on GPS-IPT determinations. Arroyo et al. (2014), extended this technique to include two linear polarizations (vertical and horizontal). In this case, the SNR metrics used were the points of maximum and minimum amplitude. The correlation was 90% with a probe from the Oznet SM soil moisture monitoring network.

Chew et al. (2014) evaluated the performance of a direct model by an empirical relationship observed in field data. GPS modulations with L2 carriers were simulated, isolating and disregarding the influence of vegetation, topography, and surface roughness in modeling. The results obtained were compared with 11 FDT probes, arranged at different depths. Authors defined a gradient of soil moisture as a function of depth. By the reflectometric phase, a 91% correlation was obtained in the range between 0 and 5 centimeters depth. In Chew et al. (2015) an algorithm was developed that started to consider the effects of vegetation on modeling.

Yan et al. (2014) conducted research using a low-cost GPS receiver with frequency L1. Yan et al. (2016) used the B1 (BeiDou) and L1 (GPS) modulations with SNR obtained via NMEA 0138 sentence. Yan et al. (2017) did not directly employ SNR, but the Signal Strength Indicator, also recorded continuously by GNSS receivers.

In Tabibi et al. (2015), soil moisture estimations were performed using L2C and L5 signals, reaching correlations with in situ probes of 70 and 80%, respectively. Roussel et al. (2016) used GPS and GLONASS modulations recorded by a station located in Lamasquère, France, considering elevation angles between 2° and 70°.

Small et al. (2016) evaluated the performance of different algorithms aimed at removing the effects of vegetation on the reflected signals; data from 11 stations of the PBO network were used. Zhang et al. (2017) carried out simultaneous monitoring of soil moisture and vegetation growth in a wheat field in France. Yang et al. (2019) used SNR by L2C, L5, B1, and B2 obtaining correlations of up to 85%. Martín et al. (2020) used modulations by multiple constellations (GPS, GLONASS, and Galileo) by a geodetic receiver and a low-cost one. The results of this research were validated by the gravimetric method, and samples were collected daily.

TABLE 1 – OVERVIEW OF RELATED RESEARCHES (PUBLISHED IN SCIENTIFIC PAPERS) RELATED TO SOIL MOISTURE ESTIMATIONS BY GNSS - R VIA SNR RECORDED IN GROUND STATIONS.

Author/year	Height (m)	Duration (days)	System	Modulation	Land cover	Validation	Corr. (%)
Larson et al. (2008a)	6	70	G	L2	Grass	Noah Model	-
Larson et al. (2008b)	1.9	83	G	L2C	Grass	TDR	85
Larson et al. (2010)	1.8	210	G	L2C	Grass	TDR	90
Rodriguez-Alvarez et al. (2009)	2.6	60	G	L1	Bare	FDR	-
Rodriguez-Alvarez et al. (2011a)	4.5	25	G	L1	Maize	FDR	-
Rodriguez-Alvarez et al. (2011b)	3	600	G	L1	Bare	Hydra	-
Chew et al. (2014)	2.4	230	G	L2	Bare	TDR	91
Arroyo et al. (2014)	3.6	11	G	L1	Grass	OzNet SM	90
Yan et al. (2014)	1	2	G	L1	Grass/bare	TDR	-
Tabibi et al. (2015)	2	153	G	L2C; L5	Sparse veg.	TDR	70; 80
Roussel et al. (2016)	1.7	40	G; R	L1	Bare	FDR	95
Chew et al. (2015)	1.5to 2.1	730	G	L2C	Sparse veg.	TDR	-
Small et al. (2016)	2	730	G	L2C	Grass	FDR	-
Vey et al. (2016)	1.5	2100	G	L2P; L2C	Bare	TDR	80
Yan et al. (2016)	2	60	B; G	B1; L1	Bare	FDR	80
Yan et al. (2017)	2	180	B; G		Bare	FDR	70
Yang et al. (2017)	2.2	105	B; G	B1, B2, L2C; L5	Sparse veg.	Permittivity	62;71
Zhang et al. (2017)	2.5	180	G	C/A	Wheat	FDR	74
Zhang et al. (2018)	29; 3.3	300; 120	G	L2C; L5	Grass	FDR	86
Han et al. (2018)	1.7	40	G	L1	Soy	FDR	95
Yang et al. (2019)	2.4	300	G; B	L2C; L5; B1; B2	Alpine veg.	TDR	80; 85
Chang et al. (2019)	1.9	450 ;14	G	L2C	Sparse veg.	Probe	61; 87
Martín et al. (2020)	1.8	66	G; R; E	L1; L1; E1	Bare	Gravimetric	70; 85
Han et al. (2020)	1.7	40	G	L1	Bare	FDR	95

SOURCE: The authors (2021).

5 DISCUSSIONS AND FINAL CONSIDERATIONS

Each of the different methods of soil moisture determination has limitations and specificities, such as the spatial scale of the measurements or footprint: sometimes punctual, as in the case of the gravimetric method and the direct in situ probes, sometimes in the order of tens of km², as in the case of remote sensing (orbital). Through these methods, there is information that may not be representative of a plot of land of interest. On the other hand, equipment such as neutron probes can provide information on an intermediate scale, however, they can be costly. In this scenario, GNSS reflectometry (GNSS-R) is an alternative or complementary method to conventional methods. Over the past decade, research has been carried out on this topic at an international level, in which results indicate a good correlation between the determinations by GNSS-R compared to conventional methods, indicating the efficiency of the technique.

GPS and GLONASS systems have global coverage and are in full operation. Currently, there are about 60 satellites considering only these two systems. Given this, there is an adequate temporal resolution for data acquisition, due to the repetition of trajectories in terms of azimuths of passage. With the modernization of GNSS, new signals are being introduced, such as the L5, L2C, and L1C. Also, new systems such as Galileo and BeiDou have been expanding the possibilities to achieve better results in the most diverse applications in which GNSS-R can be used.

Research has also been focused on the refinement of modeling, including the evaluation of different antenna patterns (LI et al., 2018), and electromagnetic properties of the soil (WU; JIN, 2019). Investigations have evaluated the combination of techniques, especially from the CYGNSS mission, which can contribute to the spatial and temporal resolution of determinations (KIM; LAKSHMI, 2018). The CYGNSS mission has great relevance in the orbital context, as it is a constellation of eight satellites aimed at monitoring the Earth via GNSS-R (CALABIA; MOLINA; JIN, 2020).

In SNR-based GNSS-R, data from conventional GNSS stations can be used, as data from RBMC stations. Historical series of these stations can be used in reflectometry, enabling the improvement of models, calibration of satellite missions, increasing the accuracy of forecasts, and contributing to the understanding of

hydrological phenomena. However, it should be noted that the use of a given sensor for this application depends on the conditions of direct visibility to the ground. In this context, many of the existing stations, mainly urban ones, do not meet this requirement.

Future research perspectives are related to investigations concerning the limitations of the technique and the improvement of modeling, highlighting the effects of the topography of the reflection surface, effects of vegetation, and roughness.

Acknowledgments

The first author would like to acknowledge CAPES (Brazilian Coordination for the Improvement of Higher Education Personnel) for a scholarship (process number: 88882.382285/2019-01).

Author Contributions

J.F.E. carried out the initial design and writing. J.F.E., F.G.N., and C.P.K. carried out the conceptualization. All authors contributed to the review, editing, and development of the article. F.G.N. supervised the execution of the research.

Conflicts of Interest

There are no conflicts of interest.

REFERENCES

ARORA, B.; DWIVEDI, D.; FAYBISHENKO, B.; JANA, R. B.; WAINWRIGHT, H. M. Understanding and Predicting Vadose Zone Processes. **Reviews in Mineralogy & Geochemistry,** v. 85, n. 1, p. 303-328, set. 2019. DOI.: 10.2138/rmg.2019.85.10

ARROYO, A. A.; CAMPS, A.; AGUASCA, A.; FORTE, G. F.; MONERRIS, A.; RÜDIGER, C.; WALKER, J. P.; PACUAL, D.; ONRUBIA, R. Dual-polarization GNSS-R interference pattern technique for soil moisture mapping. **IEEE Journal of Selected Topics in Applied Earth Observations and Remote Sensing**, v. 7, n. 5, p. 1533-1544, mai. 2014. DOI.: 10.1109/JSTARS.2014.2320792.

BABAEIAN, E.; SADEGHI, M.; JONES, S. B.; MONTZKA, C.; VEREECKEN, H.; TULLER, M.. Ground, Proximal, and Satellite Remote Sensing of Soil Moisture. **Reviews of Geophysics**, v. 57, n. 2, p. 530-616, mar. 2019. DOI.: 10.1029/2018RG000618.

BILICH, A.; LARSON, K. M. Mapping the GPS multipath environment using the signal-to-noise ratio (SNR). **Radio Science**, v. 42, n. 6, nov. 2007. DOI.: 10.1029/2007RS003652.

CALABIA, A.; MOLINA, I.; JIN, S. Soil Moisture Content from GNSS reflectometry using dielectric permittivity from fresnel reflection coefficients. **Remote Sensing**, v. 12, n. 1, p. 1-21, jan. 2020. DOI.: 10.3390/rs12010122.

CHANG, X.; JIN, T.; YU, K.; LI, Y.; LI, J.; ZHANG, Q. Soil moisture estimation by GNSS multipath signal. **Remote Sensing**, v. 11, n. 21, p. 1-16, 2019. DOI.: 10.3390/rs11212559.

CHEW, C. C.; SMALL, E. E. Soil Moisture Sensing Using Spaceborne GNSS Reflections: Comparison of CYGNSS Reflectivity to SMAP Soil Moisture. **Geophysical Research Letters**, v. 45, n. 9, p. 4049-4057, 2018. DOI.:10.1029/2018GL077905.

CHEW, C. C.; SMALL, E. E.; LARSON, K. M. An algorithm for soil moisture estimation using GPS-interferometric reflectometry for bare and vegetated soil. **GPS Solutions**, v. 20, n. 3, p. 525-537, mai. 2015. DOI.: 10.1002/2016GL068189.

CHEW, C. C.; SMALL, E. E.; LARSON, K. M.; ZAVOROTNY, V. U. Effects of near-surface soil moisture on GPS SNR data: Development of a retrieval algorithm for soil moisture. **IEEE Transactions on Geoscience and Remote Sensing**, v. 52, n. 1, p. 537-543, jan. 2014. DOI.: 10.1109/tgrs.2013.224232.

DE RIDDER, K. Surface soil moisture monitoring over Europe using Special Sensor Microwave/Imager (SSM/I) imagery. **Journal of Geophysical Research: Atmospheres**, v. 108, n. 14, 2003. DOI.: 10.1029/2002JD002796.

DESILETS, D.; ZREDA, M.; FERRÉ, T. P. A. Nature's neutron probe : Land surface hydrology at an elusive scale with cosmic rays. **Water Resources Research**, v. 46, n. 1, p. 1-7, jun. 2010. DOI.: 10.1029/2009WR008726.

DELTA-T DEVICES LTD, **User manual for the profile probe type PR1. Version PR1- UM-01-2. Delta-t Devices Ltd**, Cambridge – UK, 2001.

EDOKOSSI, K.; CALABIA, A.; JIN, S.; MOLINA, I. GNSS-reflectometry and remote sensing of soil moisture: A review of measurement techniques, methods, and applications. **Remote Sensing**, v. 12, n. 4, p. 2-26, fev. 2020. DOI.: 10.3390/rs12040614.

ENTEKHABI, D.; NJOKU, E. G.; O'NEILL, P. E.; KELLOGG, K. H.; CROW W. T.; EDELSTEIN, W N.; ENTIN, J. K.; GOODMAN, S. D.; JACKSON, T. J.; JOHNSON, J; KIMBALL, J; PIEPMEIER, J. R.; KOSTER, R. D.; NEII, M.; MCDONALD, K. C.; MOGHADDAM, M.; MORAN, S.; REICHLE, R.; SHI, J. C.; SPENCER, M. W.; THURMAN, S. W.; TSANG, L.; VAN ZYL J. The soil moisture active passive (SMAP) mission. **Proceedings of the IEEE**, v. 98, n. 5, p. 704-716, mai. 2010. DOI.: 10.1109/JPROC.2010.2043918.

EROGLU, O.; KURUM, M.; BOYD, D.; GURBUZ, A. C. High spatio-temporal resolution CYGNSS soil moisture estimates using artificial neural networks. **Remote Sensing**, v. 11, n. 19, p. 2-32, set. 2019. DOI.: 10.3390/rs11192272.

EURIQUES, J. F. **Determinação da umidade do solo por meio da técnica de Refletometria GNSS – Primeiros resultados no Brasil**. 164 f. Dissertação (Mestrado em Ciências Geodésicas) – Programa de Pós-Graduação em Ciências Geodésicas, Universidade Federal do Paraná. Curitiba, 2019. Disponível em: https://hdl.handle.net/1884/62323. Acesso em: 20 set. 2020.

GAMARO, P. E. **Medidores Acústicos Doppler de Vazão**. 1ª ed. Foz do Iguaçu: Itaipu Binacional, 2012.

GAO, H.; WOOD, E. F.; JACKSON, T. J.; DRUSCH, M.; BINDLISH, R. Using TRMM/TMI to retrieve surface soil moisture over the southern United States from 1998 to 2002. **Journal of Hydrometeorology**, v. 7, n. 1, p. 23-38, 2006.

GEORGIADOU, P. Y.; KLEUSBERG, A. On Carrier Signal Multipath Effects in Relative GPS Positioning. **Manuscripta Geodaetica**, v. 13, n. 1, p. 172-179, 1988.

GLEASON, S.; HODGART, S.; SUN, Y.; GOMMENGINGER, C.; MACKIN, S.; ADJRAD, UNWIN, M. Detection and Processing of Bistatically reflected GPS signals from Low Earth Orbit for the purpose of Ocean Remote Sensing. **IEEE Transactions on Geoscience and Remote Sensing**, v. 43, n. 6, p. 1229-1241, jul. 2005. DOI.: 10.1109/TGRS.2005.845643.

GURTNER, W.; ESTEY, L. **RINEX The Receiver Independent Exchange Format Version 3.03**. 2015. Astronomical Institute, University of Bern and UNAVCO. Disponível em: < ftp://igs.org/pub/data/format/rinex300.pdf > Acesso em 23 set. 2020.

HALLIKAINEN M.T.; F.T. ULABY; M.C. DOBSON; M. EL-RAYES; WU, L.-K. Microwave Dielectric Behaviour of Wet Soil - Part 1: Empirical Models and Experimental Observations. **IEEE Transactions on Geoscience and Remote Sensing**, v. 23, n. 1, p. 25-34, jan. 1985. DOI.: 10.1109/TGRS.1985.289497.

HAN, M.; ZHU, Y.; YANG, D.; CHANG, Q.; HONG, X.; SONG, S. Soil moisture monitoring using GNSS interference signal: proposing a signal reconstruction method. **Remote Sensing Letters**, v. 11, n. 4, p. 373-382, 2020. DOI.: 10.1080/2150704X.2020.1718235.

HAN, M.; ZHU, Y.; YANG, D.; HONG, X.; SONG, S. A semi-empirical SNR model for soil moisture retrieval using GNSS SNR data. **Remote Sensing**, v. 10, n. 2, p. 1-19, 2018. DOI.:10.3390/rs10020280.

HANSON, B. Field Estimation of Soil Water Content: A Practical Guide to Methods, Instrumentation and Sensor Technology. **Vadose Zone Journal**, v. 8, n. 3, p. 628-759, 2009. DOI.: 10.2136/vzj2008.0171.

HILLEL, D. **Environmental Soil Physics**. 1º ed. San Diego: Academic Press, 1998.

JIA, Y.; PEI, Y. Remote Sensing in Land Applications by Using GNSS-Reflectometry. In: HUNG, M.; WU, Y. **Recent Advances and Applications in Remote Sensing**. IntechOpen, 2018. p. 65-88.

JIN, S.; CARDELLACH, E.; XIE, F. **Remote Sensing and Digital Image Processing: Theory, Methods and Applications**. 2014. Dordrecht: Springer, 2014.

JIN, S.; QIAN, X.; KUTOGLU, H. Snow depth variations estimated from GPS-reflectometry: A case study in Alaska from L2P SNR data. **Remote Sensing**, v. 8, n. 1, p. 1-15 jan. 2016. DOI.: 10.3390/rs8010063.

KATZBERG, S. J.; TORRES, O.; GRANT, M. S.; MASTERS, D. Utilizing calibrated GPS reflected signals to estimate soil reflectivity and dielectric constant: Results from SMEX02. **Remote Sensing of Environment**, v. 100, n. 1, p. 17-28, set. 2006. DOI.: 10.1016/j.rse.2005.09.015.

KERR, Y. H.; WALDTEUFEL, P.; WIGNERON, J. P.; MARTINUZZI, J. M.; FONT, J.; BERGER, M. Soil Moisture Retrieval from Space: The Soil Moisture and Ocean Salinity (SMOS) Mission. **IEEE Transactions on Geoscience and Remote Sensing,** v. 39, n. 8, p. 1729-1735, 2001. DOI.: 10.1109/36.942551.

KIM, H.; LAKSHMI, V. Use of Cyclone Global Navigation Satellite System (CYGNSS) Observations for Estimation of Soil Moisture. **Geophysical Research Letters**, v. 45, n. 16, p. 8272–8282, 2018. DOI.: 10.1029/2018GL078923.

LARSON, K. M. GPS interferometric reflectometry: applications to surface soil moisture, snow depth, and vegetation water content in the western United States. **Wiley Interdisciplinary Reviews: Water,** v. 3, n. 6, p. 775-787, 2016. DOI.:10.1002/wat2.1167.

LARSON, K. M.; BRAUN, J. J.; SMALL, E. E.; ; ZAVOROTNY, V. U.; GUTMANN, E. D.; BILICH A. L. GPS Multipath and Its Relation to Near-Surface Soil Moisture Content. **IEEE Journal of Selected Topics in Applied Earth Observations and Remote Sensing**, v. 3, n. 1, p. 91-99, 2010. DOI.: 10.1109/jstars.2009.2033612.

LARSON, K. M.; NIEVINSKI, F. G. GPS snow sensing: results from the EarthScope Plate Boundary Observatory. **GPS Solutions**, v. 17, n. 1, p. 41-52, 2013. DOI.: 10.1007/s10291-012-0259-7.

LARSON, K. M.; SMALL, E. E.; GUTMANN, E.; BILICH, A. L.; AXELRAD, P.; BRAUN, J. Using GPS multipath to measure soil moisture fluctuations: Initial results. **GPS Solutions**, v. 12, n. 3, p. 173-177, 2008a. DOI.: 10.1007/s10291-007-0076-6.

LARSON, K. M.; SMALL, E. E.; GUTMANN, E. D; BILICH, A. L.; BRAUN, J. J.; ZAVOROTNY V. U. Use of GPS receivers as a soil moisture network for water cycle studies. **Geophysical Research Letters**, v. 35, n. 24, dez. 2008b. p. 1-5.DOI.:10.1029/2008gl036013.

LEICK, A. **GPS Satellite Surveying**. 2ª ed. New York: John Wiley & Sons, 1995.

LI, F.; PENG, X.; CHEN, X.; LIU, M.; XU, L. Analysis of key issues on GNSS-R soil moisture retrieval based on different antenna patterns. **Sensors,** v. 18, n. 8, p. 1-16, ago. 2018. DOI.: 10.3390/s18082498.

LIU, L.; LARSON, M. Decadal changes of surface elevation over permafrost area estimated using reflected GPS signals. **Cryosphere**, v. 12, n. 2, p. 477-489, fev. 2018. DOI.: 10.5194/tc-12-477-2018.

LIMA, J.; SILVA, E.; KOIDE, S.; SANTOS, R. Avaliação do Desempenho de Sonda de Capacitância no Monitoramento da Umidade de Latossolos do Cerrado em Condições de Campo. **Revista Brasileira de Recursos Hídricos**, v. 17, n. 1, p. 23-32, nov. 2012. DOI.:10.21168/rbrh.v17n1.p23-32.

LÖFGREN, J. S.; HAAS, R. Sea level measurements using multi-frequency GPS and GLONASS observations. **Eurasip Journal on Advances in Signal Processing**, v. 2014, n. 1, 2014. DOI: 10.1186/1687-6180-2014-50.

MARTIN-NEIRA, M. A Passive Reflectometry and Interferometry System (PARIS): application to ocean altimetry. **European Space Agency Journal**, v. 17, p. 331-355, 1993.

MARTÍN, A.; IBÁÑEZ, S.; BAIXAULI, C., BLANC, S.; ANQUELA, A. B. Multi-constellation GNSS interferometric reflectometry with mass-market sensors as a solution for soil moisture monitoring. **Hydrology and Earth System Sciences**, v. 24, p. 3573-3582, jul. 2020. DOI.: 10.5194/hess-24-3573-2020.

MASTERS, D.; AXELRAD, P.; KATZBERG, S. Initial results of land-reflected GPS bistatic radar measurements in SMEX02. **Remote Sensing of Environement**, v. 92, p. 507-20, mai. 2004. DOI.: 10.1016/j.rse.2004.05.016.

MENDES, P. C. de S. **Caracterização de um sensor para medição de umidade do solo com termo-resistor a temperatura constante**. 127 f. Tese (Doutorado em Engenharia Elétrica) – Programa de Pós-Graduação em Engenharia Elétrica, Universidade Federal da Bahia, Salvador, 2006.

MONICO, J. F. G. **Posicionamento pelo GNSS: Descrição, Fundamentos e Aplicações**. 2ª ed. Presidente Prudente: Editora Unesp, 2008.

NIEVINSKI, F. G.; LARSON, K. M. Forward modeling of GPS multipath for near-surface reflectometry and positioning applications. **GPS Solutions,** v. 18, n. 2, p. 309-322, 2014a. DOI.:10.1007/s10291-013-0331-y.

NIEVINSKI, F. G.; LARSON, K. M. An open source GPS multipath simulator in Matlab/Octave. **GPS Solutions**, v. 18, n. 3, p. 473-481, Fev. 2014b. DOI.:10.1109/tgrs.2013.2297688.

NIEVINSKI, F. G.; LARSON, K. M. Inverse modeling of GPS multipath for snow depth estimation - Part I: Formulation and simulations. **IEEE Transactions on Geoscience and Remote Sensing**, v. 52, n. 10, p. 6555-6563, 2014c. DOI.:10.1109/TGRS.2013.2297681.

NIEVINSKI, F. G.; LARSON, K. M. Inverse modeling of GPS multipath for snow depth estimation - Part II: Application and validation. **IEEE Transactions on Geoscience and Remote Sensing**, v. 52, n. 10, p. 6564–6573, 2014d. DOI.:10.1109/tgrs.2013.2297688.

NIEVINSKI, F. G., MONICO, J. F. G. GPS como um sensor remoto. In: PARANHOS FILHO, A. C.; MIOTO, C. L.; MARCATO JUNIOR, J.; CATALANI, T. G. T. (Org.). **Geotecnologias em Aplicações Ambientais**. 1ª ed. Campo Grande: Editora da UFMS, 2016, vol.1, p.234-251.

NIEVINSKI, F. G.; SILVA, M. F. E.; BONIFACE, K.; MONICO, J. F. G. GPS Diffractive Reflectometry: Footprint of a Coherent Radio Reflection Inferred from the Sensitivity Kernel of Multipath SNR. **IEEE Journal of Selected Topics in Applied Earth Observations and Remote Sensing**, v. 9, n. 10, p. 4884-4891, Out. 2016. DOI.:10.1109/jstars.2016.2579599.

OCHSNER, T. E.; COSH, M. H.; CUENCA, R. H.; DORIGO,W.A.; DRAPER, C.S.; HAGIMOTO,Y.; KERR, Y.; LARSON, K.M.; NJOKU, E. G.; SMALL, E. R.; ZREDA, M. State of the Art in Large-Scale Soil Moisture Monitoring. **Soil Science Society of America Journal**, v. 77, n. 6, p. 1888-1923, 2013. DOI.:10.2136/sssaj2013.03.0093.

PEREIRA, S. **Tecnologia da Reflectometria no Domínio do Tempo para medição da umidade do solo**. 109 f. Tese (Doutorado em Engenharia Agrícola) – Programa de Pós-Graduação em Engenharia Agrícola, Universidade Federal de Viçosa, Viçosa, 2011.

ROBINSON, D. A.; CAMPBELL, C. S.; HOPMANS, J. W.; HORNBUCKLE, B. K.; JONES, S. B.; KNIGHT, R.; OGDEN, F.; SELKER, J.; WENDROTH, O. Soil Moisture Measurement for Ecological and Hydrological Watershed-Scale Observatories: A

Review. **Vadose Zone Journal**, v. 7, n. 1, p. 358-389, fev. 2008. DOI.: 10.2136/vzj2007.0143.

RODRIGUEZ-ALVAREZ, N.; AKOS, D. M.; ZAVOROTNY, V. U.; SMITH, J. A.; CAMPS, A.; FAIRALL, C. W. Airborne GNSS-R Wind Retrievals Using Delay – Doppler Maps. **IEEE Transactions on Geoscience and Remote Sensing**, v. 51, n. 1, p. 626-641, jan. 2013. DOI.: 10.1109/TGRS.2012.2196437.

RODRIGUEZ-ALVAREZ, N.; BOSCH-LLUIS, X.; CAMPS, A.; VALL-LLOSSERA, M.; VALENCIA, E.; MARCHAN-HERNANDEZ, J. F.; RAMOS-PEREZ, I.. Soil moisture retrieval using GNSS-R techniques: Experimental results over a bare soil field. **IEEE Transactions on Geoscience and Remote Sensing**, v. 47, n. 11, p. 3616-3624, 2009. DOI.: 10.1109/TGRS.2009.2030672.

RODRIGUEZ-ALVAREZ, N.; CAMPS, A.; VALL-LLOSSERA, M.; M.; BOSCH-LLUIS, X.; MONERRIS, A.; RAMOS-PEREZ, I.; VALENCIA, E.; MARCHAN-HERNANDEZ, F.; MARTINEZ-FERNANDEZ, J.; BARONCINI-TURRICCHIA, G.; PÉREZ-GUTIÉRREZ, C,; SÁNCHEZ, N. Land geophysical parameters retrieval using the interference pattern GNSS-R technique. **IEEE Transactions on Geoscience and Remote Sensing**, v. 49, n. 1, p.71-84, Jan. 2011a. DOI.:10.1109/TGRS.2010.2049023.

RODRIGUEZ-ALVAREZ, N.; BOSCH-LLUIS, X.; CAMPS, A.; AGUASCA, A.; VALL-LLOSSERA, M.; VALENCIA, E.; RAMOS-PEREZ, I.; PARK, H. Review of crop growth and soil moisture monitoring from a ground-based instrument implementing the Interference Pattern GNSS-R Technique. **Radio Science**, v. 46, n. 5, p. 1-11, out. 2011b. DOI.: 10.1029/2011RS004680.

ROUSSEL, N.; FRAPPART, F.; RAMILLIEN, G.; DARROZES, J.; BAUP, F.; LESTARQUIT, L.; HA, M. C. Detection of Soil Moisture Variations Using GPS and GLONASS SNR Data for Elevation Angles Ranging from 2° to 70°. **IEEE Journal of Selected Topics in Applied Earth Observations and Remote Sensing**, v. 9, n. 10, p. 4781-4794, 2016. DOI.:10.1109/JSTARS.2016.2537847.

SEEBER, G. **Satellite Geodesy: Foundations, Methods, and Applications**. 2ª ed. New York: Walter de Gruyter, 2003.

SENEVIRATNE, S. I.; CORTI, T.; DAVIN, E. L.; HIRSCHI, M.; JAEGER, E. R.; LEHNER, I. ORLOWSKY, B.; TEULING, A. J. Investigating soil moisture-climate interactions in a changing climate: A review. **Earth-Science Reviews**, v. 99, n. 4, p. 125-161, fev. 2010. DOI.:10.1016/j.earscirev.2010.02.004.

SMALL, E. E.; LARSON, K. M.; CHEW, C. C.; DONG, J.; OCHSNER, T. E. Validation of GPS-IR Soil Moisture Retrievals: Comparison of Different Algorithms to Remove Vegetation Effects. **IEEE Journal of Selected Topics in Applied Earth Observations and Remote Sensing**, v. 9, n. 10, p. 4759-4770, out. 2016. DOI.: 10.1109/JSTARS.2015.2504527.

STRANDBERG, J.; HOBIGER, T.; HAAS, R. Coastal Sea Ice Detection Using Ground-Based GNSS-R. **IEEE Geoscience and Remote Sensing Letters**, v. 14, n. 9, p. 1552–1556, 2017. DOI.: 10.1109/LGRS.2017.2722041.

SWENSON, S.; FAMIGLIETTI, J.; BASARA, J.; WAHR, J. Estimating profile soil moisture and groundwater variations using GRACE and Oklahoma Mesonet soil moisture data. **Water Resources Research**, v. 44, n. 1, p. 1-12, 2008. DOI.:10.1029/2007WR006057.

TABIBI, S.; NIEVINSKI, F. G.; VAN DAM, T. Statistical Comparison and Combination of GPS, GLONASS, and Multi-GNSS Multipath Reflectometry Applied to Snow Depth Retrieval. **IEEE Transactions on Geoscience and Remote Sensing**, v. 55, n. 7, p. 3773-3785, 2017. DOI.:10.1109/tgrs.2017.2679899.

TABIBI, S.; NIEVINSKI, F. G.; VAN DAM, T.; MONICO, J. F. G. Assessment of modernized GPS L5 SNR for ground-based multipath reflectometry applications. **Advances in Space Research**, v. 55, n. 4, p. 1104-1116, 2015. DOI.:10.1016/j.asr.2014.11.019.

TEUNISSEN, P. J.; MONTENBRUCK, O. **Springer Handbook of Global Navigation Satellite Systems**. [s.l.]: Springer International Publishing, 2017. DOI 10.1007/978-3-319-42928-1

TULLER, M.; OR, D. Water Retention and Characteristic Curve. In: HILLEL, D; HATFIELD, J. L.; POWLSON, D. S.; ROSENZWEIG, C..; SCOW, K. M.; SINGER, J. M.; SPARKS, D. L. **Encyclopedia of Soils in the Environment**, 1º ed., Amsterdã, Elsevier Academic Press, 2004, p. 278-289. ISBN**:** 9780123485304.

VEY, S.; GÜNTNER, A.; WICKERT, J.; BLUME, T.; RAMATSCHI, M. Long-term soil moisture dynamics derived from GNSS interferometric reflectometry: a case study for Sutherland, South Africa. **GPS Solutions**, v. 20, n. 4, p. 641-654, 2016. DOI.: 10.1007/s10291-015-0474-0.

WU, X.; JIN, S. A Simulation Study of GNSS-R Polarimetric Scattering from the Bare Soil Surface Based on the AIEM. **Advances in Meteorology**, v. 2019, p. 1-9, mai. 2019. DOI.: 10.1155/2019/3647473.

XIE, Q.; MENENTI, M.; JIA, L. Improving the AMSR-E/NASA soil moisture data product using in-situ measurements from the Tibetan Plateau. **Remote Sensing,** v. 11, n. 23, 2019. DOI.:10.3390/rs11232748.

YAN, S.; LI, Z.; YU, K.; ZHANG, K. GPS-R L1 interference signal processing for soil moisture estimation: an experimental study. **Eurasip Journal on Advances in Signal Processing**, v. 107, n. 1, p. 1-13, 2014. DOI.: 10.1186/1687-6180-2014-107.

YAN, S. H.; ZHANG, N.; CHEN, N. C.; GONG, J. Y. Feasibility of using signal strength indicator data to estimate soil moisture based on GNSS interference signal analysis. **Remote Sensing Letters**, v. 9, n. 1, p. 61-70, 2017. DOI.:10.1080/2150704X.2017.1384587.

YAN, S. H.; ZHAO, F.; CHEN, N. C.; GONG, J. Y. Soil moisture estimation based on BeiDou B1 interference signal analysis. **Science China Earth Sciences**, v. 59, n. 12, p. 2427-2440, 2016. DOI.: 10.1007/s11430-015-0013-7.

YANG, T.; WAN, W.; CHEN, X.; CHU, T.; QIAO, Z.; LIANG, H.; WEI. J.; WANG, G.; HONG, Y. Land surface characterization using BeiDou signal-to-noise ratio observations. **GPS Solutions**, v. 23, n. 2, p. 1–12, 2019. DOI .10.1007/s10291-019-0824-4.

YANG, T.; WAN, W.; CHEN, X.; CHU, T.; HONG, Y. Using BDS SNR observations to measure near-surface soil moisture fluctuations: Results from low vegetated surface. **IEEE Geoscience and Remote Sensing Letters**, v. 14, n. 8, p. 1308-1312, 2017. DOI.: 10.1109/LGRS.2017.2710083.

ZAVOROTNY, V. U.; LARSON, K. M.; BRAUN, J. J.; SMALL, E. E.; GUTMANN, E. D.; BILICH, A. L. A Physical Model for GPS Multipath Caused by Land Reflections : Toward Bare Soil Moisture Retrievals. **IEEE Journal of Selected Topics in Applied Earth Observations and Remote Sensing**, v. 3, n.1, p. 100-110, 2010, abr. 2010. DOI.: 10.1109/JSTARS.2009.203360.

ZAVOROTNY, V. U.; GLEASON, S.; CARDELLACH, E.; CAMPS, A. Tutorial on remote sensing using GNSS bistatic radar of opportunity. **IEEE Geoscience and Remote Sensing Magazine**, v. 2, n. 4, p. 8-45, 2015. DOI.:10.1109/MGRS.2014.2374220.

ZHANG, S.; ROUSSEL, N.; BONIFACE, K.; HA, C. M.; FRAPPART, F.; DARROZES, J.; BAUP, F.; CALVET, J. C. Use of reflected GNSS SNR data to retrieve either soil moisture or vegetation height from a wheat crop. **Hydrology and Earth System Sciences**, v. 21, n. 9, p. 4767-4784, 2017. DOI.:10.5194/hess-21-4767-2017.

ZHANG, S.; CALVET, J. C.; DARROZES, J.; ROUSSEL, N.; FRAPPART, F.; BOUHOURS, G. Deriving surface soil moisture from reflected GNSS signal observations from a grassland site in southwestern France. **Hydrology and Earth System Sciences**, v. 22, n. 3, p. 1931-1946, 2018. DOI.: 10.5194/hess-22-1931-2018.

ZHANG, F.; ZHANG, L.-W.; SHI, J.-J.; HUANG, J.-F. Soil Moisture Monitoring Based on Land Surface Temperature-Vegetation Index Space Derived from MODIS Data. **Pedosphere**, v. 24, n. 4, p. 450-460, 2014. DOI.: 10.1016/S1002-0160(14)60031-X.

ZHOU, W.; LIU, L.; HUANG, L.; YAO, Y.; CHEN, J.; LI, S. A New GPS SNR-based Combination Approach for Land Surface Snow Depth Monitoring. **Scientific Reports**, v. 9, n. 1, p. 1-20, mar. 2019. DOI.: 10.1038/s41598-019-40456-2.

ZREDA, M.; SHUTTLEWORTH, W. J.; ZENG, X.; DESILETS, D.; FRANZ, T.; ROSOLEM, R. COSMOS: The cosmic-ray soil moisture observing system. **Hydrology and Earth System Sciences**, v. 16, n. 11, p. 4079-4099, 2012. DOI.:10.5194/hess-16-4079-2012.

2.2 CHAPTER 2: PAPER 2 – INPE I: IDEAL CONDITIONS

This chapter presents the manuscript *"Field-Wide Non-Contact Soil Moisture Sensing: Comparison between GNSS Interferometric Reflectometry and Cosmic-Ray Neutron Probe,"* which has been submitted for peer review in a scientific journal. This study focuses on the field application of GNSS Interferometric Reflectometry (GNSS-IR) for soil moisture estimation, comparing its performance with the Cosmic-Ray Neutron Probe under controlled conditions. The paper discusses the experimental setup, data processing techniques, and the correlation between the two methodologies.

2.2.1 Field-Wide Non-Contact Soil Moisture Sensing: Comparison between GNSS Interferometric Reflectometry and Cosmic-Ray Neutron Probe

ABSTRACT

Soil moisture is a key variable in understanding the water cycle, biogeochemical cycles, and various phenomena of the Earth System. Previous studies have demonstrated that Global Navigation Satellite Systems Interferometric Reflectometry (GNSS-IR) can be used for soil moisture remote sensing at field scale, offering advantages over traditional methods. In this study, we assessed the performance of ground-based GNSS-IR in determining soil moisture around a GNSS station in São Paulo state, Brazil. Signal-to-noise ratio (SNR) observations were collected using a geodetic-quality GNSS (GPS and GLONASS) receiver and antenna during a continuous 16-months campaign. For the first time, a neutron probe from the Cosmic-ray Soil Moisture Observing System (COSMOS) was used to validate the soil moisture estimates computed by the GNSS-IR technique. The results indicate good agreement between those two field-wide non-contact soil moisture sensing techniques, reaching a correlation of 0.73 with standard deviation of 0.0157 m^3/m^3, as derived from the RS2P signal (GLONASS L2-frequency, Protected code). The results were also compared against rain events recorded by a rain gauge, showing that peaks in soil moisture followed precipitation events. Despite differences between the methods, primarily related to different sensing depths and footprints, both methods simultaneously responded to variations in soil moisture.

Keywords Geodetic Remote Sensing. GNSS-IR. Multipath. Signal-to-Noise Ratio. Cosmic-ray.

1 INTRODUCTION

Soil moisture is the water content stored in the unsaturated soil or vadose zone (Hillel 1998). It is an essential component in several environmental, hydrological, and geophysical processes occurring at local, regional, and global scales. Accurate knowledge of soil moisture is crucial for various applications, including weather forecasting, climate monitoring, water resources management, prevention of natural hazards, geotechnical activities, engineering works, and agriculture (Hillel 1998; Robinson et al. 2008; Entekhabi et al. 2010; Seneviratne et al. 2010; Ochsner et al. 2013; Babaeian et al. 2019; Edokossi et al. 2020). The spatial distribution of soil moisture is non-uniform, both horizontally across the ground surface and vertically with increasing depth (Seneviratne et al. 2010; Tuller and Or 2004).

There are several conventional methods for soil moisture estimation, including in situ methods such as gravimetric and permittivity probes (Babaeian et al. 2019). Although these methods are highly accurate, they may not reflect the soil moisture conditions in larger surrounding areas. Orbital and airborne platforms offer the advantage of global or regional coverage, respectively, but they have large footprints and low spatial resolution, with approximately 100 m for active sensors (radars) and 10 km for passive sensors (radiometers) (Vey et al. 2016; Edokossi et al. 2020; Zhang et al. 2018). Additionally, satellite imaging has limited temporal resolution, which is related to the revisit period and may be several days. These factors make satellite sensors less suitable for applications that require high spatial and temporal resolution of soil moisture (Zhang et al. 2018).

Global Navigation Satellite Systems Interferometric Reflectometry (GNSS-IR) has recently gained attention as a promising method for soil moisture remote sensing (Larson et al. 2008a; Larson et al. 2010; Larson et al. 2008b; Rodriguez-Alvarez et al. 2009; Arroyo et al. 2014; Tabibi et al. 2015; Roussel et al. 2016; Yang et al. 2017; Martín et al. 2020; Han et al. 2020). GNSS-R allows for remote or proximal sensing depending on the sensing platform, by exploiting GNSS L-band radio (1 to 2 GHz) transmissions (Teunissen and Montenbruck 2017; Jia and Pei 2018). After reflection

off the ground surface, these radio waves reach the GNSS antenna with modified characteristics, such as propagation time delay, amplitude, phase shift, and frequency (Roussel et al. 2016). The multipath reception of direct and reflected signals enables remote sensing through the resulting interference pattern (Leick 1995; Euriques et al. 2021).

Geodetic GNSS-IR offers several unique advantages for soil moisture sensing, including: an intermediate footprint, approximately 50 meters in radius for a 2-m tall GNSS antenna (Tabibi et al. 2017); cost-effective exploitation of the existing GNSS infrastructure, constellations with hundreds of satellites and networks of thousands of tracking stations; short satellite revisit time; global coverage; and all-weather operation (Edokossi et al. 2020; Teunissen and Montenbruck 2017; Seeber 2003; Larson and Nievinski 2013). However, the method also has some limitations, such as the dependency of calibration coefficients on the antenna model and soil type, the confounding effects of vegetation and surface roughness, and its shallow sensitivity, limited to the top few centimeters of depth (Chew et al. 2014; Larson et al. 2010; Euriques et al. 2021).

Cosmic-ray soil moisture probes are another field-wide non-contact soil moisture estimation technique that spans hundreds of meters in footprint (Evans et al. 2016; Bogena et al. 2015). This technique leverages cosmic radiation from extraterrestrial sources. When fast neutrons reach and interact with the atmosphere, they create a cascade of high-energy neutrons. The return energy flow is inversely proportional to the soil moisture content (Desilets et al. 2010; Andres et al. 2013). The Cosmic-ray Soil Moisture Observing System (COSMOS) implements this methodology for soil moisture estimation (Zreda et al. 2012). However, this technique influenced by sources of hydrogen in the environment, such as litter and biomass in humid climates (Desilets et al. 2010; Zreda et al. 2012; Evans et al. 2016; Upadhyaya et al. 2021).

In this study, we evaluated the performance of GNSS-IR for soil moisture estimation at a GNSS station in Southeastern of Brazil. Our approach consisted of a reflectometric algorithm, composed of a physical forward model and a statistical inverse model, as applied to signal-to-noise ratio (SNR) observations. We assessed the performance of soil moisture retrievals over six different combinations of satellite constellation (GPS and GLONASS), carrier frequencies (L1 and L2), and modulations (civil and military). We also conducted a comparison to cosmic-ray neutron probes over a 16-month (1.3-year-long) campaign, making this the first inter-comparison

between those two field-wide non-contact soil moisture-sensing techniques, thus, validation and comparison between those two techniques are more compatible.

2 METHODOLOGY

2.1 GNSS-IR SOIL MOISTURE ESTIMATION

In this section, we provide a review of the GNSS-IR field measurements, the reflectometric algorithm, and the post-processing used in our study.

2.1.1 GNSS field measurements

A Trimble NetR8 receiver with a choke-ring antenna (TRM29659.00) was installed at the Brazilian Center for Weather Forecasting and Climate Studies (CPTEC), National Institute for Space Research (INPE) located in the city of Cachoeira Paulista, São Paulo, Brazil (Fig. 1 (a) and (b)). The study area has flat topography, uniform grassy vegetation, and an unobstructed visibility from the antenna to the main area (Fresnel zones – Fig. 1 (c)).

The GNSS data were collected from GPS and GLONASS constellations, and L1 and L2 carrier frequencies with a 1 Hz sampling rate. The data were recorded for 16 months (1.3 years), from June 2014 to October 2015, which covered all seasons and provided a comprehensive view of soil moisture dynamics. The use of two constellations improved the azimuthal coverage in the region of interest, due to the higher number of satellites (about 60) and the higher orbit altitude and larger inclination of GLONASS satellites.

FIGURE 1: LOCATION OF THE SITE INSTALLATION ON A REGIONAL SCALE (A) AND CACHOEIRA PAULISTA CITY SCALE (B). GNSS-R FOOTPRINT DEFINED BY FRESNEL ZONES (C).

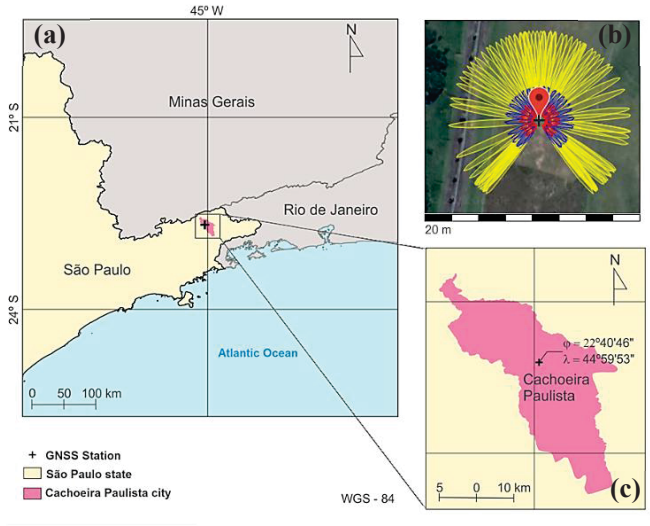

SOURCE: The authors. Credit of background image: Google Earth. Credit of Fresnel zones mapping (c): https://gnss-reflections.org/rzones.

Determination of soil moisture series by GNSS-R was performed using six series of SNR: GS1C (L1-C/A) and GS2X (L2C) for GPS, and RS1C (L1-C/A), RS1P (L1-P), RS2P (L2-P), for GLONASS. The signal nomenclature used follows the RINEX version 3.0 specification (Gurtner and Estey 2015). A multi-GNSS solution (MGNSS) is also generated by combining the five solutions listed above.

Note that there are two periods where no GNSS data is available: December 2014 due to a power failure, and February to March 2015 due to an accidental event. The GNSS antenna was replaced during the latter period, resulting in a slight change of a few centimeters in the antenna height. We have applied a visibility mask restricting satellites to elevation angles from 5 degrees to 30 degrees.

2.1.2 GNSS Reflectometry Algorithm

The algorithm employed for modeling SNR was originally developed for snow depth sensing (Nievinski and Larson 2013; Nievinski and Larson 2014a; Nievinski and Larson 2014b; Nievinski and Larson 2014c) and later adapted for sea level (Geremia-Nievinski et al. 2020; Tabibi et al. 2020) and soil moisture sensing (Tabibi et al. 2015). It was extended to multiple GNSS solutions in Tabibi et al. 2017. The determination of soil moisture using GNSS-IR involves a reflectometry algorithm based on the

combination of a forward physical model, which simulates the theoretical multipath, and a statistical inverse model, that uses GNSS SNR field data to estimate the unknown reflection parameters.

For a flat and horizontal surface, the reflection-minus-direct or interferometric propagation delay (in meters, assuming vacuum speed of light) equals simply $D_i = 2H \sin e$, where e is the satellite elevation angle and H is the antenna height above the surface (Euriques et al. 2021; Zavorotny et al. 2010). The interferometric phase equals $\phi_i = kD_i + \phi_X$, where $k = 2\pi/\lambda$ is the wavenumber and ϕ_X is a non-geometric phase function, based on surface composition, including electrical permittivity and the antenna design, including gain at each polarization (Euriques et al. 2021; Zavorotny et al. 2010). Theoretical SNR can then be expressed as:

$$S = P_n^{-1}(P_d + P_r + 2P_d^{0.5}P_r^{0.5}\cos\phi_i) \quad (1)$$

It is normalized by the noise power P_n and proportional to the sum of direct power P_d, reflection power P_r, all smooth functions of elevation angle, and their coherent superposition, modulated by interferometric phase. The total SNR can be decomposed in two terms $S = \bar{S} + s$:

$$\bar{S} = P_n^{-1}(P_d + P_r) \quad (2a)$$

$$s = 2P_n^{-1}P_d^{0.5}P_r^{0.5}\cos\phi_i = A\cos(Hk_z + \phi_X) \quad (2b)$$

where $\bar{S}$ and s are the SNR trend and detrended oscillation, respectively.

An empirical model $S_m = \bar{S}_m + s_m$ can be fit to the theoretical model above, $S_m \approx S$:

$$\bar{S}_m = c_0 + c_1k_z + c_2k_z^2 + \cdots \approx \bar{S} \quad (3a)$$

$$s_m = A_m\cos(H_mk_z + \varphi_m) \approx s \quad (3b)$$

The formulas are expressed in term of the vertical wavenumber $k_z = 2k\sin e$ (Euriques et al. 2021). The polynomial sum of coefficients, $\sum c_i k_z^i$, approximates the trend, $\bar{S}$, while the sinusoid term, $A_m\cos(\phi_m)$, approximates the oscillation, s. An amplitude

dampening is allowed through $A_m = \sum a_i k_z^i \approx A$. The empirical phase function approximating interferometric phase $\phi_m \approx \phi_i$ is defined in terms of the expectation of linear and constant coefficients:

$$H_m = \mathrm{E}\{\partial\phi_i/\partial k_z\} = H + \mathrm{E}\{\partial\phi_X/\partial k_z\} = H + \delta H \tag{4a}$$

$$\varphi_m = \mathrm{E}\{\phi_i - k_z H_m\} = \mathrm{E}\{\phi_X - k_z \delta H\} \tag{4b}$$

In practice, we measure the interferometric phase only indirectly through SNR, so the fitting is performed by means of polynomial detrending followed by spectral analysis.

Empirical height $H_m = H + \delta H$ is the most useful parameter for altimetry applications, such as water level and snow depth sensing. It equals the sum of geometric height H and the regression slope of the non-geometric interferometric phase ϕ_X over sine of elevation angle (Euriques et al. 2021). The (scalar) phase shift, φ_m, is most useful for soil moisture estimation (Chew et al. 2014); it corresponds to the regression intercept of ϕ_X on k_z.

We perform the empirical fitting above twice: once for SNR field measurements, S_f; and another time for synthetic SNR, S_0, which is simulated based only on *a priori* information about the antenna type and height as well as the surface type and composition (nominal soil moisture conditions). The discrepancy between corresponding parameters yields first guesses for a number of empirical biases:

$$\varphi_B \approx \varphi_{m0} - \varphi_{mf} \tag{5a}$$

$$H_B \approx H_{m0} - H_{mf} \tag{5b}$$

$$A_B \approx A_{m0}/A_{mf} \tag{5c}$$

$$K_B \approx c_{00}/c_{0f} \tag{5d}$$

Finally, we augment the theoretical model (Eq.1) with the above set of biases (5):

$$S_a = \bar{S}_0 K_B + A_0 A_B \cos(\phi_{i0} + k_z H_B + \varphi_B) \quad (6)$$

The first guesses values obtained by Eq. (5) are refined iteratively by means of a least-squares adjustment of the augmented model S_a (Eq. 6) to the SNR field measurements S_f: $[\varphi_B, H_B, A_B, K_B] = \mathrm{argmin}\left(S_a - S_f\right)^2$

Such a statistical inverse model still employs internally a physical forward model to simulate SNR data (Nievinski and Larson 2013; Nievinski and Larson 2014a). Hence, the algorithm allows isolating the influence of known instrumental effects and unknown environmental characteristics on the resulting parameters (Nievinski and Larson 2014b; Nievinski and Larson 2014c). SNR inversion is performed independently for each individual satellite track or arc, between the pre-defined elevation and azimuth masks.

2.1.3 Post-Processing: Parameter Refinement

With SNR inversion, we obtain tens of GNSS-IR phase shift and antenna height biases per day at irregular intervals corresponding to the satellite rising and setting times. To obtain a regularly spaced time series, several post-processing steps are necessary (Tabibi et al. 2017). First, track clustering is performed to compare results across subsequent days based on the repeatability of GNSS satellite azimuth. Secondly, quality control is carried out to detect outliers in each track cluster using a standard three-sigma rule. After this, the independent satellite estimates are combined into a site-wide average over time, using a moving average, typically with a window duration of one day and an advancing step of 6 hours

For soil moisture estimation, a special procedure is applied during post-processing to account for the correlation between phase shift and antenna height biases. Soil moisture affects the penetration depth of electromagnetic waves into the soil, causing variations in the effective antenna height (Larson 2016). To improve the precision of phase shift estimates, a median height bias is defined as a constant for each track cluster and introduced as a constraint to decorrelate the two biases. A

similar procedure was applied in Tabibi et al., (2020) for sea level sensing, but in that case the phase shift was constrained to yield more precise height estimates. In our study, the processing was divided into two periods, before and after the antenna setup change, with each period having a piecewise constant effective height.

Finally, the phase shift φ_B series obtained from post-processing is converted into soil moisture SM_V through a polynomial calibration curve:

$$SM_V = a\,\varphi_B + b \tag{7}$$

where the slope, $a = 0.0148\ (\mathrm{m}^3/\mathrm{m}^3)/°$, is determined from physical simulations; it is often reported in the literature in reciprocal form as $a^{-1} = 65\,°/(\mathrm{m}^3\mathrm{m}^{-3})$(Chew et al. 2016). The intercept, $b = 0.05\ \mathrm{m}^3/\mathrm{m}^3$ is associated to the residual soil moisture for each soil type (Vey et al. 2016).

2.2 Cosmic-neutral soil moisture datasets

To validate the GNSS-R results, a cosmic-ray neutron probe (model CRS-1000/B from Hydroinnova) is used. This probe is available in the study area and it is located approximately 15 m from the GNSS-IR station (Fig. 2). Additionally, we also evaluated the response of both methods to precipitation events using rain gauge data.

The cosmic probe used in this study is part of the COSMOS network and provides measurements of soil moisture content at a variable nominal depth, ranging from approximately 15 cm in wet soils to 70 cm in dry soils (Babaeian et al. 2019). The data are transmitted through the Iridium satellite constellation to a data center in Arizona, wich is responsible for data processing, quality control, and dissemination of results (Zreda et al. 2012). The data can be accessed directly on the COSMOS website (http://cosmos.hwr.arizona.edu). To account for the variability of the data, we defined the COSMOS probe time series using a moving average with a window duration of one day, as done for GNSS-IR. To ensure a more consistent comparison, we rescaled the GNSS-IR series to match the depth of COSMOS data.

FIGURE.2: ARRANGEMENT OF THE EQUIPMENT USED IN THE STUDY AREA. THE FOOTPRINT OF EACH TECHNIQUE IS HIGHLIGHTED IN CIRCLES, APPROXIMATELY 50 M FOR GNSS-IR AND 350 M FOR THE COSMOS PROBE.

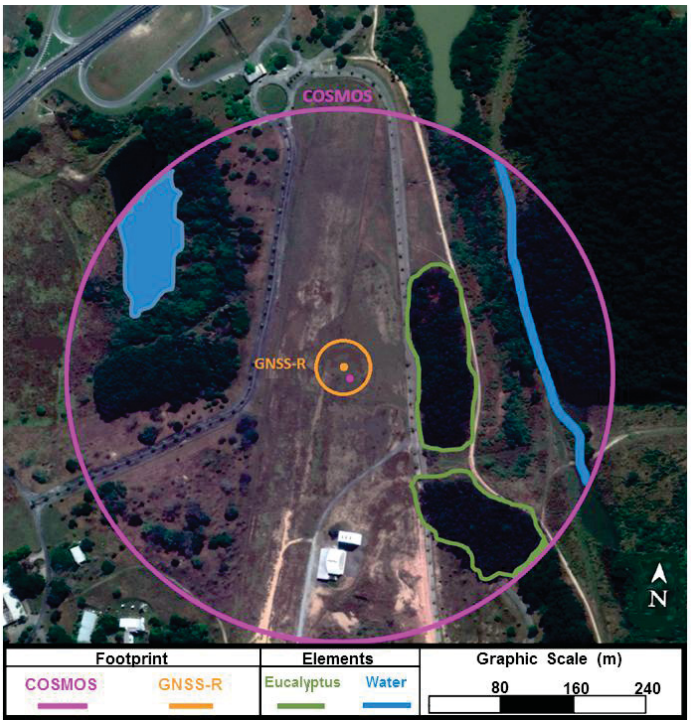

SOURCE: The authors. Credit of background image: Google Earth.

It is important to note that the standard deviation of soil water content determined by a cosmic-ray probe is highly dependent on the temporal resolution of the data and several other factors, including soil moisture itself and site-specific conditions, accounted for in the probe calibration. Previous studies have shown that the mean of absolute differences between the cosmic-ray neutron probe and the gravimetric method is typically less than 0.01 m^3/m^3 (Zreda et al. 2012). In a worst-case scenario evaluation in a humid forest, the accuracy was found to be 0.03 m^3/m^3 for 24-h averages, even in the case of an exceptionally high soil moisture of 0.70 m^3/m^3 (Bogena et al. 2013).

3 RESULTS AND DISCUSSION

We compared and evaluated six soil moisture GNSS-IR series with the COSMOS probe data and to rain events for validation. Fig. 3 shows the best GNSS-IR series and COSMOS series (top panel) as well as daily rainfall (bottom panel). It is evident that there is a sudden increase in soil moisture after precipitation events, which

is clearly visible in both soil moisture series. Subsequently, soil moisture decreases over time, until the next precipitation event.

During dry periods (such as winter in South Hemisphere), the two soil moisture series correspond well, while differences between the methods become more pronounced during the rainy season (summer). The timing of soil moisture peaks is nearly simultaneous due to rainfall, with small differences due to the different nominal depth of the two methods. The largest differences between the series occur during the soil moisture peaks, which may have been over-smoothed in moving average procedure.

FIGURE. 3 GNSS-R (RS2P) (BLACK) AND COSMOS PROBE (MAGENTA) SOIL MOISTURE SERIES (TOP PANEL) AND RAINFALL EVENTS (BOTTOM PANEL). THE BOTTOM PANEL SHOWS THE RAINFALL PRECIPITATION EVENTS (MM/H) STORED BY A RAIN GAUGE.

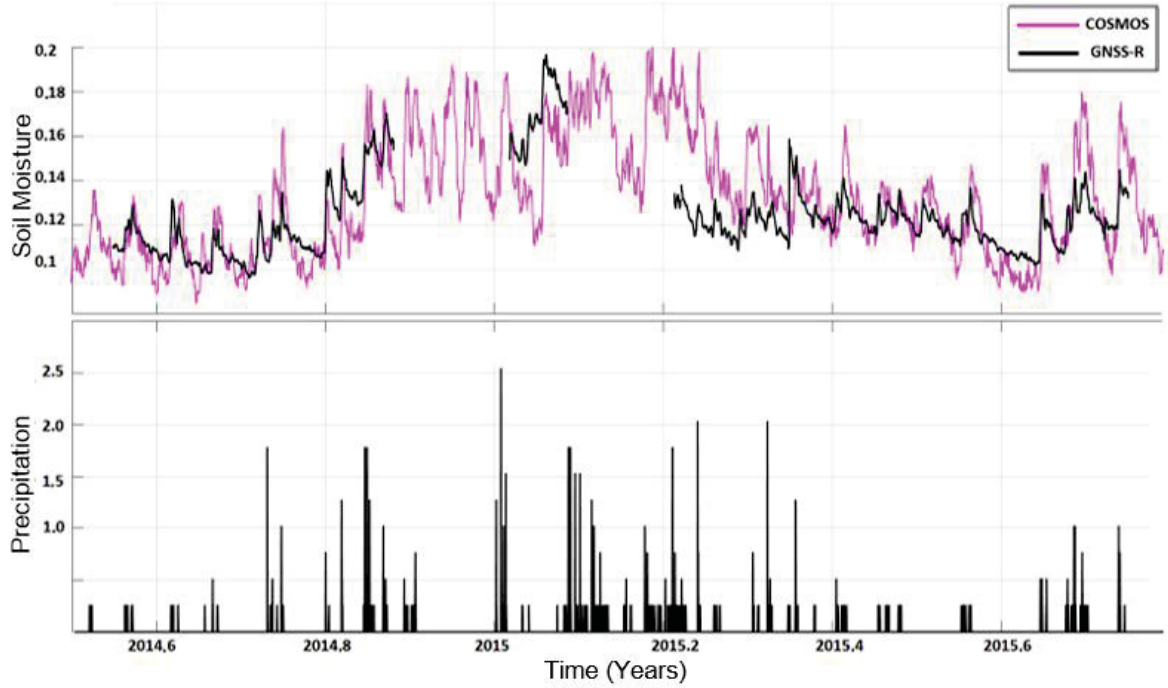

SOURCE: The authors

TABLE 1 shows a more detailed comparison of COSMOS to each of the GNSS-R series. The correlation values are around 0.7, with a minimum of 0.65 (GS1C) and a maximum of 0.73 (RS2P). The highest values were found for RS2P and GS2X signals, while the lowest correlations were found for the RS1P and GS1C signals, with values of 0.64 and 0.65, respectively. The minimum root mean square error (RMSE) of 0.0157 m^3/m^3 was achieved in the RS2P signal.

TABLE 1 – STATISTICS OF COMPARISON BETWEEN GNSS-R AND COSMOS

GNSS Signal	Correlation coefficients	RMSE (m^3/m^3)
GS1C	0.65	0.0181
GS2X	0.72	0.0160
RS1C	0.69	0.0171
RS1P	0.64	0.0178
RS2P	0.73	0.0157
MGNSS	0.68	0.0167

SOURCE: The authors.

The best GNSS-IR soil moisture series, RS2P, is used for further evaluations. FIGURE 4 presents a scatterplot between the GNSS-IR and COSMOS soil moisture series, which reveals an increase in variance (heteroscedasticity) between the methods under higher soil moisture conditions.

FIGURE 4 SCATTERPLOT OF GNSS-IR (RS2P) VERSUS COSMOS PROBE (BOTH IN M^3/M^3) SOIL MOISTURE SERIES. THE ONE-TO-ONE LINE DIAGONAL IS SHOWN AS A RED LINE

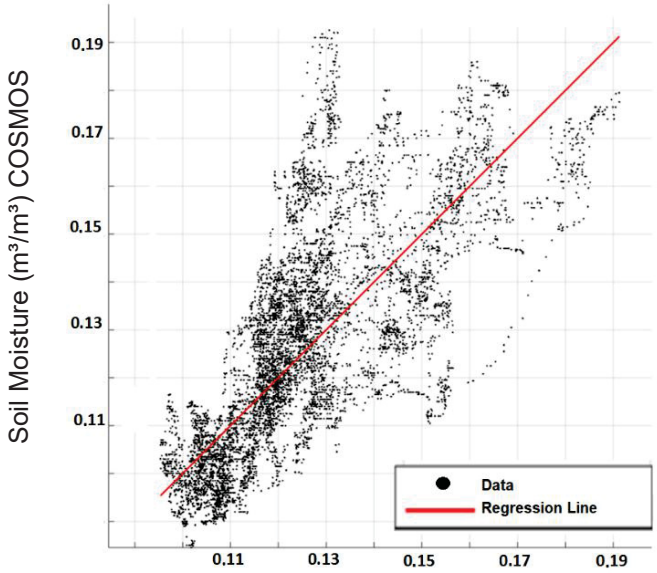

SOURCE: The authors.

FIGURE 5 shows the discrepancies between the GNSS-IR and COSMOS time series as a function of soil moisture. the red line represents a moving average (not to be confused with the previous 24-h temporal moving average). these discrepancies are predominantly within ± 0.02 m^3/m^3 and increase with soil moisture, especially above ~ 0.12 m^3/m^3. this was verified in all combination analyses.

FIGURE 5 SHOWS THE DISCREPANCIES BETWEEN THE GNSS-IR AND COSMOS TIME SERIES

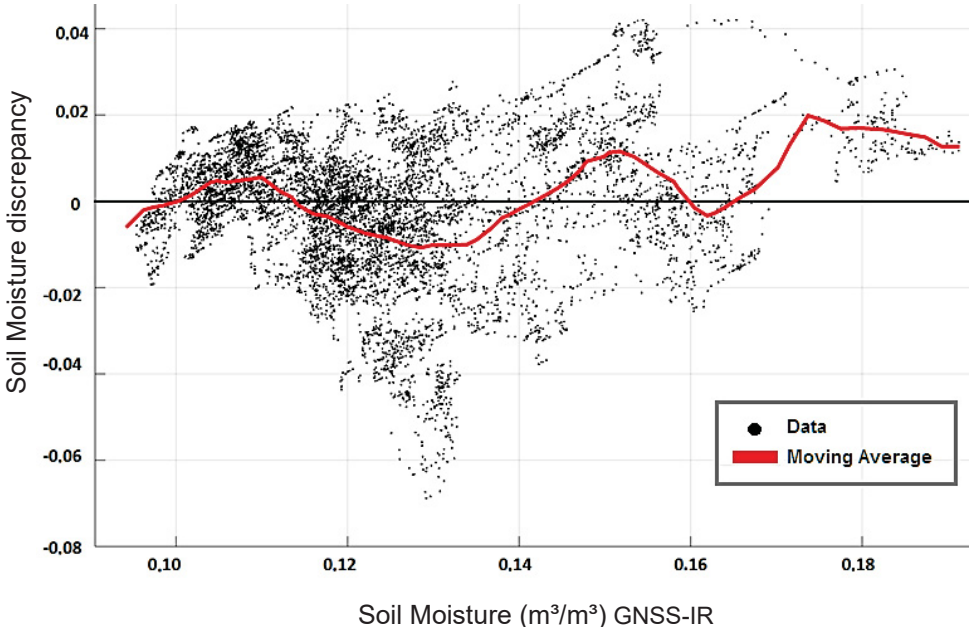

SOURCE: The authors.

The GNSS-IR and COSMOS soil moisture series show good agreement, which may be attributed to their large sensing footprints despite the lack of spatial coincidence. The main exception is the period from 2015.2 to 2015.3, which is believed to have resulted from the saturation of water around the probe due to a prolonged period of uninterrupted rain. Cosmic-ray neutron probes are sensitive to these hydrogen sources (Bogena et al. 2013; Evans et al. 2016). Furthermore, the near-surface or shallow depth sensed by GNSS-R is more susceptible to variations and moisture losses due to factors such as infiltration and evapotranspiration.

Improved results provided by L2/R2 frequencies in both GPS and GLONASS could be a result of their different penetration depths. The L1 frequency has a wavelength of 19 cm, resulting in a shallower penetration depth compared to the L2 (≈24 cm). Shallow soil regions tend to be more variable, whereas deeper regions tend to be more stable.

4 CONCLUSIONS

We evaluated the performance of GNSS-IR in determining soil moisture using data collected over a 16-month period (1.3 years). Six soil moisture time series were generated using L1/R1 and L2/R2 carrier frequencies from both U.S. GPS and Russian GLONASS. The GNSS-R soil moisture series was validated using the cosmic-ray neutron probe from the COSMOS network.

The results showed that all the GNSS-IR soil moisture series performed similarly, with the best correlations with COSMOS obtained from the R2/L2 carrier frequency (RS2P and GS2X). The worst correlation was related to the L1/R1 carrier frequency (RS1P and GS1C).

Although the multi-GNSS solution (MGNSS) did not provide the best results, it is still important for GNSS-IR purposes due to the potential reduction in uncertainties, improvement in azimuthal coverage, and avoidance of gaps in the time series.

It should be noted the correlation between GNSS-IR and COSMOS results was impacted by differences in the footprints and nominal depths of each method. These differences naturally result in discrepancies between soil moisture estimates, as they vary horizontally and vertically. Despite these differences, the methods still responded simultaneously to variations in soil moisture at precipitation events. These results demonstrate that GNSS-IR has the potential to be a valuable alternative or complementary method for soil moisture monitoring.

It should be emphasized that GNSS-IR can leverage existing geodetic continuously operating reference stations and their historical data series. However, it is crucial to consider the location and surrounding characteristics of the GNSS stations (Geremia-Nievinski and Hobiger 2019), such as ensuring unobstructed visibility to the ground and sky in the azimuths of interest. Additionally, land cover and vegetation effects must be considered in some environments, as they can affect the GNSS-IR reflections.

REFERENCES

ARROYO A A, CAMPS A, AGUASCA A, FORTE GF, MONERRIS A, RÜDIGER C, WALKER JP, PARK H, PASCUAL D, ONRUBIA R (2014) Dual-polarization GNSS-R

interference pattern technique for soil moisture mapping. **IEEE J Sel Top Appl Earth Obs Remote Sens** 7(5):1533–1544. https://doi.org/10.1109/JSTARS.2014.2320792

BABAEIAN E, SADEGHI M, JONES SB, MONTZKA C, VEREECKEN H, TULLER M (2019) Ground, Proximal, and Satellite Remote Sensing of Soil Moisture. **Rev.Geophys**.57:530616. https://doi.org/10.1029/201808

BOGENA HR, HUISMAN JA, GÜNTNER A, HÜBNER C, KUSCHE J, JONARD F, VEY S, VEREECKEN H (2015) Emerging methods for noninvasive sensing of soil moisture dynamics from field to catchment scale: a review. **WIREs Water** 2(6):635–647. https://doi.org/10.1002/wat2.1097

CHEW CC, SMALL EE, LARSON KM, ZAVOROTNY VU (2014) Effects of near-surface soil moisture on GPS SNR data: Development of a retrieval algorithm for soil moisture. **IEEE Trans Geosci Remote Sens** 52(1):537–543. https://doi.org/10.1109/TGRS.2013.2242332

DESILETS D, ZREDA M, FERRÉ TPA (2010) Nature's neutron probe: Land surface hydrology at an elusive scale with cosmic rays. 46 (W11505):1–7. https://doi.org/10.1029/2009WR008726

EDOKOSSI K, CALABIA A, JIN S, MOLINA I (2020) GNSS-reflectometry and remote sensing of soil moisture: A review of measurement techniques, methods, and applications. **Remote Sens** 12(4). https://doi.org/10.3390/rs12040614

ENTEKHABI D, NJOKU EG, O'NEILL PE, KELLOGG KH, CROW WT, EDELSTEIN WN, ENTIN JK, GOODMAN SD, JACKSON TJ, JOHNSON J, KIMBALL J, PIEPMEIER JR, KOSTER RD, MARTIN N, MCDONALD KC, MOGHADDAM M, MORAN S, REICHLE R, SHI JC, SPENCER MW, THURMAN SW, TSANG L, VAN ZYL J (2010) The soil moisture active passive (SMAP) mission. **Proc IEEE** 98(5):704–716. https://doi.org/10.1109/JPROC.2010.2043918

EURIQUES JF, KRUEGER CP, MACHADO WC, SAPUCCI LF, GEREMIA-NIEVINSKI F (2021) Soil Moisture Estimation with GNSS Reflectometry: A Conceptual Review. **Rev Bras Cartogr** 73(2):413–434. https://doi.org/10.14393/rbcv73n2-55033

EVANS JG, WARD HC, BLAKE JR, HEWITT EJ, MORRISON R, FRY M, BALL LA, DOUGHTY LC, LIBRE JW, HITT OE, RYLETT D, ELLIS RJ, WARWICK AC, BROOKS M, PARKES MA, WRIGHT GMH, SINGER AC, BOORMAN DB, JENKINS A (2016) Soil water content in southern England derived from a cosmic-ray soil moisture observing system – COSMOS-UK. **Hydrol Process** 30(26):4987–4999. https://doi.org/10.1002/hyp.10929

GEREMIA-NIEVINSKI F, HAAS THR, STRANDBERG WLJ, VEY STS (2020) SNR - based GNSS reflectometry for coastal sea - level altimetry : results from the first IAG inter - comparison campaign. **J Geod** 74(70). https://doi.org/10.1007/s00190-020-01387-3

GURTNER W, ESTEY L (2015) RINEX The Receiver Independent Exchange Format Version 3.03

HAN M, ZHU Y, YANG D, CHANG Q, HONG X, SONG S (2020) Soil moisture monitoring using GNSS interference signal: proposing a signal reconstruction method. **Remote Sens Lett** 11(4):373–382. https://doi.org/10.1080/2150704X.2020.1718235

HILLEL D (1998) **Environmental Soil Physics**, 1st ed. Academic Press, San Diego

JIA Y, PEI Y (2018) Remote Sensing in Land Applications by Using GNSS-Reflectometry. In: **Recent Advances and Applications in Remote Sensing**. InTech, pp 65–88

LARSON KM, BRAUN JJ, SMALL EE, ZAVOROTNY VU, GUTMANN ED, BILICH AL (2010) GPS Multipath and Its Relation to Near-Surface Soil Moisture Content. **IEEE J Sel Top Appl Earth Obs Remote Sens** 3(1):91–99. https://doi.org/10.1109/JSTARS.2009.2033612

LARSON KM, NIEVINSKI FG (2013) GPS snow sensing: Results from the EarthScope Plate Boundary Observatory. **GPS Solut** 17(1):41–52. https://doi.org/10.1007/s10291-012-0259-7

LARSON KM, SMALL EE, GUTMANN E, BILICH A, AXELRAD P, BRAUN J (2008a) Using GPS multipath to measure soil moisture fluctuations: Initial results. **GPS Solut** 12(3):173–177. https://doi.org/10.1007/s10291-007-0076-6

LARSON KM, SMALL EE, GUTMANN ED, BILICH AL, BRAUN JJ, ZAVOROTNY VU (2008b) Use of GPS receivers as a soil moisture network for water cycle studies. **Geophys Res Lett** 35(24). https://doi.org/10.1029/2008GL036013

LEICK A (1995) **GPS Satellite Surveying,** 2nd. John Wiley & Sons, New York

MARTÍN A, IBÁÑEZ S, BAIXAULI C, BLANC S, ANQUELA AB (2020) Multi-constellation GNSS interferometric reflectometry with mass-market sensors as a solution for soil moisture monitoring. **Hydrol Earth Syst Sci** 24(7):3573–3582. https://doi.org/10.5194/hess-24-3573-2020

NIEVINSKI FG, LARSON KM (2013) Forward modeling of GPS multipath for near-surface reflectometry and positioning applications. **GPS Solut** 18(2):309–322. https://doi.org/10.1007/s10291-013-0331-y

NIEVINSKI FG, LARSON KM (2014a) An open source GPS multipath simulator in Matlab/Octave.**GPSSolut**18(3):473–481. https://doi.org/http://dx.doi.org/10.1109/tgrs.2013.2297688

Nievinski FG, Larson KM (2014b) Inverse modeling of GPS multipath for snow depth estimation - Part I: Formulation and simulations. **IEEE Trans Geosci Remote Sens** 52(10):6555–6563. https://doi.org/10.1109/TGRS.2013.2297681

NIEVINSKI FG, LARSON KM (2014c) Inverse modeling of GPS multipath for snow depth estimation - Part II: Application and validation. **IEEE Trans Geosci Remote Sens** 52(10):6564–6573. https://doi.org/10.1109/TGRS.2013.2297688

OCHSNER TE, COSH MH, CUENCA RH, DORIGO WA, DRAPER CS, HAGIMOTO Y, KERR YH, NJOKU EG, SMALL EE, ZREDA M (2013) State of the Art in Large-Scale Soil Moisture Monitoring. **Soil Sci Soc Am J** 77(6):1888–1923. https://doi.org/10.2136/sssaj2013.03.0093

RIVERA VILLARREYES AC, BARONI G, (2013) Calibration approaches of cosmic-ray neutron sensing for soil moisture measurement in cropped fields. **Hydrol Earth Syst Sci** 10 (July 2014):4237–4274. https://doi.org/10.5194/hessd-10-4237-2013

ROBINSON DA, CAMPBELL CS, HOPMANS JW, HORNBUCKLE BK, JONES SB, KNIGHT R, OGDEN F, SELKER J, WENDROTH O (2008) Soil Moisture Measurement for Ecological and Hydrological Watershed-Scale Observatories: A Review. **Vadose Zo** J 7(1):358–389. https://doi.org/10.2136/vzj2007.0143

RODRIGUEZ-ALVAREZ N, BOSCH-LLUIS X, CAMPS A, VALL-LLOSSERA M, VALENCIA E, MARCHAN-HERNANDEZ JF, RAMOS-PEREZ I (2009) Soil moisture retrieval using GNSS-R techniques: Experimental results over a bare soil field. **IEEE Trans Geosci Remote Sens** 47(11):3616–3624. https://doi.org/10.1109/TGRS.2009.2030672

ROUSSEL N, FRAPPART F, RAMILLIEN G, DARROZES J, BAUP F, LESTARQUIT L, HA MC (2016) Detection of Soil Moisture Variations Using GPS and GLONASS SNR Data for Elevation Angles Ranging from 2° to 70°. **IEEE J Sel Top Appl Earth Obs Remote Sens** 9(10):4781–4794. https://doi.org/10.1109/JSTARS.2016.2537847

SEEBER G (2003) **Satellite Geodesy: Foundations, Methods, and Applications**, 2nd. New York

SENEVIRATNE SI, CORTI T, DAVIN EL, HIRSCHI M, JAEGER EB, LEHNER I, ORLOWSKY B, TEULING AJ (2010) Investigating soil moisture-climate interactions in a changing climate: A review. **Earth-Science Rev** 99(3–4):125–161. https://doi.org/10.1016/j.earscirev.2010.02.004

TABIBI S, GEREMIA-NIEVINSKI F, FRANCIS O, DAM T VAN (2020) Remote Sensing of Environment Tidal analysis of GNSS reflectometry applied for coastal sea level sensing in Antarctica and Greenland. **Remote Sens Environ** 248(June):111959. https://doi.org/10.1016/j.rse.2020.111959

TABIBI S, NIEVINSKI FG, VAN DAM T (2017) Statistical Comparison and Combination of GPS, GLONASS, and Multi-GNSS Multipath Reflectometry Applied to Snow Depth Retrieval. **IEEE Trans Geosci Remote Sens** 55(7):3773–3785. https://doi.org/10.1109/TGRS.2017.2679899

TABIBI S, NIEVINSKI FG, VAN DAM T, MONICO JFG (2015) Assessment of modernized GPS L5 SNR for ground-based multipath reflectometry applications. **Adv Sp Res** 55(4):1104–1116. https://doi.org/10.1016/j.asr.2014.11.019

TEUNISSEN PJG, MONTENBRUCK O (2017) **Springer Handbook of Global Navigation Satellite Systems**. Springer International Publishing

TULLER M, OR D (2004) Water Retention and Characteristic Curve. In: **Encyclopedia of Soils in the Environment**. pp 278–289

UPADHYAYA DB, EVANS J, MUDDU S, TOMER SK, BITAR A AL, YEGGINA S, S T, MORRISON R, FRY M, TRIPATHI SN, MUJUMDAR M, GOSWAMI M, GANESHI N, NEMA MK, JAIN SK, ANGADI SS, YENAGI BS (2021) The Indian COSMOS network (ICON): Validating L-band remote sensing and modelled soil moisture data products. **Remote Sens** 13(3):1–25. https://doi.org/10.3390/rs13030537

VEY S, GÜNTNER A, WICKERT J, BLUME T, RAMATSCHI M (2016) Long-term soil moisture dynamics derived from GNSS interferometric reflectometry: a case study for Sutherland, South Africa. **GPS Solut** 20(4):641–654. https://doi.org/10.1007/s10291-015-0474-0

YANG T, WAN W, CHEN X, CHU T, HONG Y (2017) Using BDS SNR observations to measure near-surface soil moisture fluctuations: Results from low vegetated surface. **IEEE Geosci Remote Sens Lett** 14(8):1308–1312. https://doi.org/10.1109/LGRS.2017.2710083

ZHANG S, CALVET JC, DARROZES J, ROUSSEL N, FRAPPART F, BOUHOURS G (2018) Deriving surface soil moisture from reflected GNSS signal observations from a grassland site in southwestern France. **Hydrol Earth Syst Sci** 22(3):1931–1946. https://doi.org/10.5194/hess-22-1931-2018

ZREDA M, SHUTTLEWORTH WJ, ZENG X, ZWECK C, DESILETS D, FRANZ T, ROSOLEM R (2012) COSMOS: The cosmic-ray soil moisture observing system. **Hydrol Earth Syst Sci** 16(11):4079–4099. https://doi.org/10.5194/hess-16-4079-2012.

2.3 CHAPTER 3: PAPER 3 – ARIZONA: NON-DEIAL STATIONS

2.3.1 Soil moisture with GNSS-IR in challenging environments: evaluating processing configurations for improved results

ABSTRACT

The Global Navigation Satellite Systems (GNSS) has been utilized to monitor terrestrial dynamics. Soil moisture is a critical variable within the hydrological cycle, linked to various planetary phenomena. GNSS Interferometric Reflectometry (GNSS-IR) is a geodetic technique that leverages multipath effects, as recorded in the signal-to-noise ratio (SNR), to estimate geophysical variables in the vicinity of the GNSS antenna, including soil moisture. SNR modeling can be performed using a reflectometric algorithm. This study aimed to estimate soil moisture by GNSS-IR around two GNSS stations, Luck Hills and Kendall, in Arizona, USA. These stations are considered non-ideal for GNSS-IR due to surrounding topography, vegetation, and structural interference. Soil moisture time series were generated for these stations through various processing configurations. The resulting series was validated by calculating correlations with soil moisture time series from conventional probes and by comparing them to precipitation events recorded by rain gauges. Specific azimuth masks were established for each station based on the evaluation of reflected signals. The GS2L (GPS L2) and RS2P (GLONASS L2) signals obtained the most favorable results, considering elevation angles between 15 and 30 degrees. Correlation differences of up to 54% were observed between series, influenced by the width of the window moving average. Minimum and maximum correlation coefficients of 0.53 and 0.85 were achieved at the Lucky Hills station, while Kendall station recorded 0.50 and 0.82. These findings suggest that employing specific processing configurations can enhance the accuracy of soil moisture estimates, even in non-ideal stations.

1 INTRODUCTION

Over the past few decades, the Global Navigation Satellite Systems (GNSS) has been employed in numerous other scientific applications beyond PNT, enabling the estimation of parameters associated with phenomena and physical processes of the Earth System. In this context, it is possible to mention ionospheric monitoring and the neutral layers of the atmosphere, which contribute to the observation of the planet. According to Teunissen and Montenbruck (2017), in the former case, these investigations allow for mitigating the influence of ionospheric errors, improving positioning accuracy, as well as exploring the dynamics of ionospheric processes, such as the origin and propagation of ionospheric storms. In the case of neutral layers, investigations enable the estimation of variables used in numerical weather prediction and climate monitoring, including atmospheric water vapor, which is a fundamental component of the hydrological cycle. In this regard, the technique known as GNSS Meteorology has emerged, which can be conducted using data recorded by ground stations (VAQUERO-MARTÍNEZ; ANTÓN, 2021).

Soil moisture is another variable of great relevance in the context of the hydrological cycle and terrestrial dynamics. Due to its relationship with energy fluxes between the Earth's physical surface and the atmosphere, soil moisture must be considered in numerical weather prediction and climate studies. Furthermore, quantifying soil moisture is essential for geotechnical activities, engineering projects, agriculture, delineation of flood areas, and groundwater recharge (ROBINSON et al., 2008; ENTEKHABI et al., 2010; SENEVIRATNE et al., 2010; OCHSNER et al., 2013; BABAEIAN et al., 2019; EDOKOSSI et al., 2020; ZHANG et al. 2021; WU et al., 2021).

GNSS Interferometric Reflectometry (GNSS-IR) is another recent technique in Geodesy that enables geodetic remote sensing and has been employed in the estimation of soil moisture (LARSON et al., 2008a; LARSON et al., 2008b; RODRIGUEZ-ALVAREZ et al., 2009; LARSON et al., 2010; CHEW et al., 2014; ARROYO et al., 2014; TABIBI et al., 2015; ROUSSEL et al., 2016; VEY et al., 2016; YAN et al., 2018; CHANG et al., 2019; EURIQUES, 2019; YANG et al., 2019; ZHANG et al., 2021).

GNSS-IR exploits GNSS multipath signals, that reach the antenna after reflecting off surrounding surfaces. These reflected signals are recorded by the

antenna with a time delay due to the additional path compared to the direct signal. When interacting with the reflecting surfaces, the characteristics of these signals are changed (amplitude, phase, frequency, and polarization) depending on the composition, dielectric properties, and surface roughness. These alterations are also related to the signal's angle of incidence and the GNSS antenna's height relative to the reflecting surface (LARSON; NIEVINSKI, 2013; ROUSSEL et al., 2015; ZAVOROTNY et al., 2014).

Although all GNSS observables are affected by multipath, the signal-to-noise ratio (SNR) is the observable that best reveals this effect and is widely used in GNSS-IR. Besides, the SNR is resilient to common errors affecting other observables, such as orbit, clock synchronization, and a large portion of atmospheric delay (LARSON et al., 2010).

By modeling the SNR recorded in RINEX files, along with a combination of properties of the reflecting surface and characteristics of the GNSS equipment, it becomes possible to estimate geophysical parameters related to the reflection surfaces of these signals, such as soil moisture, vegetation growth, and water levels (JIN et al., 2014).

The main limitations of this methodology are the effects of topography and vegetation on the reflected signals modeling and the inaccuracies of the theoretical coefficients in the calibration curve (EURIQUES et al., 2021; ZHANG et al., 2017; GEREMIA-NIEVINSKI, HOBINGER 2019).

The main advantages of GNSS-IR compared to conventional soil moisture estimation methods are the intermediate coverage area, approximately 50 meters for a 2-meter high antenna, and the use of the well-established GNSS infrastructure, which ensures appropriate continuity and temporal resolution (TABIBI et al., 2017; EURIQUES et al., 2021).

In this context, a research project is currently under development "*The Atmospheric Hydrological Cycle and Deep Convective Activity: Observations from the North American Monsoon GPS Hydrometeorological Network (2017) and follow-on Campaigns*". In this project, hydrological cycle variables are being estimated to investigate soil-atmosphere interactions, such as convective activities, using GNSS data obtained from ground stations located in Arizona, USA. Historical time series from hundreds of active GNSS stations were employed to estimate water vapor. Additionally, two GNSS stations were installed next to Eddy covariance towers from

the United States Department of Agriculture (USDA), soil moisture sensors, and rain gauges. This paper aims to estimate soil moisture by GNSS-IR around two GNSS stations with challenging surrounding characteristics of the abovementioned project.

2 METHODOLOGY

The GNSS data collected by these two stations, named Lucky Hills and Kendall, were used to estimate soil moisture using GNSS-IR. FIGURE 1 shows the location map of these stations situated in the state of Arizona, USA. The Lucky Hills station is indicated in blue, and the Kendall station is shown in red.

FIGURE 1 – VIEW TO THE AZIMUTH 60º FROM LUCKY HILLS STATION – ARIZONA – USA

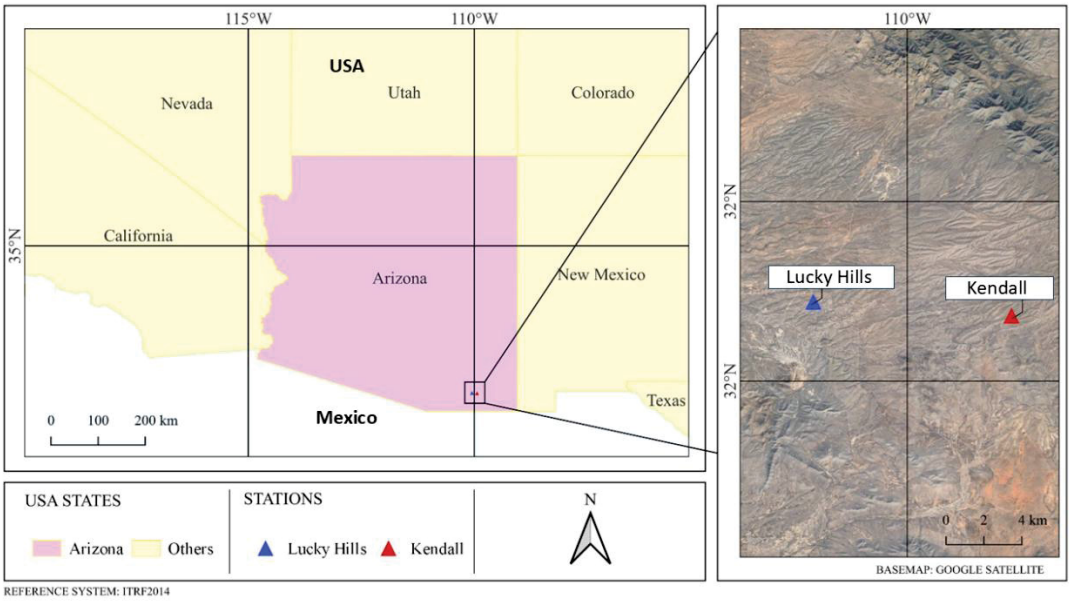

SOURCE: T

The authors (2024).

The Lucky Hills Station is a Septentrio receiver (SEPT POLARX5) and the Trimble Zephyr 2 antenna (TRM59800.00) mounted on a fixed-height pole of 2 meters, at a point with geodetic coordinates latitude 31.74420973 degrees; longitude -110.0522557 degrees; ellipsoidal altitude: 1346.376 meters in the ITRF 2014. These coordinates were determined using the GNSS Precise Point-Processing (PPP) geodetic method. This antenna allowed the recording of the following GNSS signals,

according to RINEX version 3.0 nomenclature, GPS (G): S1C; S1L; S1W; S2L; S2W; S5Q; and GLONASS (R): S1C; S1P; S2C; S2P. The GNSS data recording interval was 1 Hz, and the GNSS tracking campaign lasted from July 1, 2021, to November 8, 2021, covering Day of Year (DoY) 182 to 312, totaling 130 days.

In FIGURE 2, the Lucky Hills station is indicated. The GNSS antenna, located in the center of the image, has a non-ideal surrounding for soil moisture estimation via GNSS-IR due to several factors. The shrubs in the antenna surrounding area affect the roughness of the reflection surface, which impacts the coherence of the reflected signals, and consequently, the results of GNSS-IR. Additionally, on the right side of FIGURE 2, the metal structures such as a container, and other metallic structures like meteorological measurement equipment. Both these structures and the vegetation affect the indirect multipath signals, as they act as obstructions between the direct line of sight from the GNSS antenna to the ground.

FIGURE 2 – VIEW TO THE AZIMUTH 60º FROM LUCKY HILLS STATION

SOURCE: The authors (2021).

The Kendall Station has the same characteristics as the Lucky Hills station in terms of equipment and recorded signals. It has geodetic coordinates of latitude 31.73641974 degrees; longitude -109.9419851 degrees; ellipsoidal altitude of 1501.77 meters in the ITRF 2014. The GNSS campaign lasted from June 30, 2021, to October 27, 2021, covering DoY 181 to 300, totaling 119 days. In FIGURE 3, the Kendall station is indicated. The GNSS antenna, located in the center of the image, has a non-ideal

surrounding for soil moisture estimation, similar to the Lucky Hills station. The vegetation around the antenna, although not as tall as that at Lucky Hills, has a greater volume, which is evident from the reduced area of exposed soil. This characteristic can more significantly hinder the results of GNSS-IR. Additionally, on the right side of FIGURE 3, the presence of metal structures around the station is highlighted, also related to meteorological variable measurement equipment, as well as small trees.

FIGURE 3 – VIEW TO THE AZIMUTH 30º FROM THE KENDALL STATION

SOURCE:The author (2021).

To model the SNR observations, the reflectometric algorithm developed by Nievinski and Larson (2014a, 2014b, 2014c, 2014d) was employed, adapted for soil moisture estimation by Tabibi et al. (2015), and expanded for Multi-GNSS by Tabibi et al. (2017). This algorithm is based on the combination of a direct physical model that simulates the theoretical multipath at the station and an inverse statistical model that uses the SNR observables recorded in the field to estimate the parameters associated with the reflected signals. Additionally, post-processing and quality control steps are applied to improve the results and obtain the metrics of interest.

In the case of soil moisture, the desired metric is the interferometric phase of the signal. These values are converted into soil moisture through a calibration curve. A polynomial is used to establish the relationship between the parameters of the interferometric phase and the soil moisture values (CHEW et al., 2014; VEY et al.,

2016). FIGURE 4 presents the flowchart of the methodology for estimating soil moisture using GNSS-IR.

FIGURE 4 – GRAPHICAL REPRESENTATIONS OF METHODOLOGY STEPS

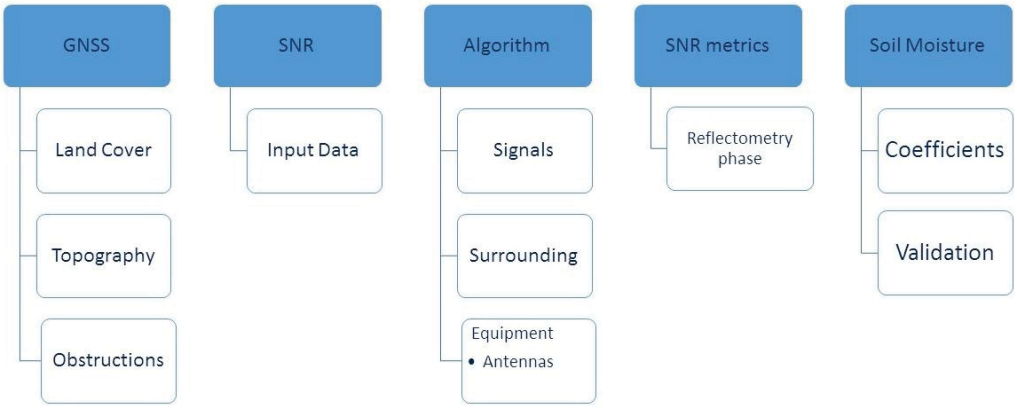

SOURCE: the authors (2024).

This algorithm requires daily Rinex observation files as input data, preferably in version 3, from which the SNR observables can be accessed through various frequency/modulation combinations. It is essential that these files are standardized to facilitate the automation of the processing.

2.1 STANDARDIZATION OF INPUT DATA

The standardization process involved stages of extraction, concatenation, conversion, filtering, and systematic naming of files. To automate this process, a .bash file was generated using the MSYS terminal. Initially, the data were recorded in the native binary format of Septentrio through compressed hourly files.

The first step in the standardization involved decompressing and concatenating these files to obtain daily files in the native Septentrio format. Subsequently, these files were converted to the RINEX format using Septentrio's RxTools software accessed via command-line instructions, thereby eliminating the need for graphical user interface interaction.

Following the conversion, the RINEX files were filtered to retain only the SNR observations, thereby reducing memory usage and optimizing processing efficiency. Finally, the files were renamed according to the standard nomenclature of the software:

statDoY0.yyo, where “stat” represents the station code; “DoY”; “0” indicates that it is a daily file; “yy” indicates the year; and “o” signifies the RINEX observation file.

2.2 EVALUATION OF SNR OSCILLATIONS

The performance of the reflected signals at the stations was assessed through the visible fluctuations in the SNR series. For this purpose, the RTKLIB software, the GNSS-Reflections tool, and the resulting graphs from the inversion stage of the reflectometry algorithm were employed.

The SNR fluctuations were evaluated using RTKPLOT tool from RTKLIB version 2.4.2. The SNR curves for each combination of satellite and signal modulation from the GPS and GLONASS systems were analyzed. Well-defined oscillations occurring near the satellite's rise and set (at low elevation angles) indicate the intact reception of the reflected signals. Thus, it is possible to estimate whether the reflections are affected by obstructions, as this introduces noise into the series and disrupts the pattern of these fluctuations, compromising the results. It was observed that the fluctuations at low elevation angles were not well-defined at either station.

Subsequently, the oscillations were evaluated using the GNSS-Reflections tool http://gnss-reflections.org/. FIGURE 5 presents this evaluation for the Kendall station. In FIGURE 5 (a), quality indicators for the reflections are shown based on the quadrants. It is noted that the southern quadrants exhibit better quality than the northern quadrants. The northwest quadrant shows the poorest results, which can be primarily attributed to the influence of variations in topography and the structures located in that direction, as seen in FIGURE 5 (c). FIGURE 5 (b) presents the ellipses of the Fresnel Zones, representing the reflection areas surrounding the Kendall station. In this case, considering that low elevation angles were found to be inadequate in the previous evaluation, the coverage area was defined with elevation angles ranging from 5° (yellow) to 25° (cyan) in 5° intervals. As the elevation angle increases, the semi-major axis of the ellipse decreases, therefore, the footprint becomes smaller.

FIGURE 5 – VIEW TOWARD THE 30º AZIMUTH OF THE KENDAL STATION

a)

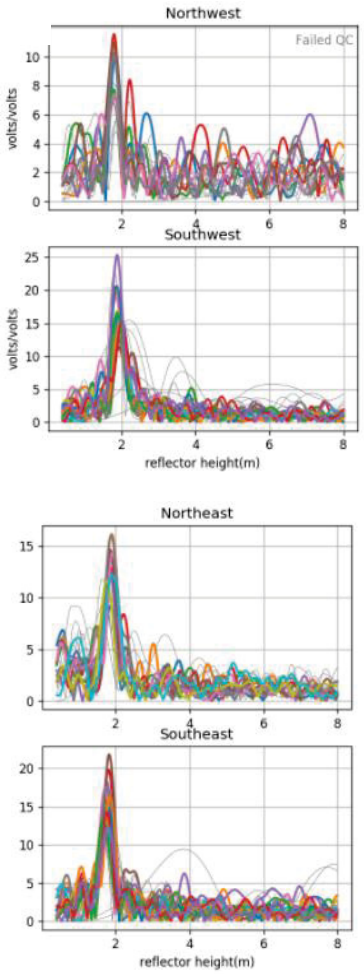

b)

c)

SOURCE: The authors (2024).

Graphs of SNR oscillations are some of the initial results from the reflectometric algorithm. FIGURE 6 presents two examples of these graphs for the Kendall Station. The SNR oscillations simulated by the direct model (red), those obtained from the GNSS field data resulting from the inversion (gray), and the residual between them (blue) are displayed.

In the upper panel, FIGURE 6 (a) shows an example of SNR oscillation from GPS satellite PRN01, with an azimuth of 211 degrees (southwest quadrant) and elevation angles between 5 and 30 degrees. The oscillations are well-defined, with a residual level between -2 and 2 dB. Conversely, FIGURE 6 (b) illustrates an example of inadequate oscillations. The modeled SNR does not exhibit well-defined oscillations and fails to align with the behavior of the simulated SNR. This is expected for directions affected by obstructions.

FIGURE 6 – KENDALL STATION OSCILLATIONS

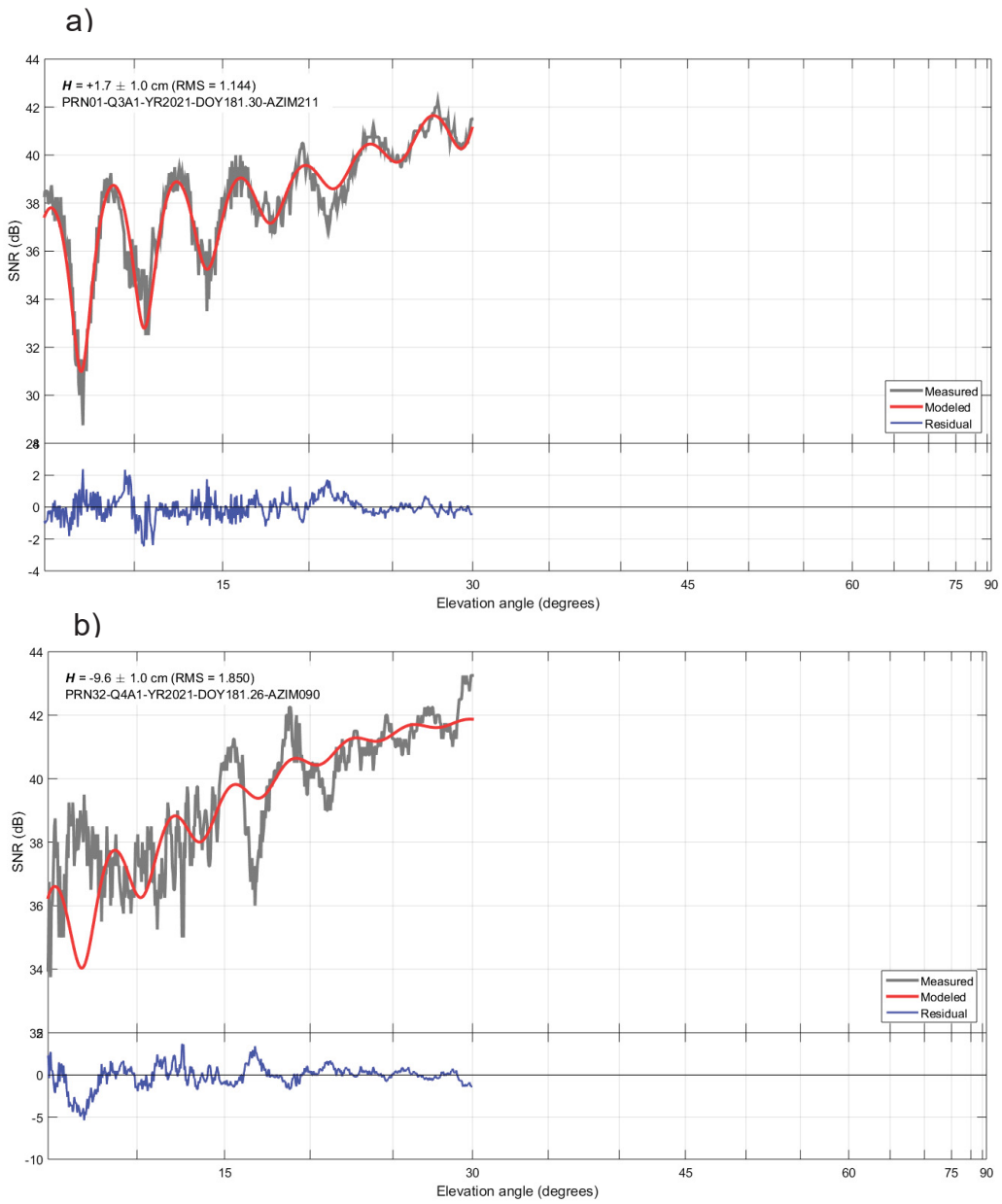

SOURCE: The authors (2024).

As the investigation progressed, it became evident that these graphs exhibited significant variability in oscillations over time, which is expected during periods associated with changes in the surrounding landscape of the stations. In the case of these stations, such changes primarily resulted from the growth of vegetation during the rainy season.

2.3 REFLECTOMETRIC ALGORITHM PROCESSING SETTINGS

Due to the non-ideal surrounding conditions of the stations, influenced by vegetation and irregular topography, numerous configurations and processing strategies were tested to enhance the results. Consequently, the following were evaluated: the GNSS signal, azimuth masks, elevation angle ranges, and configurations for moving averages (spacing and window width).

All available GPS and GLONASS signals were processed in the reflectometry algorithm across L1, L2, and L5 frequencies. Based on the analyses conducted to evaluate oscillations, specific azimuth masks were established for the two stations to exclude SNR arcs from processing where oscillations in certain directions proved unsuitable

After extensive processing, it was determined that an elevation angle mask was also necessary, as low elevation angles (near-horizon) were significantly affected, primarily by surrounding vegetation. The standard elevation angle range for GNSS-IR is generally between 0 and 30 degrees. Consequently, masks were applied incrementally, adjusting the elevation angle range, and the results were evaluated accordingly.

FIGURES 7 (a) and (b) display graphs of antenna height bias as a function of azimuth for the Lucky Hills station. Since the antenna height relative to the reflection surface is highly correlated with phase parameters, accurate height determination influences the reflectometric phase series and, consequently, the precision of soil moisture estimates.

FIGURE 7 (a) illustrates an initial scenario without azimuth masks, considering elevation angles between 0 and 30 degrees. Due to the inclination of the orbital plane of global GPS and GLONASS satellites, Fresnel zones are absent in the northern direction for stations in the Northern Hemisphere. This explains the lack of data in the region between azimuths 330 to 30 degrees, even without applying an azimuth mask.

FIGURE 7 (b) shows the scenario with an elevation mask applied, considering only the range between 15 and 30 degrees, and azimuth masks that retain only the SNR arcs in the quadrant between 180 and 270 degrees of azimuth. It is observed that, with these masks applied, the graph presents bias values that are more consistent with each other, which can be interpreted as yielding more precise results.

FIGURE 7 – ANTENNA HEIGHT BIAS AS A FUNCTION OF AZIMUTH – LUCKY HILLS

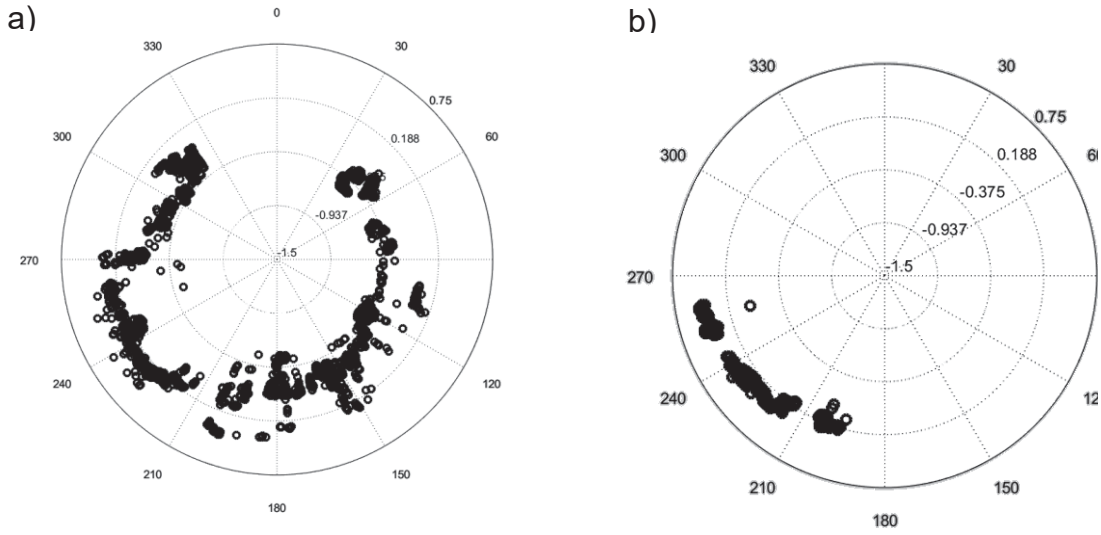

SOURCE: The authors (2024).

A moving average is used in the post-processing of the reflectometric algorithm to smooth short-term fluctuations and highlight trends in the series. Therefore, it is essential to carefully consider these settings, as applying a moving average can remove noise from the series but may also mask information if the smoothing is too aggressive.

The spacing of the moving average specifies the data interval that will comprise the smoothed series. Meanwhile, the width of the moving average window defines how many original data points are used to calculate the average value at a given point in the new series. For example, if the window is set to 24 hours, each point in the smoothed series is based on the data from the previous 24 hours up to the point in question. The smaller the window width, the more detailed the resulting series. This way, a series based on a 2-hour window is more detailed than one using a 24-hour width.

Series with different moving average configurations were created, primarily adjusting the window width while maintaining hourly spacing to preserve moisture peaks associated with precipitation events. Window widths of 2, 3, 4, 6, 8, 12, and 24 hours were tested.

To assess the quality of the results, the soil moisture series obtained through GNSS-IR were validated using different processing strategies and configurations against the soil moisture series recorded by the respective permittivity probes installed near each station. The correlation between these series was calculated. Additionally,

the soil moisture series were evaluated in relation to precipitation events recorded by rain gauges.

3 RESULTS

By calculating the correlation between the series, it was possible to establish a quantitative parameter indicating the best processing strategies, considering the evaluation of the GNSS signal, azimuth and elevation masks, spacing, and the width of the moving average window. The combinations that yielded the best results were obtained with the GS2L and RS2P signals at both stations. Among all the evaluated signals, these two provided the highest correlations between the series obtained from the different GNSS-IR processing strategies and the moisture series recorded by the probes.

The superior performance of the L2 frequency signals compared to the L1 frequency signals was anticipated, as previous studies have indicated this behavior (TABIBI et al, 2015). Regarding the L5 signals, only 12 GPS satellites transmitted this frequency in 2021. Therefore, when applying the filters, this resulted in a low amount of data, limiting the results.

Specific azimuth masks were defined for each station based on the evaluation of the oscillations, and the elevation angles were restricted to the range between 15 and 30 degrees. The following are considerations regarding the best results obtained.

3.1 LUCKY HILLS STATION

TABLE 1 shows the correlation between the soil moisture series obtained from the permittivity probe and the GNSS-IR series using the GS2L signal as a function of different moving average window widths in Lucky Hills station. The highest correlation occurred in the series with a moving average window width of 24 hours, with a correlation of 0.85. The lowest correlation was found in the series with a 2-hour window width, which a correlation 0.58.

TABLE 1 – CORRELATION BETWEEN SOIL MOISTURE ESTIMATED THROUGH PROBE AND GNSS-IR (GS2L) BY DIFFERENT MOVING AVERAGE WINDOW WIDTH

Window Width Day (h)	Correlation: Probe x GNSS-IR – GS2L
24	**0.85**
12	**0.81**
8	**0.79**
6	0.74
4	0.74
3	0.65
2	**0.58**

SOURCE: The authors (2024).

TABLE 2 presents the correlation between soil moisture estimated by GNSS-IR using the RS2P signal and the soil moisture series determined by the permittivity probe. For the RS2P signal, the highest correlation (0.82) was also obtained with a moving average window width of 24 hours. Similarly, the lowest correlation (0.58), indicating the worst result, was achieved with a window width of 2 hours.

TABLE 2 – CORRELATION BETWEEN SOIL MOISTURE ESTIMATED THROUGH PROBE AND GNSS-IR (RS2P) BY DIFFERENT MOVING AVERAGE WINDOW WIDTH

Window Width Day (h)	Correlation: Probe x GNSS-IR – GS2L
24	**0,82**
12	0,77
8	0,74
6	0,71
4	0,63
3	0,59
2	**0,53**

SOURCE: The authors (2024).

FIGURE 8 shows the soil moisture series and precipitation events at the Lucky Hills station in the GNSS-IR configuration that exhibited the highest correlation with the permittivity probe, using the GS2L signal with a 24-hour moving average window. In the upper panel, the soil moisture obtained by the permittivity probe installed near the GNSS station Lucky Hills is displayed, with a range of approximately 0.05 m^3/m^3 to 0.25 m^3/m^3

Central panel of FIGURE 8, the precipitation events (rain) recorded by a rain gauge are displayed. The maximum recorded precipitation event during the considered period was approximately 25 mm. In the lower panel, the soil moisture estimated by GNSS-IR by the GS2L signal is shown. It is noted that the GNSS- IR series begins approximately around 2021.5, indicating that it started later than the other series due to the commencement of the GNSS campaign, or rather, due to the input data itself.

FIGURE 8 – LUCKY HILLS STATION – VALIDATION OF THE SOIL MOISTURE SERIES GNSS-IR (GS2L) WITH A 24-HOUR MOVING AVERAGE WINDOW WIDTH.

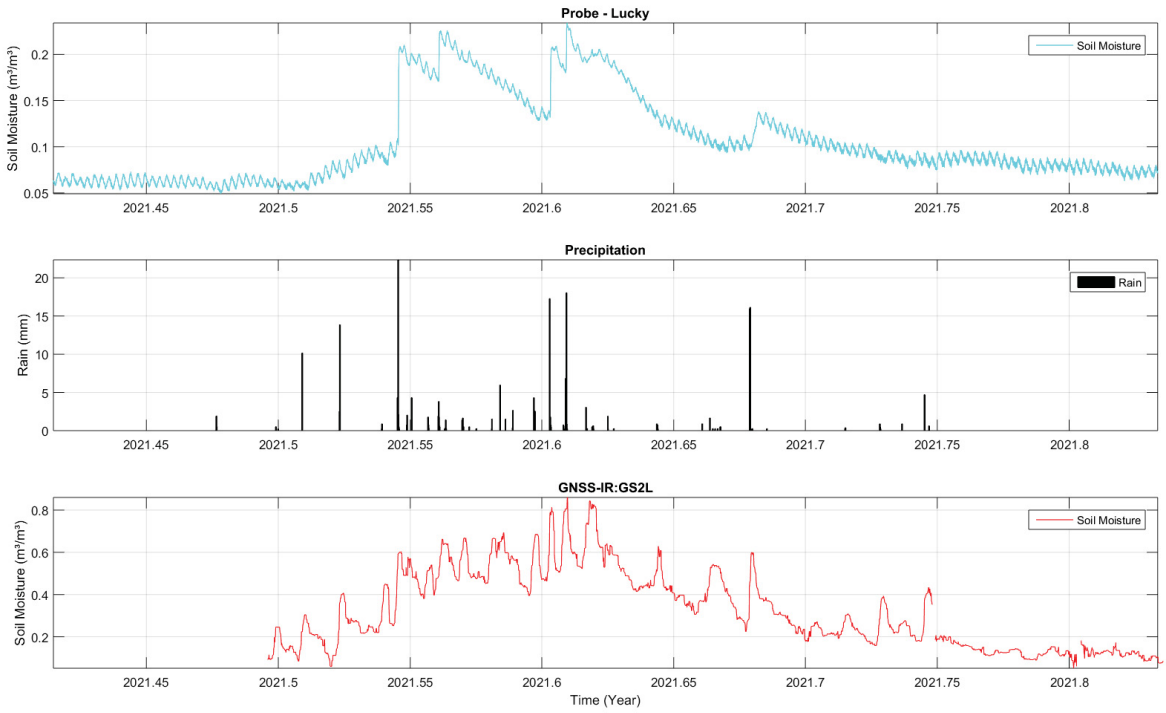

SOURCE: The authors (2024).

The soil moisture estimated by GNSS-IR corresponded well to precipitation events, as each precipitation event (middle panel) is associated with a peak in the moisture curve (lower panel). This correspondence is noted to occur simultaneously, even for lower magnitude precipitation events, such as those observed between 2021.7 and 2021.75, which had precipitation amounts of less than 2.5 mm.

Comparing the soil moisture series recorded by the sensor, it can be observed that precipitation events do not always lead to moisture peaks. For example, the two events occurring after 2021.5, with precipitation of 10 and 15 mm consecutively, did not result in peaks in the moisture series recorded by the sensor. However, these

events did lead to a gradual and continuous increase in moisture. This trend is interrupted by a sharp increase resulting in a moisture peak due to the precipitation event (25 mm) that occurred at 2021.55. In this case, as well as in the peak observed at 2021.6, it can be noted that the highlighted moisture peaks appear when the soil is already moist.

It is noticeable that when these peaks are recorded by the sensor, they occur after a certain period, as seen with the precipitation event (15 mm) that occurred between 2021.65 and 2021.7. The differences in sensitivity to precipitation events between the sensor and GNSS-IR are explained by the variation in reference depths of each technique. GNSS-IR has a reference depth of up to 5 cm, which is related to the penetration capability of the L-band electromagnetic waves and is conditioned by the soil moisture content.

On the other hand, the permittivity sensor depends on the depth at which the sensor is buried in the soil (10 cm). Since soil moisture does not distribute homogeneously in the soil, both horizontally across the terrain and vertically with depth, it is expected that there would be natural divergences in the series obtained at different depths.

In the GNSS-IR series, where moisture is associated with the upper layer of the soil, there is greater variability in moisture values, as these regions are more subject to the influence of phenomena such as evaporation, runoff, as well as the precipitation events themselves that contribute to increased soil moisture. Thus, it is observed that each precipitation event correlates with a peak in soil moisture in the GNSS-IR series; furthermore, these peaks occur simultaneously with the precipitation events.

FIGURE 9 presents the validation of the GNSS-IR series by altering only the moving average window width to 2 hours. In this case, it is observed that the GNSS-IR series exhibits greater data variability than in the series generated with a 24-hour window, as expected. Although this window could reveal the genuine variations in soil moisture in the upper layers of the soil, the series appears to be quite noisy, affecting the analysis and proper characterization of soil moisture, as numerous spurious values are present in the series, such as many values exceeding 1 m^3/m^3 and below 0 m^3/m^3, which indicate inconsistencies. These occurrences happen even for periods that do not directly correspond to precipitation events, as can be seen in the spikes that occur

after 2021.75, where spikes of spurious data appear in the GNSS-IR series despite no precipitation events having occurred.

FIGURE 9 – LUCKY HILLS STATION – VALIDATION OF THE GNSS-IR (GS2L) SOIL MOISTURE SERIES WITH A 2-HOUR MOVING AVERAGE WINDOW WIDTH.

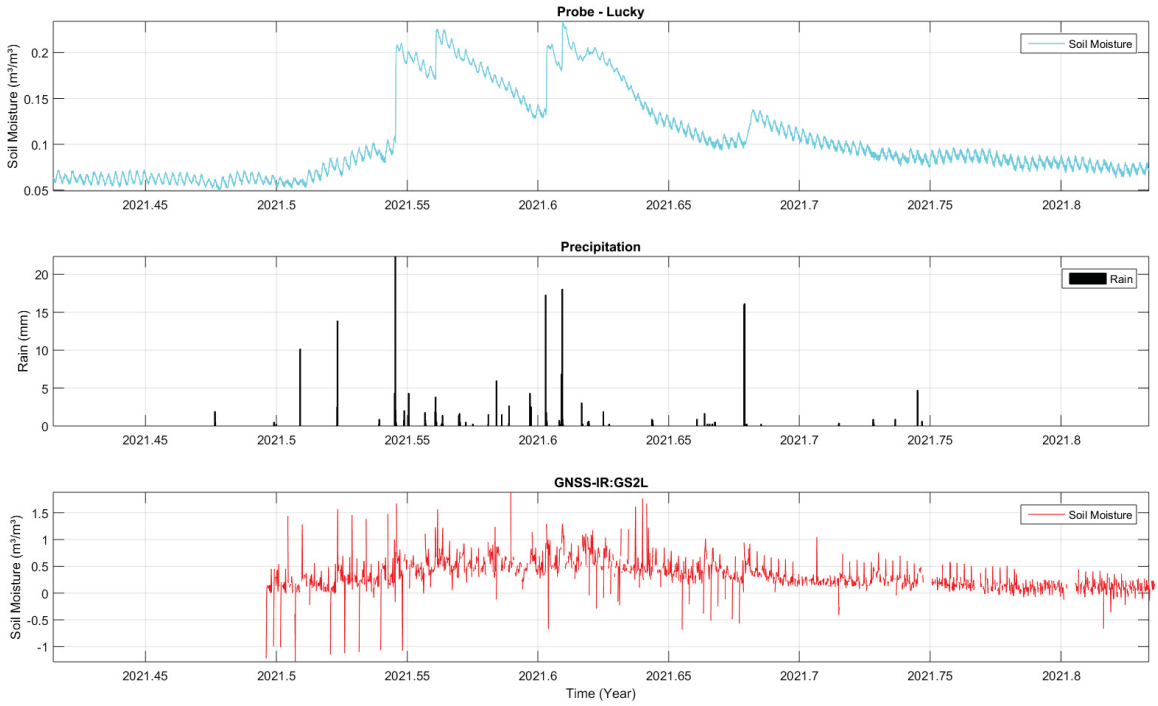

SOURCE: The authors (2024).

FIGURE 10 presents the validation graphs of the GNSS-IR series for the same case, but with an 8-hour moving average window. In this case, the third-best correlation (0.79) was achieved among all the observed windows. This series was generated with the minimum moving average window width at which no spurious data appeared, as seen in the series with a 2-hour width. Thus, this processing configuration preserved the advantages observed in the other strategies.

In this intermediate smoothing (8-hour), the prominent humidity peaks in the series are directly related to precipitation events, as occurred with the 24-hour width. On the other hand, with this width, the genuine fluctuations that occur in the upper layers of the soil between precipitation events are preserved, which do not appear in the 24-hour series due to excessive smoothing. Thus, this can be considered the configuration that provided the best result, although there is a 6% difference compared to the series with the highest correlation (24-hour width).

FIGURE 10 – LUCKY HILLS STATION – VALIDATION OF THE GNSS-IR (GS2L) SOIL MOISTURE SERIES WITH A MOVING AVERAGE WINDOW WIDTH OF 8 HOURS.

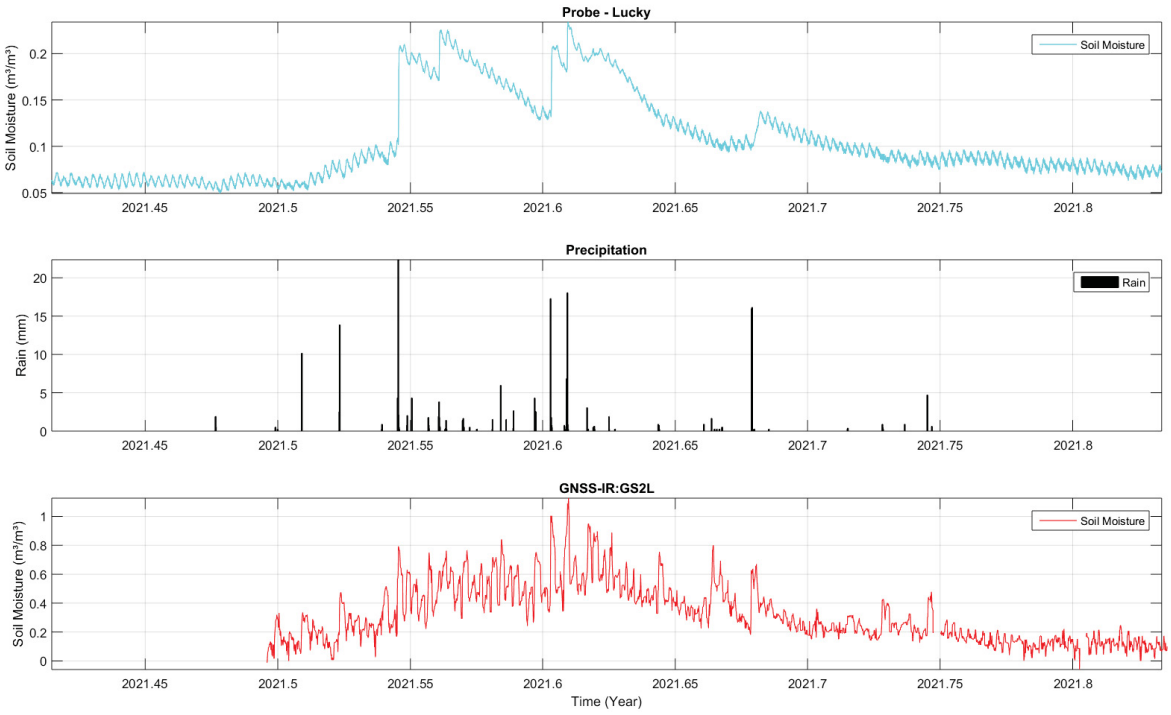

SOURCE: The authors (2024).

The scatter plot between the soil moisture series estimated by GNSS-IR and the series recorded by the permittivity probe is presented in FIGURE 11. The Root Mean Square Error (RMSE) was 0.03 m³/m³. The regression line is shown in red, and the data points, represented by black dots, become more dispersed as the soil moisture increases.

In FIGURE 12 the discrepancies between these series are highlighted as a function of soil moisture. It was observed that there is a tendency for discrepancies to increase with rising moisture levels; however, these discrepancies predominantly remain within the range of 0.1 and -0.1 m³/m³. The red line represents a moving average applied to the discrepancy values. At the beginning of the series, the values and the moving average line are close to the x-axis, indicating low discrepancies between the series. The gray-shaded area denotes a prediction interval based on the standard deviation of the data.

FIGURE 11 – SCATTER PLOT BETWEEN THE SOIL MOISTURE GNSS-IR (GS2L) AND THE PROBE. LUCKY HILLS STATION

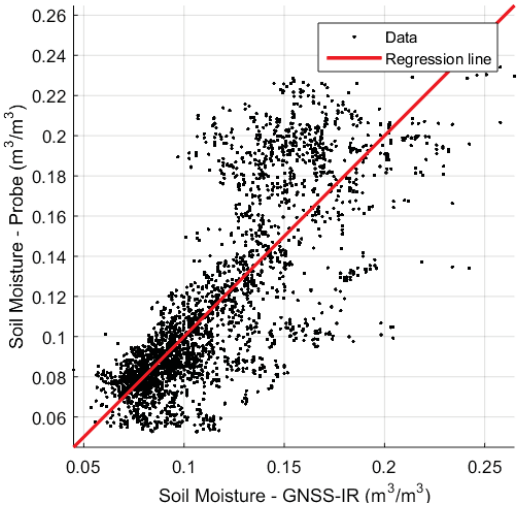

SOURCE: The authors (2024).

FIGURE 12 – DISCREPANCY GRAPH BETWEEN THE GNSS-IR

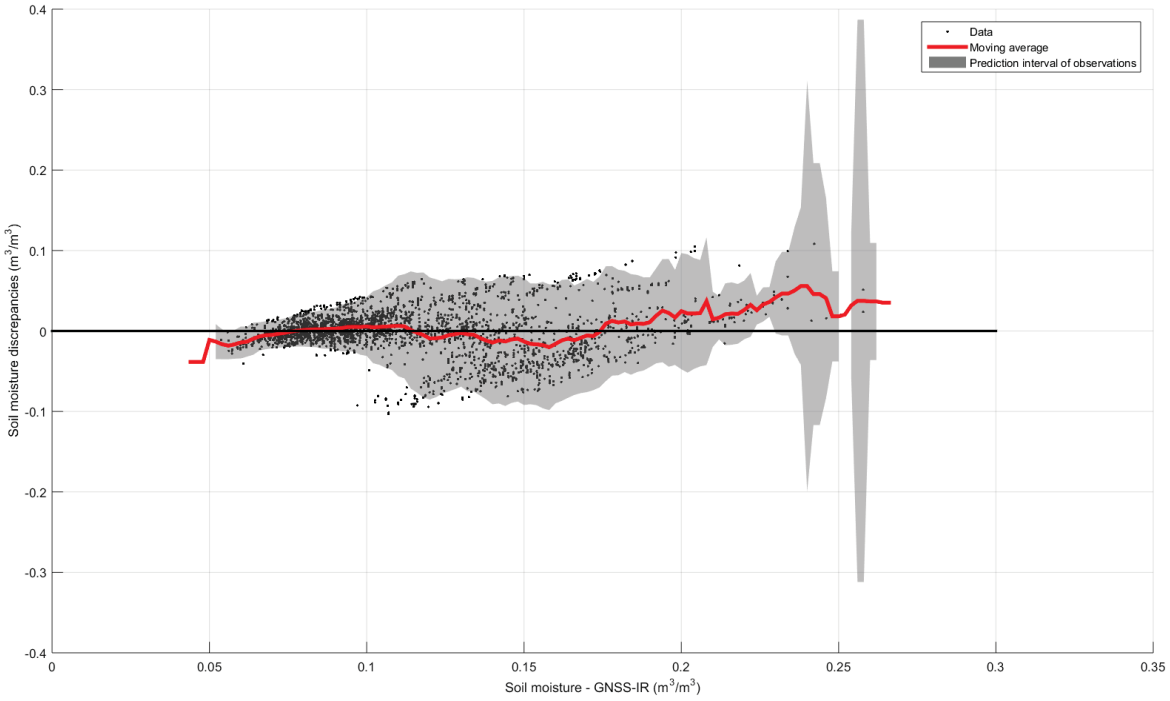

SOURCE: The authors (2024).

In FIGURE 13 the best result for soil moisture series obtained at the Lucky Hills station using GNSS-IR with the RS2P signal. Based on the previously discussed considerations. The correlation achieved was 0.74 for the series with an 8-hour moving

average window. When comparing with FIGURE 10, which was produced with the same characteristics except for the GNSS signal used, it is evident that the series obtained with the RS2P signal shows greater data variability. This is primarily due to the orbital plane and period characteristics of the GLONASS system, leading to a degree of variability in satellite passes over time, unlike GPS, where satellite passes occur more regularly.

There are advantages and disadvantages to considering each specific case. For instance, variability in the satellite pass directions may provide better spatial resolution for estimates. However, this same characteristic can lead to noisier SNR arcs due to data variability. In this context, a multi-GNSS signal might combine the benefits obtained from both cases, offering a more robust approach.

FIGURE 13 – LUCKY HILLS STATION – VALIDATION OF THE GNSS-IR (RS2P) SOIL MOISTURE SERIES WITH A MOVING AVERAGE WINDOW WIDTH OF 8 HOURS.

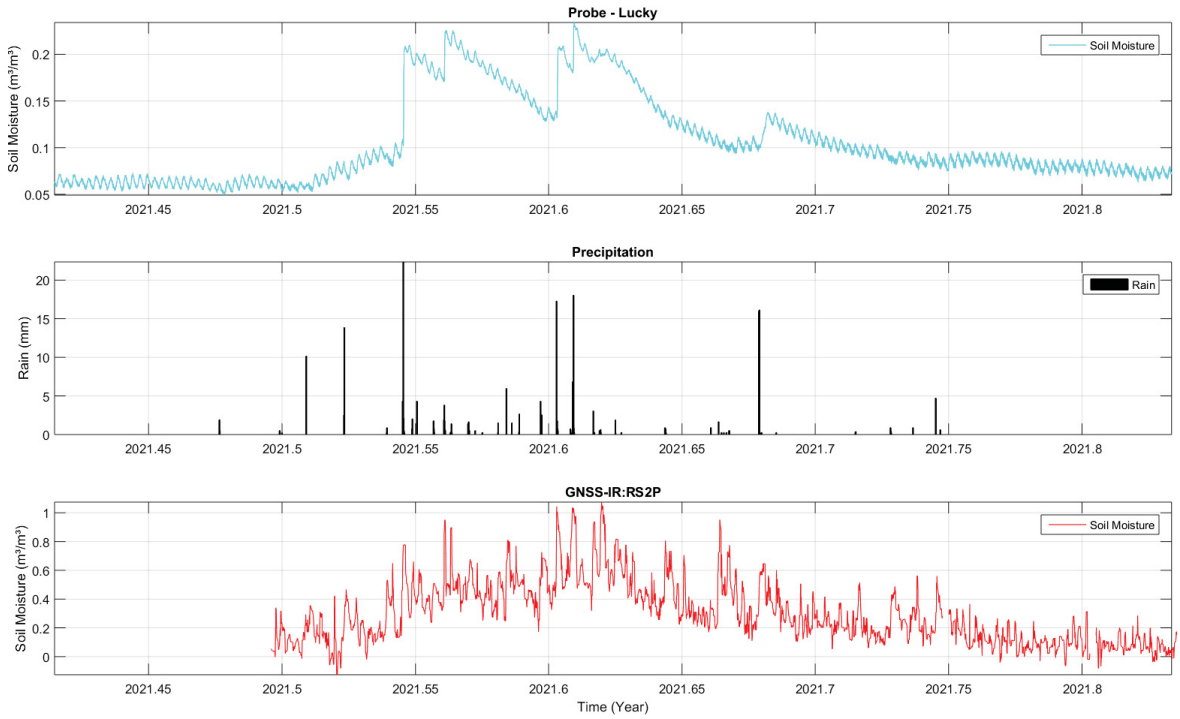

SOURCE: the author (2024).

The results obtained at Lucky Hills, considering the signals with the best outcomes, GS2L and RS2P, showed a maximum correlation of 0.85 and 0.82,

respectively. The average correlation was 0.74 for the series generated with the GS2L signal and 0.68 for the series generated with the RS2P signal.

3.2 KENDALL STATION

TABLE 3 presents the correlation values for the Kendall station between the soil moisture series obtained by the permittivity probe and the GNSS-IR series using the GS2L signal, considering different moving average window widths. Unlike the behavior observed at the Lucky Hills station, the highest correlation was found in the series with a 6-hour moving average window width, with a correlation of 0.71 (FIGURE 14).

TABLE 3 – CORRELATION BETWEEN SOIL MOISTURE ESTIMATED THROUGH PROBE AND GNSS-IR (GS2L) BY DIFFERENT MOVING AVERAGE WINDOW WIDTH.

Window Width Day (h)	**Correlation: Probe x GNSS-IR – GS2L**
24	0.55
12	0.65
8	0.69
6	**0.71**
4	0.68
3	0.67
2	0.65

SOURCE: The authors (2024).

In the case of the Kendall station, the series with the highest correlation (0.71) was obtained with a moving average width of 6 hours. This series was considered the best since the 8-hour width, which was the best at the Lucky Hills station, ended up smoothing out important peaks associated with precipitation events. Furthermore, widths shorter than 6 hours exhibited spurious data.

In FIGURE 14, the graphs associated with these series are presented. It can be observed that at this station, the GNSS-IR series shows two periods without data. This occurred due to problems in recording GNSS data. It was found that the raw data files had a much smaller size compared to other days, indicating that the issue was related to the actual recording of the input data. The two periods following these gaps in the series, that is, when data was available again (2021.6 and 2021.7), were

indicated in the post-processing as equipment changes related to variations in the height of the GNSS antenna.

This strategy contributed to the results, as, in practical terms, the growth of vegetation during the rainy season leads to variations in vegetation height and, consequently, in the distance between the GNSS antenna and the reflection surface.

FIGURE 14 – KENDALL STATION – VALIDATION OF THE GNSS-IR (GS2L) SOIL MOISTURE SERIES WITH A MOVING AVERAGE WINDOW WIDTH OF 6 HOURS.

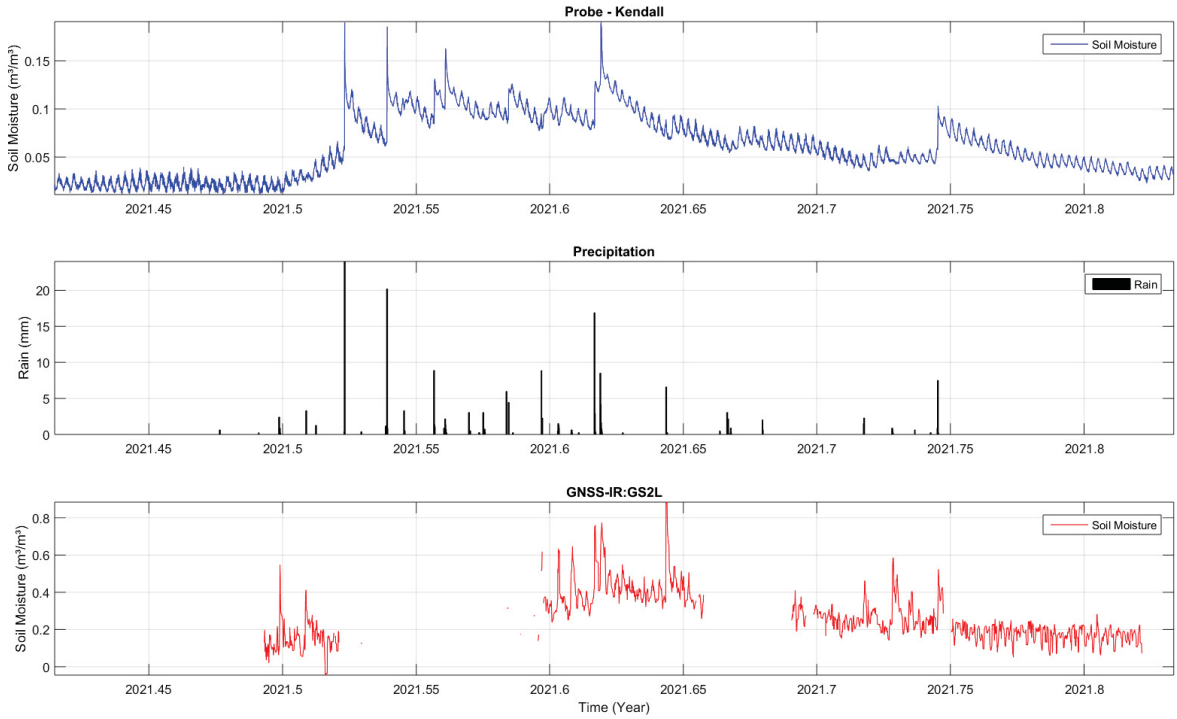

SOURCE: The authors (2024).

The lowest correlation in the GS2L series was obtained with a 24-hour window, where the correlation was 0.55, contrary to what occurred at the Lucky Hills station, where the 24-hour series provided the best correlation. FIGURE 15 shows the scatter plot between the soil moisture series estimated by GNSS-IR and the series recorded by the permittivity probe. The root mean square error (RMSE) was 0.02 m³/m³.

FIGURE 15 – SCATTER PLOT BETWEEN THE SOIL MOISTURE GNSS-IR (GS2L) AND THE PROBE. KENDALL STATION.

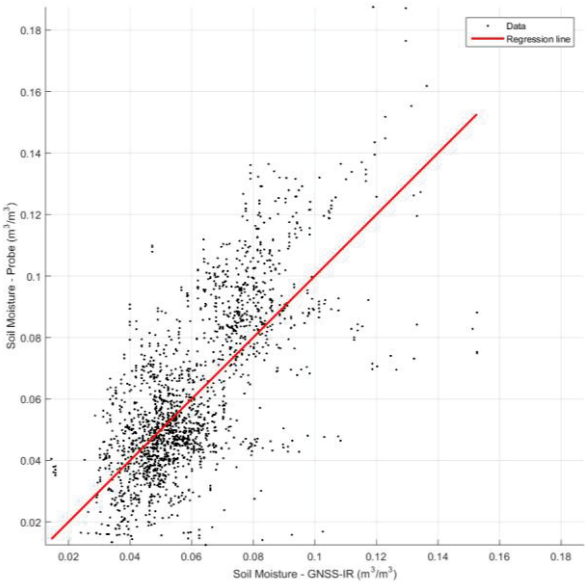

SOURCE: the author (2024).

FIGURE 16 presents the discrepancy plot between the series as a function of soil moisture. A slight trend of increasing discrepancy with rising soil moisture levels was observed; however, these discrepancy values between the series remain predominantly within a range of -0.05 to 0.05 m³/m³, indicating less discrepancy than at the Lucky Hills station.

FIGURE 16 – DISCREPANCY GRAPH BETWEEN THE GNSS-IR

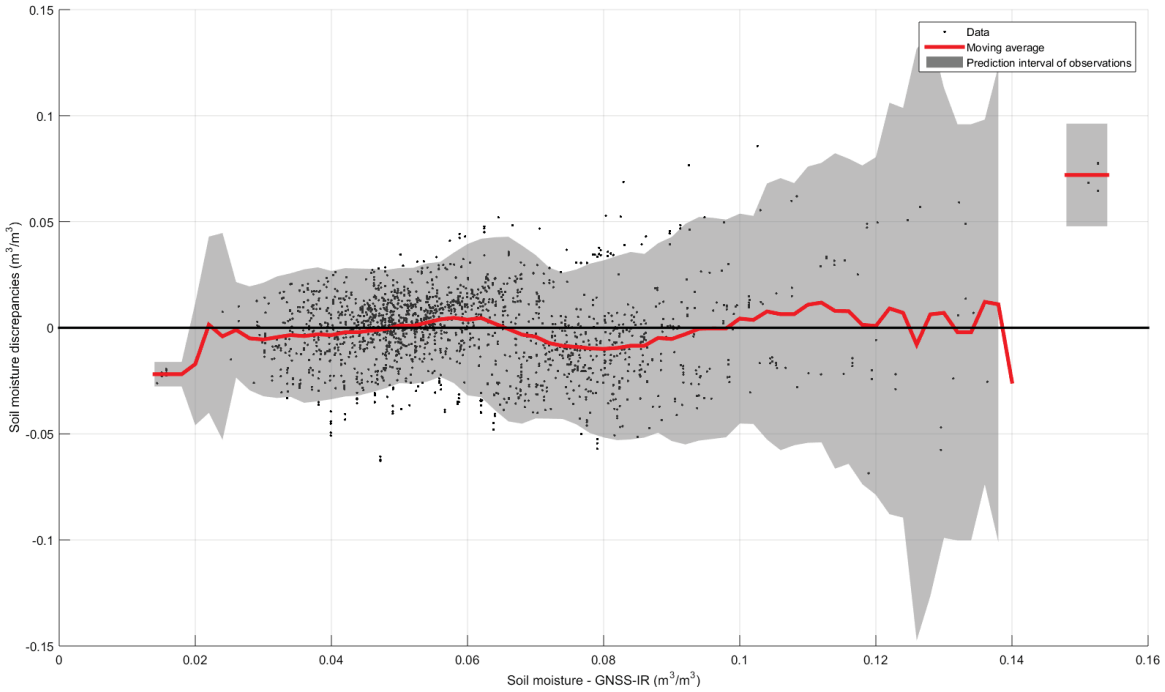

SOURCE: The authors (2024).

TABLE 4 shows the correlation values between the soil moisture series measured by the permittivity probe and the GNSS-IR series from the Kendall station using the RS2P signal, across different moving average window widths.

TABLE 4 – CORRELATION BETWEEN SOIL MOISTURE ESTIMATED THROUGH PROBE AND GNSS-IR (RS2P) BY DIFFERENT MOVING AVERAGE WINDOW WIDTH.

Window Width Day (h)	Correlation: Probe x GNSS-IR – RS2P
24	0,53
12	**0,66**
8	**0,66**
6	0,63
4	0,53
3	0,53
2	**0,50**

SOURCE: The authors (2024).

The results presented in TABLE 4 show that the RS2P signal, across different moving average window widths, yielded series with lower correlation to the series estimated by the permittivity probe compared to the GS2L signal.

Considering the signals with the best results, GS2L and RS2P, maximum correlations of 0.71 and 0.66, respectively, were obtained. The GS2L signal achieved an average correlation of 0.66, while the RS2P signal had an average correlation of

0.58. This pattern was also observed at the Lucky Hills station and differs from other studies, in which the RS2P signal showed better results. However, a common characteristic in those studies is that they were conducted at stations considered ideal for reflectometry. In these cases, the variability in the passage of GLONASS satellites may contribute to a more homogeneous representation of soil moisture around the station due to its variation in terms of azimuth with each pass over the antenna horizon.

3.3 COMPARING OF RESULTS

The stations evaluated in this study can be considered non-ideal due to the surrounding vegetation and topography. Consequently, it is suggested that the variability in GLONASS satellite passages, combined with the random distribution of vegetation affecting reflected signals, hinders the accuracy of estimates made using signals from this system.

For the GPS, however, since satellite passages occur more consistently, the application of azimuth masks based on prior assessments helped minimize the impact of vegetation on the reflected signal, as well as the influence of topography, which varies more significantly at the Kendall station.

TABLE 5 shows the highest and lowest correlations between the series considering the GS2L and RS2P signals across different processing strategies. The last column indicates the optimization from the series with the lowest to the highest correlation.

TABLE 5– HIGHEST AND LOWEST CORRELATIONS BETWEEN GNSS-IR SOIL MOISTURE SERIES AND PROBE SERIES.

Station	GNSS Signal	Lowest correlation	Highest correlation	Optimization (%)
Lucky Hills	GS2L	0,58	0,85	47
	RS2P	0,53	0,82	54
Kendall	GS2L	0,60	0,71	18
	RS2P	0,50	0,66	32

SOURCE: The authors (2024).

At the Lucky Hills station, using the GS2L signal, the maximum correlation was achieved with the series generated using a 24-hour moving average window. The lowest correlation was obtained with a 2-hour window. In this case, the choice of

window width impacts the correlation by up to 47%, highlighting the importance of conducting investigations to determine the optimal GNSS-IR processing configuration for each station. TABLE 6 shows the average correlation values for each station based on the GS2L and RS2P signals.

TABLE 6 – AVERAGE CORRELATION BETWEEN GNSS-IR SOIL MOISTURE SERIES AND PROBE MEASUREMENTS.

Station	GNSS Signal	Average correlation
Lucky Hills	GS2L	0,74
	RS2P	0,68
Kendall	GS2L	0,66
	RS2P	0,58

SOURCE: The authors (2024).

The average values provide a more realistic basis for comparison, as correlation alone does not fully reflect the series' quality. Applying processing strategies with varied configurations proved effective in refining the results, achieving up to a 54% optimization between strategies at the Lucky Hills station with the RS2P signal. However, it is essential to consider two main factors that impacted the results: the difference in reference depth between techniques and the surrounding vegetation at the stations.

These influences are evident when comparing GNSS-IR time series with those obtained from the capacitive probes used for validation (FIGURES 8, 9, 10, 13, 14). It is observed that, despite the degree of correlation between the series, their behavior diverges, especially during the rainy season between 2021.5 and 2021.7.

Due to the differences in reference depth between the techniques, in the GNSS-IR series, which are associated with the more superficial soil layers, moisture peaks and those corresponding to precipitation events occur more simultaneously. In contrast, the peaks recorded by the probes occur after a certain period, as the water gradually infiltrates deeper layers, resulting in a time lag between the series and potentially affecting the correlation calculation.

These differences, combined with the influence of vegetation on GNSS-IR estimates, led to discrepancies in the series. This remains a limitation of the technique, as isolating the effect of vegetation in modeling is highly complex, though numerous studies have shown promising results in this area (Lv et al., 2021; Ding et al., 2023)

4 CONCLUSIONS

This research concerns soil moisture estimative around two stations located in the state of Arizona, USA. These stations are not considered ideal for GNSS-IR due to the topography, vegetation, and metal structures present in their surroundings. Using data from permittivity probes and rain gauges, it was possible to validate the estimates and evaluate different processing configurations.

Investigations were conducted to adjust azimuthal masks; masks for elevation angles; GNSS signals; spacing; and window width for moving averages. The best results were obtained using the GS2L and RS2P signals, with an elevation mask of 15 to 30 degrees and specific azimuth masks for each station.

At the Lucky Hills station, the best series was defined by considering the smallest window width to better represent the genuine variations in soil moisture that occur in the surface layers, as this width smoothed the series sufficiently to prevent spurious peaks from appearing. In this sense, the best series was considered to be the one using the GS2L signal with an 8-hour width, which presented a correlation of 0.79 with the series recorded by the probe. With the RS2P signal, the series defined as the best was also with an 8-hour width, which presented a correlation of 0.74.

At the Kendall station, the best series using the GS2L signal presented a correlation of 0.71 and was defined by a moving average width of 6 hours. For the RS2P signal, the best series was defined with an 8-hour width, showing a correlation of 0.66. It was found that a higher correlation does not always indicate the series that best represents the soil moisture estimated by GNSS-IR. This occurs due to the differences in reference depths between the techniques and the influence of vegetation. In the case of GNSS-IR, a series with greater variability in soil moisture behavior is expected, as it reflects the natural variations occurring in the surface layers of the soil, up to 5 cm, which corresponds to the reference depth of the technique.

The investigations aimed at defining the best processing configuration resulted in an optimization of up to 54% in the results, considering only the difference in moving average width. The variability in the influence of moving average width on the series may be related to the peculiarities and specific characteristics of each station. Therefore, it is evident that each station should be evaluated individually to ensure that the configurations are appropriate. This is particularly important in non-ideal stations,

which have restrictions regarding the prerequisites of the technique, such as the presence of vegetation and irregular topography.

The Lucky Hills station, although surrounded by taller shrub vegetation compared to the Kendall station, yielded the best results. One factor to consider that may have contributed to this outcome is the nature of the shrubs; despite their greater height, they are sparser. In areas without shrubs, there is exposed soil, which simplifies modeling. In contrast, the Kendall station features a type of grass that has a significant height. Vegetation with such vertical patterns has a greater impact on signal coherence. Moreover, this type of vegetation appears dense, occupying a large portion of the reflection area, and consequently affecting reflectometric modeling.

The irregular topography at the stations, particularly at the Kendall station, may have impacted the consistent modeling of the station height about the reflection surface, consequently affecting the accuracy of the results. This parameter has a high correlation with the reflectometric phase, meaning that any variations or inaccuracies in the station's height can lead to significant discrepancies in the estimations of soil moisture and other related variables.

GNSS-IR enabled consistent estimates of soil moisture, considering the correlation between the generated series and those recorded by the sensors. The generated series displayed peaks that coincided with precipitation events recorded by rain gauges. The differences observed between the GNSS-IR series and those obtained from the sensors were anticipated due to the varying reference depths of each technique. This indicates that while GNSS-IR provides valuable insights into soil moisture dynamics, it is essential to account for the differences in measurement depths when interpreting the results.

The application of specific configurations for each station significantly contributed to the refinement of results and enabled the use of non-ideal stations. The width of the moving average window had a direct influence on the results, both in terms of correlation and in the representation of phenomena associated with the upper soil layers. It is worth noting that a specific width must be defined for each station to optimize the accuracy of the estimates. This tailored approach ensures that the unique characteristics of each station are taken into account, leading to more reliable soil moisture estimations.

The negative influence of vegetation and existing structures around the stations was minimized through the use of azimuth and elevation masks. However, the impact

of vegetation cannot be overlooked and remains a limitation of GNSS-IR in estimating soil moisture. Numerous studies are being developed on this topic (Li et al. 2023; Wei et al. 2023; Shekhar et al. 2024).

It is recommended that specific investigations be conducted regarding the processing configurations for reflectometry at each GNSS station to be employed in GNSS-IR. This initial step should include the use of sensors for validation purposes. By tailoring the processing configurations and validating them with sensors, the accuracy and reliability of soil moisture estimations can be enhanced, ultimately leading to more effective applications of the GNSS-IR technique.

This research is part of the North American Monsoon scientific investigation project, in which variables of the hydrological cycle have been estimated using GNSS techniques to contribute to analyses of soil-atmosphere interactions. These results demonstrate the feasibility of using GNSS not only for its traditional applications in positioning, navigation, and synchronization but also for monitoring Earth dynamics and various environmental variables. The findings highlight the potential of GNSS technology in advancing our understanding of hydrological processes and improving environmental monitoring efforts.

In future works, it is recommended to conduct new investigations using a Multi-GNSS signal, generated from a combination of signals from different constellations and frequencies. With the increase in the number of satellites transmitting the L5 frequency, there is the potential for improved accuracy in soil moisture estimates, as this frequency offers advantages such as greater resistance to interference. Furthermore, the use of signals from multiple constellations can provide more robust and continuous coverage.

Investigations into the influence of vegetation and tools to minimize this effect in GNSS-IR estimates remain a relevant area of research. Operational considerations suggest that future studies should establish strategies to monitor data recording to avoid losses at the end of campaigns. Additionally, it is recommended that the GNSS receiver be installed close to the receiving antenna, as long cables between these devices can result in signal power loss.

REFERENCES

BABAEIAN, E.; SADEGHI, M.; JONES, S. B.; et al. Ground, Proximal, and Satellite

Remote Sensing of Soil Moisture. **Reviews of Geophysics**, v. 57, n. 2, p. 530–616, 19. jun. 2019. [s.l.]. Disponível em: <https://onlinelibrary.wiley.com/doi/abs/10.1029/2018RG000618>.

CHANG, X.; JIN, T.; YU, K.; et al. Soil moisture estimation by GNSS multipath signal. **Remote Sensing**, v. 11, n. 21, p. 1–16, 2019.

CHEW, C. C.; SMALL, E. E.; LARSON, K. M.; ZAVOROTNY, V. U. Effects of near-surface soil moisture on GPS SNR data: Development of a retrieval algorithm for soil moisture. **IEEE Transactions on Geoscience and Remote Sensing**, v. 52, n. 1, p. 537–543, 2014.

DING, R.; ZHENG, N.; ZHANG, H.; ZHANG, H.; LANG, F.; BAN, W. A Study of GNSS-IR Soil Moisture Inversion Algorithms Integrating Robust Estimation with Machine Learning. ***Sustainability***, vol. *15*, 6919, 2023. https://doi.org/10.3390/su15086919.

EDOKOSSI, K.; CALABIA, A.; JIN, S.; MOLINA, I. GNSS-reflectometry and remote sensing of soil moisture: A review of measurement techniques, methods, and applications. **Remote Sensing**, v. 12, n. 4, 2020.

ENTEKHABI, D.; NJOKU, E. G.; O'NEILL, P. E.; et al. The soil moisture active passive (SMAP) mission. **Proceedings of the IEEE**, v. 98, n. 5, p. 704–716, 2010.

EURIQUES, J. F. **Determinação da umidade do solo por meio da técnica de Refletometria GNSS – Primeiros resultados no Brasil**, 2019. Universidade Federal do Paraná. Disponível em: <https://acervodigital.ufpr.br/bitstream/handle/1884/62323/R - D - JORGE FELIPE EURIQUES.pdf?sequence=1&isAllowed=y>. .

EURIQUES, J. F.; KRUEGER, C. P.; MACHADO, W. C.; SAPUCCI, L. F.; GEREMIA-NIEVINSKI, F. Soil Moisture Estimation with GNSS Reflectometry: A Conceptual Review. Revista Brasileira de Cartografia, v. 73, n. 2, p. 413–434, 2021.

GEREMIA-NIEVINSKI, F.; HOBIGER, T. **Site guidelines for multi-purpose GNSS reflectometry stations**. 2019.

JIN, S.; CARDELLACH, E.; XIE, F. **Remote Sensing and Digital Image Processing: Theory, Methods and Applications**. Springer International Publishing, 2014.

LARSON, K. M.; BRAUN, J. J.; SMALL, E. E.; et al. GPS Multipath and Its Relation to Near-Surface Soil Moisture Content. **IEEE Journal of Selected Topics in Applied Earth Observations and Remote Sensing**, v. 3, n. 1, p. 91–99, 2010.

LARSON, K. M.; NIEVINSKI, F. G. GPS snow sensing: Results from the EarthScope Plate Boundary Observatory. **GPS Solutions**, v. 17, n. 1, p. 41–52, 2013.

LARSON, K. M.; SMALL, E. E.; GUTMANN, E.; et al. Using GPS multipath to measure soil moisture fluctuations: Initial results. **GPS Solutions**, v. 12, n. 3, p. 173–177, 2008a.

LARSON, K. M.; SMALL, E. E.; GUTMANN, E. D.; et al. Use of GPS receivers as a soil moisture network for water cycle studies. **Geophysical Research Letters**, v. 35, n. 24, 2008b.

LI, J. ; YANG D.; WANG, F.; HONG, X. Hong A New Algorithm for Measuring Vegetation Growth Using GNSS Interferometric Reflectometry. **IEEE Journal of Selected Topics in Applied Earth Observations and Remote Sensing,** v. 16, 2023

LV, J.; ZHANG, R.; TU, J.; LIAO, M.; PANG, J.; YU, B.; LI, K.; XIANG, W.; FU, Y.; LIU, G. A GNSS-IR Method for Retrieving Soil Moisture Content from Integrated Multi-Satellite Data That Accounts for the Impact of Vegetation Moisture Content. **Remote Sens**. 2021, 13, 2442. https://doi.org/ 10.3390/rs13132442

NIEVINSKI, F. G.; LARSON, K. M. Forward modeling of GPS multipath for near-surface reflectometry and positioning applications. **GPS Solutions**, v. 18, n. 2, p. 309–322, 2014a. Springer Verlag.

NIEVINSKI, F. G.; LARSON, K. M. An open source GPS multipath simulator in Matlab/Octave. **GPS Solutions**, v. 18, n. 3, p. 473–481, 2014b. Springer Verlag.

NIEVINSKI, F. G.; LARSON, K. M. Inverse modeling of GPS multipath for snow depth estimation - Part I: Formulation and simulations. **IEEE Transactions on Geoscience and Remote Sensing**, v. 52, n. 10, p. 6555–6563, 2014c. Institute of Electrical and Electronics Engineers Inc.

NIEVINSKI, F. G.; LARSON, K. M. Inverse modeling of GPS multipath for snow depth estimation - Part II: Application and validation. **IEEE Transactions on Geoscience and Remote Sensing**, v. 52, n. 10, p. 6564–6573, 2014d. Institute of Electrical and Electronics Engineers Inc.

OCHSNER, T. E.; COSH, M. H.; CUENCA, R. H.; et al. State of the Art in Large-Scale Soil Moisture Monitoring. **Soil Science Society of America Journal**, v. 77, n. 6, p. 1888–1923, 2013. Disponível em: <https://www.soils.org/publications/sssaj/abstracts/77/6/1888>. .

ROBINSON, D. A.; CAMPBELL, C. S.; HOPMANS, J. W.; et al. Soil Moisture Measurement for Ecological and Hydrological Watershed-Scale Observatories: A Review. **Vadose Zone Journal**, v. 7, n. 1, p. 358–389, 2008.

RODRIGUEZ-ALVAREZ, N.; BOSCH-LLUIS, X.; CAMPS, A.; et al. Soil moisture retrieval using GNSS-R techniques: Experimental results over a bare soil field. **IEEE Transactions on Geoscience and Remote Sensing**, v. 47, n. 11, p. 3616–3624, 2009.

ROUSSEL, N.; FRAPPART, F.; RAMILLIEN, G.; et al. Detection of Soil Moisture Variations Using GPS and GLONASS SNR Data for Elevation Angles Ranging from 2° to 70°. **IEEE Journal of Selected Topics in Applied Earth Observations and Remote Sensing**, v. 9, n. 10, p. 4781–4794, 2016.

ROUSSEL, N.; RAMILLIEN, G.; FRAPPART, F.; et al. Sea level monitoring and sea state estimate using a single geodetic receiver. **Remote Sensing of Environment**, v. 171, p. 261–277, 2015. Elsevier Inc. Disponível em: <http://dx.doi.org/10.1016/j.rse.2015.10.011>. .

SENEVIRATNE, S. I.; CORTI, T.; DAVIN, E. L.; et al. Investigating soil moisture-climate interactions in a changing climate: A review. **Earth-Science Reviews**, v. 99, n. 3–4, p. 125–161, 2010.

SHEKHAR, S. et al. Comparative Analysis of NavIC Multipath Observables for Soil Moisture over Different Field Conditions. ***Progress In Electromagnetics Research,*** v. 117, p. 25-35, 2023

TABIBI, S.; NIEVINSKI, F. G.; VAN DAM, T. Statistical Comparison and Combination of GPS, GLONASS, and Multi-GNSS Multipath Reflectometry Applied to Snow Depth Retrieval. **IEEE Transactions on Geoscience and Remote Sensing**, v. 55, n. 7, p. 3773–3785, 2017. Institute of Electrical and Electronics Engineers Inc.

TABIBI, S.; NIEVINSKI, F. G.; VAN DAM, T.; MONICO, J. F. G. Assessment of modernized GPS L5 SNR for ground-based multipath reflectometry applications. **Advances in Space Research**, v. 55, n. 4, p. 1104–1116, 2015. Elsevier Ltd.

TEUNISSEN, P. J. G.; MONTENBRUCK, O. **Springer Handbook of Global Navigation Satellite Systems**. Springer International Publishing, 2017.

VAQUERO-MARTÍNEZ, J.; ANTÓN, M. Review on the Role of GNSS Meteorology in Monitoring Water Vapor for Atmospheric Physic. **Remote Sensing** *13*, 2287. https://doi.org/10.3390/rs13122287

VEY, S.; GÜNTNER, A.; WICKERT, J.; BLUME, T.; RAMATSCHI, M. Long-term soil moisture dynamics derived from GNSS interferometric reflectometry: a case study for Sutherland, South Africa. **GPS Solutions**, v. 20, n. 4, p. 641–654, 2016. Springer Verlag.

WEI, H.; YANG, X.; PAN, Y.;SHEN, F. GNSS-IR Soil MoistureInversion Derived from Multi-GNSS and Multi-Frequency Data Accounting for Vegetation Effects. ***Remote Sens***.v.15, 5381, 2023. https://doi.org/10.3390/rs15225381

WU, X.; MA, W.; XIA, J.; et al. Spaceborne gnss-r soil moisture retrieval: Status, development opportunities, and challenges. **Remote Sensing**, v. 13, n. 1, p. 1–24, 2021.

YAN, S. H.; ZHANG, N.; CHEN, N. C.; GONG, J. Y. Feasibility of using signal strength indicator data to estimate soil moisture based on GNSS interference signal analysis. **Remote Sensing Letters**, v. 9, n. 1, p. 61–70, 2018. Taylor & Francis. Disponível em: <https://doi.org/10.1080/2150704X.2017.1384587>.

YANG, T.; WAN, W.; CHEN, X.; et al. Land surface characterization using BeiDou signal-to-noise ratio observations. **GPS Solutions**, v. 23, n. 2, p. 1–12, 2019. Springer Berlin Heidelberg. Disponível em: <http://dx.doi.org/10.1007/s10291-019-0824-4>. .

ZAVOROTNY, V. U.; GLEASON, S.; CARDELLACH, E.; CAMPS, A. Tutorial on remote sensing using GNSS bistatic radar of opportunity. **IEEE Geoscience and Remote Sensing Magazine**, v. 2, n. 4, p. 8–45, 2014. Institute of Electrical and Electronics Engineers Inc.

ZHANG, S.; ROUSSEL, N.; BONIFACE, K.; et al. Use of reflected GNSS SNR data to retrieve either soil moisture or vegetation height from a wheat crop. **Hydrology and Earth System Sciences**, v. 21, n. 9, p. 4767–4784, 2017. Copernicus GmbH.

ZHANG, X.; NIE, S.; ZHANG, C.; ZHANG, J.; CAI, H. Soil moisture estimation based on triple-frequency multipath error. **International Journal of Remote Sensing**, v. 42, n. 15, p. 5953–5968, 2021. Taylor & Francis. Disponível em: <https://doi.org/10.1080/01431161.2021.1933246> .

2.4 CHAPTER 4: PAPER 4 – CONTINUOUSLY OPERATING GNSS STATION UFPR/RBMC

This chapter presents the paper "Soil Moisture Estimation by GNSS-IR from Active Stations: Case Study – RBMC/IBGE, UFPR Station," which has been accepted for publication in *Anuário do Instituto de Geociências*. This study explores the application of GNSS Interferometric Reflectometry (GNSS-IR) for soil moisture monitoring using an active GNSS station from the Brazilian Network for Continuous Monitoring (RBMC/IBGE). The manuscript details the methodological framework, data processing techniques, and results obtained for the UFPR station. The findings highlight the potential of GNSS-IR for integrating soil moisture monitoring into existing geodetic infrastructures.

Reference: EURIQUES, J. F; VEIGA, L. A. K.; MACHADO, W. Carrupt; KRUEGER, C. P.; GEREMIA-NIEVINSKI, F. Soil moisture estimation by GNSS-IR from active stations: case study – RBMC/IBGE, UFPR station. Anuário do Instituto de Geociências, Rio de Janeiro, v. 48, 2025. e65911. DOI: https://doi.org/10.11137/1982-3908_2025_48_65911.

2.4.1 Soil Moisture Estimation by GNSS-IR from Active Stations: Case Study – RBMC/IBGE, UFPR Station

ABSTRACT

The Earth is a dynamic planet subject to numerous natural phenomena and processes that human activities have intensified. Monitoring variables associated with these phenomena is essential. Soil moisture, for example, plays a crucial role in climate systems, agriculture, and the hydrological cycle. The Global Navigation Satellite System (GNSS) is one of the Geodesy tools used for monitoring the Earth, through which the GNSS Interferometric Reflectometry (GNSS-IR) technique can be employed to estimate soil moisture. In this study, the UFPR station, part of the Brazilian Continuous Monitoring Network of GNSS Systems (RBMC) was selected for investigation. A Python script was developed to automate the preparation of GNSS data from any RBMC station. Different processing configurations of a reflectometric

algorithm were evaluated, resulting in a set of time series of soil moisture for 2022. Results indicate that configurations adapted to the station's local conditions contribute to the enhancement of the results. The best signal among the 24 evaluated was the precise signal from the L2 frequency of GLONASS (RS2P). Peaks in precipitation were aligned with peaks in soil moisture, with soil moisture ranging from 0 to 0.35 m^3/m^3. The results support the development of a methodology for monitoring soil moisture in the vicinity of GNSS-RBMC stations that meet GNSS-IR requirements, expanding the potential applications of this network.
Keywords: Interferometric Reflectometry. Geodetic Remote Sensing. Hydrological Cycle

1 INTRODUCTION

Earth is a dynamic planet susceptible to numerous processes. Changes in the Earth System are a natural consequence of these processes. However, due to human activities, the changes occurring over the last 150 years are incomparable to those that occurred previously (Simon et al. 2006). Population growth, combined with increasing exploitation of natural resources, has led to drastic changes on the planet, such as global warming, which affects the climate system and, consequently, Earth's dynamics. This scenario has resulted in a decrease in freshwater reserves and an increase in the occurrence of extreme phenomena (Awange & Kiema 2013). According to Plag and Pearlman (2009), sustainable development is crucial for achieving a stable future for the planet.

Monitoring processes related to the Earth System is one of the prerequisites for sustainable development (Paganini et al. 2018). These considerations are highlighted in the plan titled "Transforming Our World: The 2030 Agenda for Sustainable Development" (Agenda 2030), proposed by the United Nations in 2014 (Acharya & Lee 2019).

Soil moisture is the water content present in the vadose zone of the soil and is a quantity related to numerous hydrological, geophysical, and environmental phenomena of the Earth that manifest at different scales (Hillel 1998; Seneviratne et al. 2010). It plays an essential role in biogeochemical cycles, such as those of water and carbon, and is related to the energy flows between the Earth's physical surface and the atmosphere. Soil moisture quantification is critical for managing water resource

management and has numerous applications, including weather forecasting; delineation of flood areas and groundwater recharge; geotechnics; engineering works; and agriculture (Robinson et al. 2008; Entekhabi et al. 2010; Seneviratne et al. 2010; Ochsner et al. 2013; Edokossi et al. 2020; Zhang et al. 2021; Wu et al. 2021).

Contact probes and Remote Sensing are the most common methods for estimating soil moisture (Babaeian et al. 2019). In the former case, measurements are point-based and may not represent an area of interest. On the other hand, Remote Sensing offers global coverage, but with generalized information due to the spatial resolution of approximately 100 m for radars and 10 km for radiometers (Edokossi et al. 2020; Vey et al. 2016).

According to Plag and Pearlman (2009), geodesy provides fundamental information on changes in the Earth's shape, gravitational field, and rotation, referred to as the pillars of geodesy. The quantities associated with these pillars are directly related to mass transport and the dynamics of the Earth System.

The Global Navigation Satellite System (GNSS) is one of the four space techniques in geodesy (Altamimi et al. 2016). GNSS encompasses various satellite positioning systems, originally developed for determining position, navigation, and timing (Seeber, 2003). However, the signals transmitted by GNSS satellites have been explored for other purposes, such as Remote Sensing through the technique known as GNSS Reflectometry (GNSS-R), which involves the joint reception of direct signals intended for positioning and indirect signals resulting from reflections over surfaces surrounding the GNSS antenna, giving rise to the so-called multipath effect (Zavorotny & Voronovich 2000; Georgiadou, Kleusberg 1988; Teunissen & Montenbruck 2017; Leick 1995).

GNSS Reflectometry conducted from conventional GNSS stations focused on positioning and exploiting the multipath effect, is called GNSS Interferometric Reflectometry (GNSS-IR). Indirect signals, therefore, those that do not originate from a direct path between the satellite and the GNSS antenna, affect accurate positioning but enable GNSS-IR. These indirect signals are recorded by the antenna with a time delay due to the additional path compared to the direct signal. When interacting with reflecting surfaces, these signals have their characteristics (amplitude, phase, frequency, and polarization) changed based on the composition, dielectric properties, and roughness of the surface. These changes are also related to the angle of incidence of the signal and the height of the GNSS antenna relative to the reflecting surface

(Larson & Nievinski 2013; Roussel et al. 2015; Zavorotny et al. 2014). By combining information from direct and reflected signals, properties of the reflecting surface, and characteristics of the GNSS equipment, it is possible to estimate attributes of these surfaces, such as soil moisture, vegetation growth, and water levels (Jin et al. 2014).

Estimating soil moisture is one of the applications in which GNSS-IR has been successfully employed (Larson et al. 2008a; Rodriguez-Alvarez et al. 2009; Larson et al. 2010; Chew et al. 2014; Arroyo et al. 2014; Tabibi et al. 2015; Roussel et al. 2016; Vey et al. 2016; Yan et al. 2018; Euriques, 2019; Yang et al. 2019; Zhang et al. 2021; Li et al. 2022; Wang et al. 2022; Wei et al. 2023). Two of the main advantages of GNSS-IR over conventional soil moisture estimation methods are an intermediate coverage area of about 50 meters for an antenna at a height of 2 meters; and the use of the well-established GNSS infrastructure, which ensures appropriate temporal resolution (Tabibi et al. 2017; Euriques et al. 2021).

Although all GNSS observables are affected by multipath, the Signal-to-Noise Ratio (SNR) is the observable that best reveals this effect. SNR is invariant to common effects between direct and indirect paths that impact other observables, such as relative orbital errors; much of the atmospheric delays; and clock synchronization errors (Larson et al. 2010).

In the case of soil moisture, the desired metrics from SNR modeling are the phase parameters of the reflected signal. These values are converted into soil moisture through a calibration curve. A polynomial establishes the relationship between the interferometric phase parameters and the soil moisture values (Chew et al. 2014; Vey et al. 2016). The main limitations of this methodology are the imprecision of the theoretical coefficients of the calibration curve and factors related to the modeling of reflected signals, such as the effects of topography and vegetation (Euriques et al. 2021; Zhang et al. 2017).

A reflectometric algorithm via SNR was developed in Matlab by Nievinski & Larson (2014a, 2014b, 2014c, 2014d) for snow altimetry; it was adapted for soil moisture estimation by Tabibi et al. (2015) and expanded for Multi-GNSS by Tabibi et al. (2017). Euriques (2019), used this algorithm to estimate soil moisture around a station installed at the National Institute for Space Research (In Portuguese, Instituto Nacional de Pesquisas Espaciais - INPE) in Cachoeira Paulista - SP, marking the first results of this application in Brazil. In this research, a correlation of 73% was obtained between the GNSS-IR estimates and a probe from the Cosmic-ray Soil Moisture

Observing System, used for validation. Alternatively, the software Gnssrefl was made available to the scientific community; this is an open-source software developed in Python for GNSS-IR (Larson, 2024). The Gnssrefl includes specific modules for various applications, including a module for estimating soil moisture.

The efficiency of the technique has been demonstrated by numerous international studies that reported a high correlation with conventional equipment. For example, Larson et al. (2008b) achieved an 85% correlation between GNSS-IR and moisture results from ten Time Domain Reflectometry (TDR) probes; Roussel et al. (2016) obtained correlations of up to 95% with capacitance probes; Yang et al. (2017) validated GNSS-R results using modeled values of soil permittivity, achieving correlations of up to 70%; in turn, Martín et al. (2020) validated GNSS-IR results with the gravimetric method, considered the most accurate method, obtaining correlations of up to 85%.

Every GNSS antenna is subject to receiving indirect signals and, consequently, to the multipath effect. Thus, reflectometric determinations can be made from GNSS tracking aimed at positioning, without requiring modifications to the equipment or the antenna installation (Larson et al. 2010). This allows for the possibility of employing historical series, for example, from active GNSS stations, for reflectometric applications, enabling the enhancement of phenomenon modeling.

In this context, data from continuously operating GNSS stations, referred to as active stations, such as those in the Brazilian Continuous Monitoring Network of GNSS Systems (RBMC), maintained by the Brazilian Institute of Geography and Statistics (IBGE), can be used, expanding the range of applications for this network. However, not all stations are suitable for GNSS-IR, as certain assumptions are required (Nievinski et al. 2016). First, the location of the GNSS station must be considered. For soil moisture estimation, the area surrounding the antenna must be predominantly bare soil or low vegetation. Additionally, there must be unobstructed visibility to the ground in that area (Geremia-Nievinski; Hobiger 2019).

The scope of this research consisted of estimating soil moisture around a RBMC station by GNSS-IR, aiming to present methodological guidelines for automating the processing of SNR data via a reflectometric algorithm to enable soil moisture monitoring, thereby expanding the range of applications of the RBMC.

2 METHODOLOGY AND DATA

Figure 1 corresponds to the methodological flowchart of this research, which began with an evaluation of RBMC stations to select one for the study. Next, the SNR recorded in the station's RINEX files was analyzed using the RTKlib software and the GNSS Reflections tool (https://gnss-reflections.org/rzones). An algorithm was developed in Python to enable the download, conversion, and standardization of GNSS data from the RBMC. A topographic survey was conducted to map the obstructions surrounding the station to establish processing configurations. Subsequently, the data were processed using the reflectometric algorithm developed by Nievinski and Larson, from which two signals that showed the best results were selected: one from the United States Global Positioning System (GPS) and another from the Russian system (GLONASS). Thus, two series of reflectometric phase data were obtained, and then converted to soil moisture series using the calibration curve, employing coefficients established in the literature. The results were compared with precipitation events recorded by an automatic station from the National Institute of Meteorology (In Portuguese, Instituto Nacional de Meteorologia - INMET).

FIGURE 1 – FLOWCHART OF METHODOLOGY

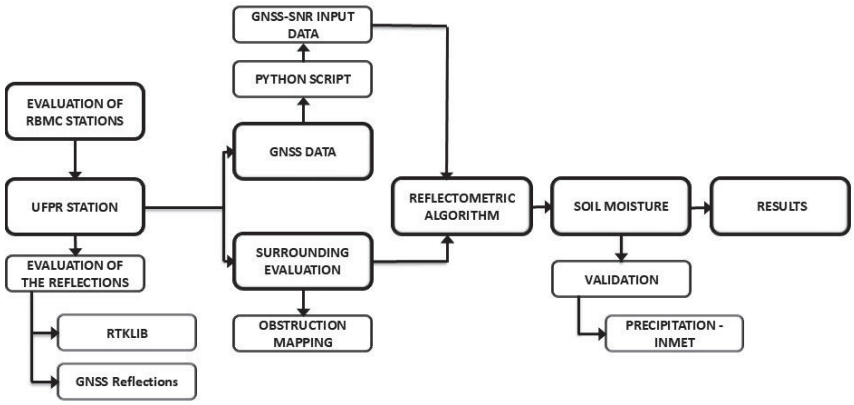

SOURCE: The authors (2024)

1.1 SELECTION OF REFERENCE STATION: UFPR-RBMC

The RBMC currently has 146 active GNSS stations distributed throughout the national territory (IBGE 2024). However, not all stations are suitable for estimating soil

moisture using GNSS-IR. This technique has assumptions, primarily related to the characteristics of the reflected signals.

One initial condition is the ground cover in the area of interest, also called the footprint, which should be predominantly exposed soil or low vegetation. This area refers to the surface reflecting the GNSS signals, which can be approximated by a set of ellipses known as Fresnel zones (Geremia-Nievinski & Hobiger 2019). This coverage varies for each station, as the dimensions of each ellipse depend on the height of the antenna, the elevation angle, and the wavelength of the signal. Another requirement is that there must be unobstructed visibility between the GNSS antenna and the ground so that the reflected signals are not affected by obstructions. In this sense, most stations are often not suitable for this application, as they are predominantly located in urban areas near buildings or on paved ground.

A preliminary selection of the stations was made by visually evaluating the surrounding composition using the station memorial provided by IBGE, Google Earth, and Street View. TABLE 1 lists some of the pre-selected stations and their classifications. After the visual assessment of the surrounding areas of the stations, the UFPR station, located in Curitiba-PR, was chosen. Although this station was classified with a 'moderate' status in the visual evaluation presented in TABLE 1, due to the presence of some obstructions such as trees, buildings, metal structures, and mainly a wall, the UFPR station was selected based on the following considerations: 1) defining a methodology using a non-ideal station allows for easier replication in other stations; 2) one of the existing buildings in the area and the metal structures belong to an INMET station. The presence of a nearby INMET station is beneficial, as it allows for a more accurate comparison of the results with the meteorological variables observed by that station; 3) logistical advantages allowed for better control of factors affecting reflections, such as controlling the height of the grass; 4) due to the inclination of the orbital plane of global GNSS satellites, there is an absence of Fresnel zones in the southern direction for stations located in the Southern Hemisphere, and it is in this region that the surrounding buildings of the antenna are located.

TABLE 1 – EXAMPLES OF ANALYZED RBMC STATIONS. THE STRIKETHROUGH LINE (MSCG) REFERS TO A DEACTIVATED STATION. THE BOLDED LINE REFERS TO THE STATION UNDER STUDY IN THIS RESEARCH (UFPR).

Station	Location	% of ground visibility	notes	Status
RSAL	Alegrete - RS	40	Parking	Bad
MSAQ	Aquidauana - MS	90	Bare Soil/fence	Good
SEAJ	São Cristóvão - SE	30	Large Trees/Buildings	Bad
ALAR	Arapiraca - AL	10	Buildings e sidewalk	Bad
SCAQ	Araquari - SC	70	Access roads and trees	Bad
MGBH	B. Horizonte - MG	0	Without ground visibility	Bad
MTCA	Cáceres - MT	90	Cropland/fence	Good
MSCG	C. Grande - MS	70	Inactive Station	Good
MSNV	Naviraí - MS	90	Cropland/fence	Good
SPBO	Botucatu - SP	40	Grassland/Buildings	Moderate
UFPR	Curitiba	70	Grassland/wall	Moderate
BOAV	Boa Vista - RR	80	Bare Soil/fence	Good

SOURCE: The authors (2024).

The UFPR station (FIGURE 2) is located on the Polytechnic Center campus of the Federal University of Paraná. It began operations in 2007, replacing the old PARA station. The structure consists of a pillar with a height of 1.20 meters above the ground, equipped with a forced centering device and an extension. The antenna, a Zephyr 3 Geodetic model (TRM115000.00), has a height of 0.10 meters between the Antenna Reference Point (ARP) and the top of the pillar. The GNSS receiver of this station is a Trimble NETR9. The current antenna and receiver set were installed on April 4, 2018 (IBGE 2024).

The INMET meteorological station, named CURITIBA-A807, is located about 30 meters from the GNSS station. This station is part of a network of automatic stations, consisting of a central memory unit connected to various sensors for measuring meteorological parameters such as atmospheric pressure, air temperature and relative humidity, precipitation, solar radiation, wind direction, and speed (INMET 2024). The data recorded by these sensors are integrated and automatically stored every hour and can be accessed through the INMET portal. Precipitation events, measured by a rain gauge at this station, were used for comparison with the GNSS-IR soil moisture estimates.

FIGURE 2 – UFPR STATION LOCATION

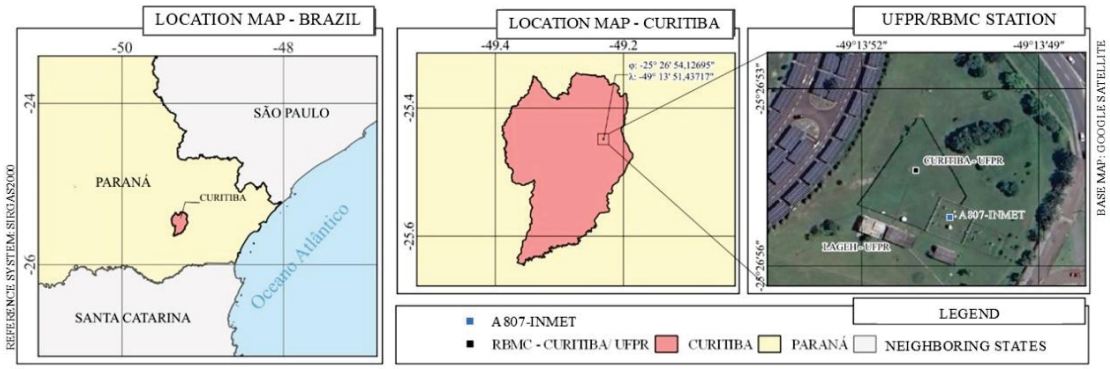

SOURCE: The authors (2024).

2.2 EVALUATION OF REFLECTED SIGNALS

The behavior of reflected signals at the UFPR station was evaluated through visible oscillations in the SNR series. This step is performed by analyzing the oscillations present in the SNR time series, allowing for an estimation of whether the reflections are being affected by obstructions. Obstructions generate noise in the series and impair the pattern of these oscillations. The lower the satellite's elevation angle, the greater the chance of being affected by obstructions around the antenna. Thus, well-defined oscillations near the satellite's rise and set, coming from low elevation angles, indicate the intact reception of reflected signals for the considered azimuth. It is worth noting that GNSS-IR exploits signals from satellites with elevation angles up to 30 degrees, with exceptions for studies addressing specific methodologies.

To perform this step, the RTKPLOT software from the RTKLIB package, version 2.4.2, was used, along with RINEX observation files (RINEX.o) and navigation files (RINEX.n) from the UFPR station for the first week of 2022, each of these files corresponding to 24 hours. This analysis could have been performed with just one day's RINEX files; however, the consistency of the analysis was evaluated over seven days to refine the results. The SNR curves for each combination of satellite and modulation from the GPS and GLONASS systems were assessed.

FIGURE 3A refers to the skyplot, which shows the satellite (G15) trajectories during two passes over the antenna's horizon during the evaluation period. The first pass occurred on the Western (W) portion of the GNSS station, following approximately

the North (N) – South (S) direction. The second pass occurred on the Eastern (E) portion. In FIGURE 3B there is a southeast view of the station, where obstructions such as trees, metal structures, and buildings can be observed.

FIGURE 3 – SKYPLOT, OSCILLATIONS ANALYSIS, AND OBSTRUCTIONS OF UFPR STATION: A. SKYPLOT GPS SATELLITES - L1 SIGNAL, RTKLIB SOFTWARE; B. SOUTHEAST VIEW OF THE RBMC-UFPR STATION; C. OSCILLATION IN RTKLIB SOFTWARE.

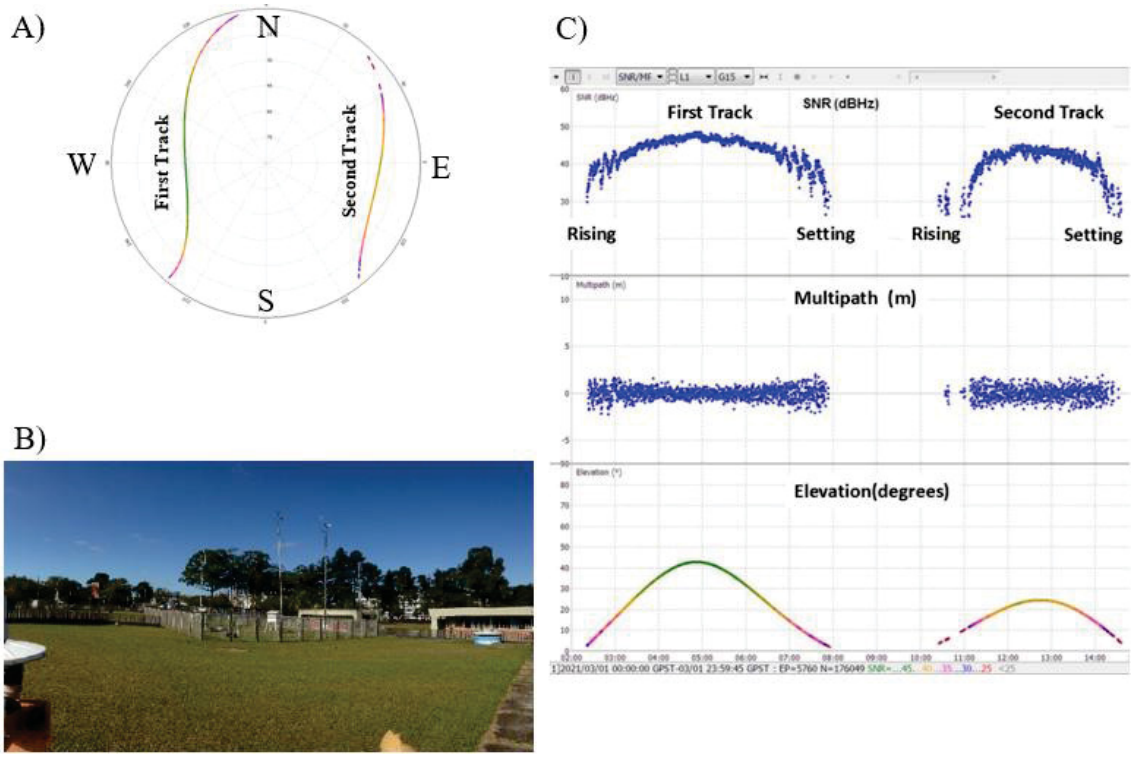

SOURCE: The authors (2024).

Subsequently, an evaluation was conducted using the GNSS-IR Reflection Zone Mapping tool (http://gnss-reflections.org/), which allows for preliminary analyses of the station directly related to GNSS-IR. FIGURE 4 presents the reflection surfaces of the signals (Fresnel zones), considering two scenarios. In the first scenario (FIGURE 4A), the coverage area was defined considering elevation angles between 5° (yellow) and 25° (cyan) with an interval of 5°. The higher the elevation angle, the smaller the semi-major axis of the ellipse. It can be noted that with this configuration, the reflection area encompasses direct obstructions to the reflected signals, such as solar panels (left side), a building, trees, and many metal structures from the meteorological station. In the second scenario (FIGURE 4B), a mask was applied in terms of elevation angles to consider elevation angles between 10 and 15 degrees (10° in yellow, and 20° in

red). In this case, although there is a smaller area, it will be less susceptible to obstructions for the reflected signals, making it more suitable for the technique.

FIGURE 4 – GNSS-IR FOOTPRINT - GNSS-IR REFLECTION ZONE MAPPING: A. ELEVATION ANGLES BETWEEN 5° IN YELLOW AND 25° IN CYAN; B. ELEVATION ANGLES BETWEEN 10° (YELLOW) AND 20° (RED).

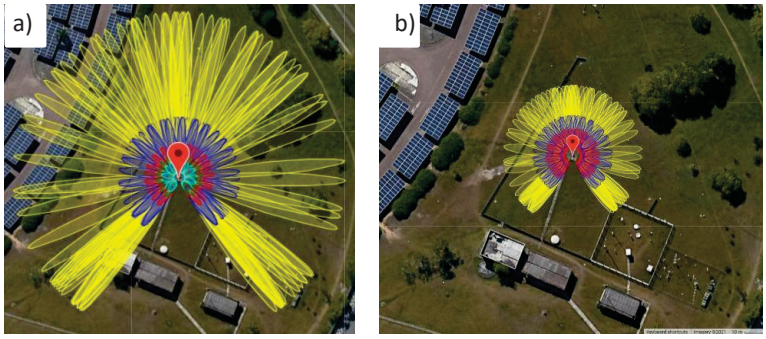

SOURCE: The authors (2024).

The results of this stage were combined with the obstruction mapping to define a filter in terms of azimuth and elevation so that signals from areas with significant obstructions could be disregarded in the processing stage.

2.3 OBSTRUCTION MAPPING

A topographic mapping of the obstructions surrounding the station was conducted to enhance the evaluation of the reflected signals through the SNR series. In this survey, the surrounding elements were categorized and mapped regarding azimuth and elevation, considering a horizontal plane common to the GNSS station. FIGURE 5A shows the obstruction map.

The main obstructions at this station are trees, indicated in green. There are several metal structures in the vicinity, many of which, in the southeastern portion of the area, correspond to the instruments of the meteorological station. Buildings and some concrete lighting poles are indicated in yellow. On average, these obstructions are at an elevation of 5°. The southern portion concentrates most of the buildings, which, in this case, do not significantly affect the oscillations due to the satellites' orbits. Furthermore, the topographic survey indicated that these buildings are below the antenna horizon.

It can be observed that the trees located to the south (on the right in FIGURE 3B) correspond to the most significant obstructions, with approximately 20 degrees from the antenna horizon. This leads to a greater restriction in terms of elevation angles in the surroundings. The metal structures of the meteorological instrumentation can also be seen. These obstructions may affect the reflected signals at low elevation angles; therefore, these conditions were taken into account in the processing configurations of the reflectometry algorithm.

FIGURE 5B shows a panoramic view of the northeastern portion of the UFPR station. The largest obstruction in this case is a tree in the center of the image, which has an elevation of approximately 7 degrees above the antenna horizon. In FIGURE 5C, the western portion of the station can be seen. As can be observed, the Western area has significantly fewer obstructions. The height of the wall is below the GNSS antenna horizon. Furthermore, well-defined oscillations originating from this region were observed by analyzing the oscillations.

FIGURE 5 - UFPR STATION SURROUNDINGS: A. OBSTRUCTION MAPPING OF RBMC-UFPR; B. UFPR STATION SURROUNDINGS – NORTHEAST DIRECTION; C. UFPR STATION SURROUNDINGS – WEST DIRECTION.

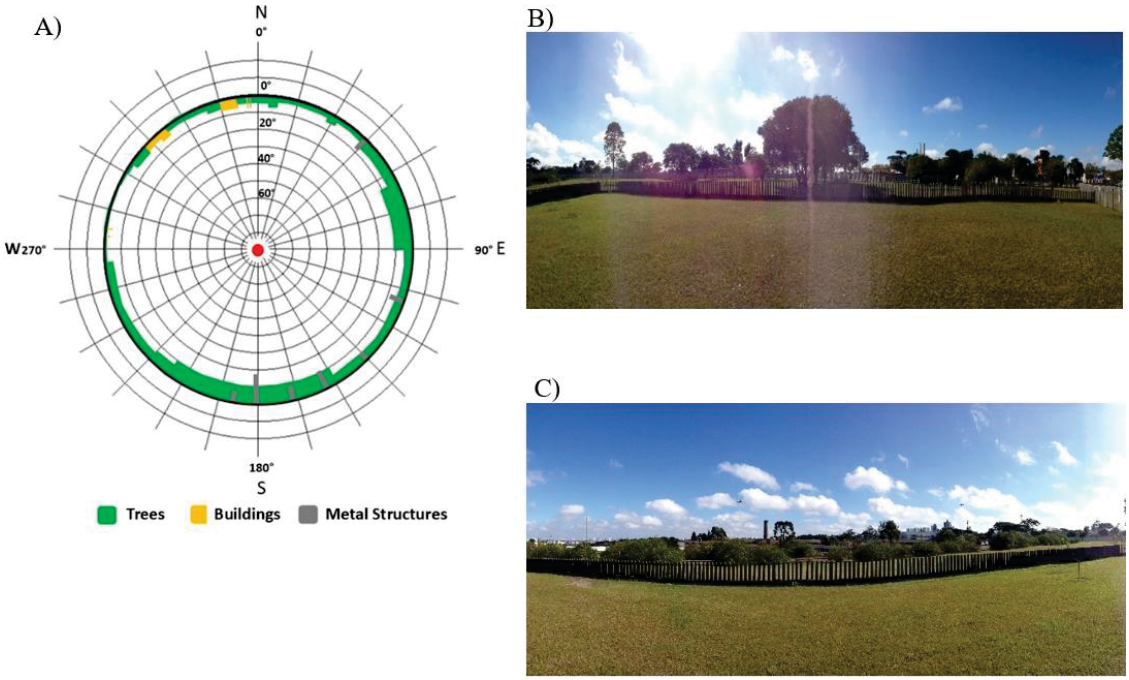

SOURCE: The authors (2024).

Based on the evaluation stages of the reflected signals, it was observed that the signals coming from satellites close to the horizon (low elevation angles) were being affected by the surrounding obstructions. The combination of this information, along with assessments made during the quality control of the processing, will enable the establishment of a mask that defines the appropriate GNSS-IR coverage area for the UFPR station.

2.4 INPUT DATA

The input data for the reflectometry algorithm are SNR information recorded in GNSS tracking files in the standard observation RINEX format (.o), in version 3 or higher, as from this version the SNR observable is recorded separately for each combination of GNSS signals in terms of frequency and available code. Since January 1, 2020, IBGE has been providing 1-second tracking files in RINEX version 3 format.

The equipment that makes up the UFPR station is multi-GNSS. Thus, various signals are recorded, including legacy signals and modern signals such as L5, L2C, and L1C. The signals from the GPS (G) and GLONASS (R) systems were used in this research, totaling 24 signals, 12 for each system, indicated here according to the Rinex nomenclature standard: G - C1C, C2W, C2X, C5X, L1C, L2W, L2X, L5X, S1C, S2W, S2X, and S5X; R - C1C, C1P, C2C, C2P, L1C, L1P, L2C, L2P, S1C, S1P, S2C, S2P.

Access to the RINEX files recorded by the UFPR station can be done through the IBGE website. The files are provided as daily files for each station and are downloaded individually. Accessing the SNR observations from the RBMC for a given station and day requires: 1 – Download; 2 – Decompression of the file (.gz to .crx); 3 – Decompression of the compressed Rinex file (.crx to .rnx).

In this research, a period of 1 year (2022) was chosen for the investigations, based on several considerations: a complete year encompasses phenomena related to the different seasons, allowing for more consistent analyses of soil moisture patterns; since 2021, it has been possible to access GNSS data from the station with 1-second recording in RINEX format 3; from this period, there has been a gradual return to in-person activities in the context of the COVID-19 pandemic, so regular mowing activities around the station were already occurring normally; furthermore, as of November 27, 2022, the International GNSS Service (IGS) began adopting the

IGS20 reference system, replacing IGb14 (IGS 2022; Altamini et al. 2021). This change requires an adaptation of the employed reflectometry algorithm.

In addition to the procedures for obtaining the RINEX files, the reflectometry algorithm requires that these files for the entire period of interest be in the same directory, properly organized with standard and sequential nomenclature, as per the example: ufpr0010.22o, where: "ufpr" is the station code; 001 is the day of the year (DOY - Day of Year), which can be checked using the GNSS Calendar tool (https://www.gnsscalendar.com/); "0" is the 8th digit, indicating the duration of the file is 24 hours, completing the standard RINEX nomenclature format with 8 digits. The extension ".22o" is the standard RINEX format to indicate the year corresponding to the file (2022) and the type of file, in this case, the observation file (.o). Other types of RINEX files, such as navigation files, e.g., .22n, are not used in reflectometry processing, as the algorithm automatically downloads the precise ephemerides during processing.

The exclusion of unnecessary observables for this processing is recommended. Thus, the carrier phase and pseudorange data also present in the observation files can be filtered out, as this information is not used in the reflectometry modeling. This filtering improves processing efficiency by reducing memory space.

Automating data processing is recommended when managing large volumes of information. In this context, an algorithm was developed in Python to download, convert, standardize, and filter GNSS data from the RBMC. Following IBGE guidelines, this algorithm was designed to prepare input data for any RBMC station by simply providing the station code and the period of interest. This algorithm makes it possible to automatically obtain RINEX files for the indicated period, for positioning or GNSS-IR. The algorithm is freely available on the GitHub platform (https://github.com/jorgeeuriques/gnssdata_rbmc). This algorithm includes the use of the tools crx2rnx (Hatanaka 2008), and gfzrnx (Nischan 2016). FIGURE 6 illustrates the flowchart of the algorithm's steps.

FIGURE 6 - PYTHON ALGORITHM PROCESSING FLOW.

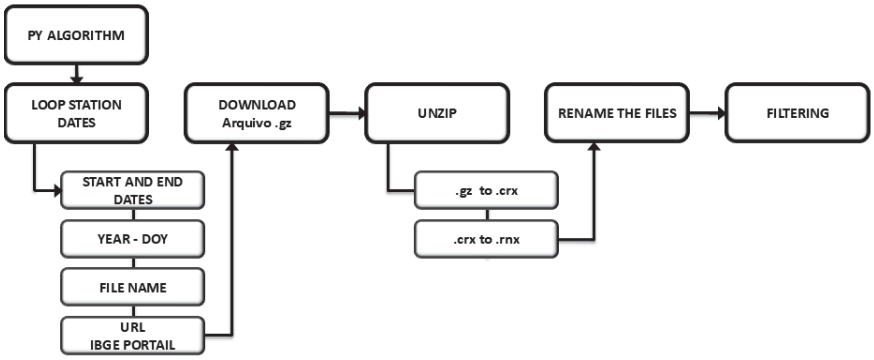

SOURCE: The authors (2024).

2.5 REFLECTOMETRIC ALGORITHM

The employed reflectometric algorithm (Nievinski & Larson 2014a, 2014b, 2014c, 2014d) enables SNR modeling to facilitate GNSS-IR through two stages: inversion and post-processing. In the first stage, a combination of a physical model, related to the theoretical simulation of multipath, and an inverse model, through which parameters are estimated from GNSS observations measured in the field, is performed. The various configurations associated with these processes in the algorithm are crucial for obtaining consistent results.

Among these configurations are: satellite observation conditions; reference system; signal processing parameters; GNSS antenna electromagnetic responses; conditions related to reflections involving the reflecting surface; propagation medium; and parameter biases. Next, post-processing is carried out, which involves a quality control process and refinement of previously estimated parameters. In the case of processing to estimate soil moisture, values of the reflectometric phase are of particular interest (Euriques et al. 2021).

The algorithm in question is highly automated; however, during the post-processing stage, some interventions were necessary to define strategies that allowed the refinement of the results. These strategies included the introduction of constraints on certain correlated parameters, such as the antenna height and the reflectometric phase measurements, derived from the SNR series. Additionally, based on the results of this stage, new processing steps were conducted to adjust some configurations, such as applying azimuth and elevation angle masks to disregard directions affected by obstructions. These filters were applied by combining analyses performed with the

RTKLIB software, the GNSS-IR Reflection Zone Mapping tool, and the topographic mapping, along with the analysis of the reflectometric processing results. Elevation masks were applied with three configurations: 0º to 30º; 5º to 30º; and 10º to 30º. The azimuth mask was gradually expanded, yielding better results when applied over the entire eastern portion of the station.

As a main result of these processes, reflectometric phase time series were obtained for each signal. All 24 signals, GPS and GLONASS, listed in section 2.4, were processed, with one processing run for each of these modulations. Other configurations were adjusted to present these results, which were refined by applying a moving average. A moving average is applied during the post-processing stage of the reflectometric algorithm to smooth short-term fluctuations and highlight trends in the phase time series. The moving average settings should be carefully evaluated to ensure an appropriate representation of the variables of interest.

Finally, after the reflectometric processing, an additional step was required to convert the reflectometric phase time series into soil moisture time series. This was accomplished through a calibration curve using theoretical coefficients indicated in the literature (Chew et al. 2014). The best results of this stage were achieved with the GS2X and RS2P signals. The time series obtained from these signals were compared with the precipitation events recorded by the INMET 807 station.

3 RESULTS AND DISCUSSIONS

In FIGURES 7A and 7B the results of SNR modeling in the reflectometric processing can be observed. In red, the simulated SNR from the direct model is shown. In gray, the observed SNR adapted in the inversion module is displayed. In blue, the residual SNR represents the difference between the simulated and observed SNR. These figures are generated for each modulation, satellite (PRN), and segment (ascending or descending arc of the satellite's position) within a given quadrant. FIGURE 7A corresponds to the SNR modeling of GPS satellite PRN08, DOY 001 (01/01/2022) at azimuth 220, considering the GS5X signal.

It can be indicated that the processing under these conditions was adequate, as the observed SNR series (dB) closely follows the simulated series, with residuals of ±1 dB. In FIGURE 7B, the same configurations are applied, but for the GS2X signal. In this case, the magnitude of the residuals is around ±2 dB. Although the GS2X signal

shows a larger residual amplitude, it is worth noting that it was available on 24 satellites in 2022, while the GS5X signal was only available on 16 satellites. The L5 carrier presented a smaller magnitude of residuals; however, in addition to being associated only with GPS, it is not available for all satellites in this system. Thus, the SNR from the L2 carrier provided the best results in the processing stage for both evaluated systems, G and R. These findings are consistent with those reported in previous research, such as in Euriques (2019).

FIGURE 7 - SNR PLOTS BY REFLECTOMETRIC ALGORITHM: A. SNR PLOT BY GS5X SIGNAL, AZIMUTH 220, DOY 001; B. SNR PLOT BY GS2X SIGNAL, AZIMUTH 220, DOY 001.

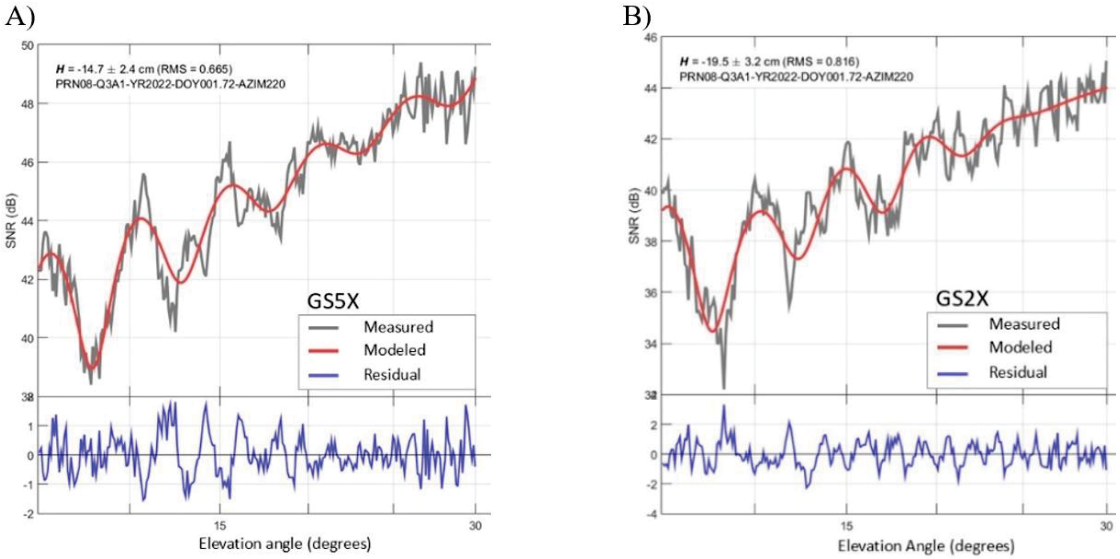

SOURCE: The authors (2024).

As with any modeling process, uncertainties are associated with the estimated parameters, which can be influenced, e.g. by the growth of vegetation around the antenna. Generally, it should be noted that the same satellite will have a series of figures associated with it, representing the daily measurements by satellite, quadrant, year, and day. These figures were investigated as a complementary step to the prior evaluation of oscillations. The analysis of residuals also contributed to identifying azimuths that did not provide good reflections or were affected by obstructions.

The combination of these factors allowed for the establishment of masks in terms of azimuths or elevation angles in post-processing to filter the data. It was found that the best elevation angle mask used only the range between 10º and 30º above the antenna horizon. It should be noted that a very restrictive mask can affect the

estimates, so it must be applied with caution. Additionally, the higher the elevation angle, the smaller the ellipses that compose the Fresnel surface, thus reducing the reflection area, which limits one of the advantages of GNSS-IR over other conventional soil moisture estimation techniques.

In FIGURES 8A and 8B, the biases and antenna height variation are presented for the different clusters defined by data grouping based on the satellite's azimuthal track. In FIGURE 8B, an azimuth mask was applied to filter the range defined by azimuths from 0 to 210. In the case of a flat and horizontal surface, radial variability would be due only to estimation residuals. However, in practice, this variability occurs due to various factors, including instrumental noise, irregular surrounding topography, and genuine natural variability caused by vegetation growth around the station. These characteristics complicate the automation of this process.

FIGURE 8 - ANTENNA HEIGHT BIASES AS A FUNCTION OF AZIMUTH: A. BEFORE FILTERING; B. AFTER FILTERING

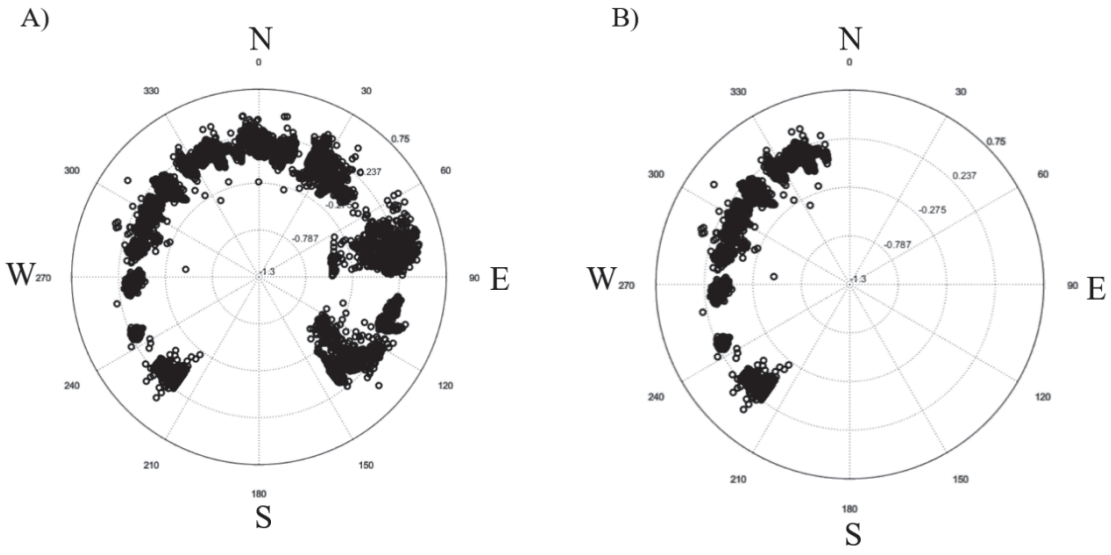

SOURCE: The authors (2024).

Regarding the moving average settings applied to the reflectometric phase time series, the hourly spacing was defined (1 phase value per hour), and different window widths were evaluated. Finally, from the reflectometric phase series, soil moisture is obtained through a calibration curve, which is applied after the processing by the reflectometric software. The theoretical coefficients of the calibration curve frequently reported in the literature the slope or angular coefficient $\mathrm{a} = 0{,}015\ \mathrm{m^3 m^{-3 o-1}}$

(Chew et al. 2014) or reciprocally $a^{-1} = 65\,°/(\mathrm{m}^3/\mathrm{m}^3)$ (Vey et al. 2016). This means that a change of 1° in phase corresponds to a change of 0.015 m³/m³ in the soil moisture content. These coefficient values were determined from physical simulations, considering the specific antenna models of the study receivers. The intercept or constant coefficient of the regression (b) is associated with the residual soil moisture, which represents the minimum soil moisture value, usually assumed to be $b = 0{,}05\ \mathrm{m}^3\mathrm{m}^{-3}$(Vey et al. 2016). According to Chew et al. (2014), this coefficient can also be obtained by interpolation of soil texture maps. This minimum soil moisture value is associated with a minimum phase, which, in turn, depends on the antenna model used and can take an arbitrary value based on the characteristics of the considered station.

FIGURE 9 illustrates the reflectometric phase series (in degrees) throughout the epochs of the year 2022 (decimal year), obtained from the GS2X signal with a window width of the moving average of 6h. It is observed that the series is interrupted around 2022.9. This happens because the period between 2022.9 and 2022.10 corresponds to the satellite orbit reference system change, officially adopted by the IGS, took place.

FIGURE 9 - REFLECTOMETRIC PHASE

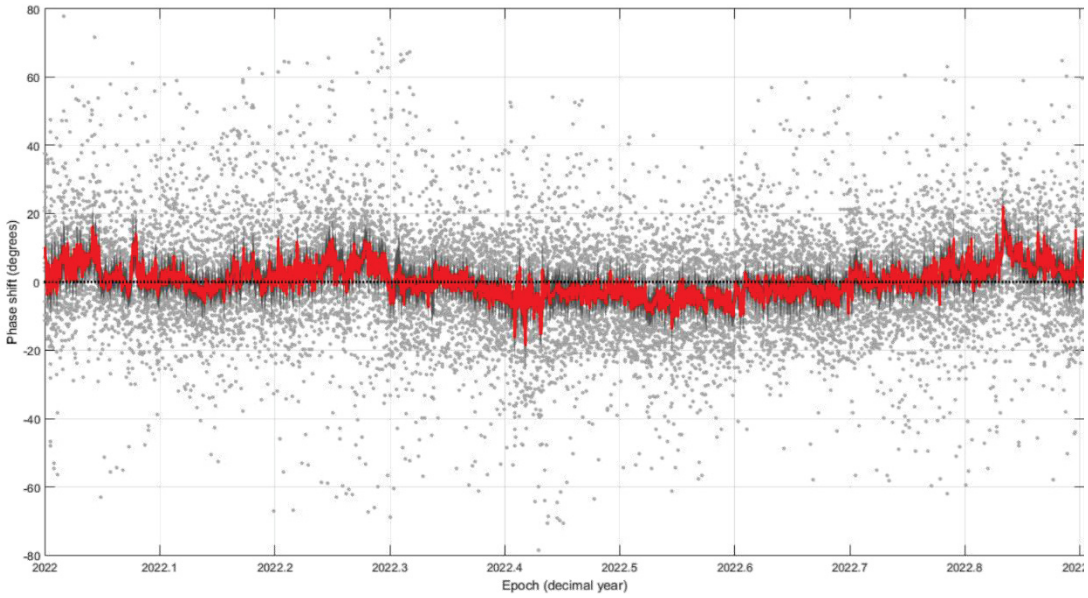

SOURCE: The authors (2024).

FIGURE 10 shows the soil moisture series derived from the reflectometric series presented in Figure 9. In this series, soil moisture ranges between 0 and 0.4

m³/m³. It is noted that the series is discontinued at epoch 2022.9, which coincides with the period when the reference system for satellite orbits was changed.

FIGURE 10 - SOIL MOISTURE TIME SERIES: GNSS-IR– GS2X

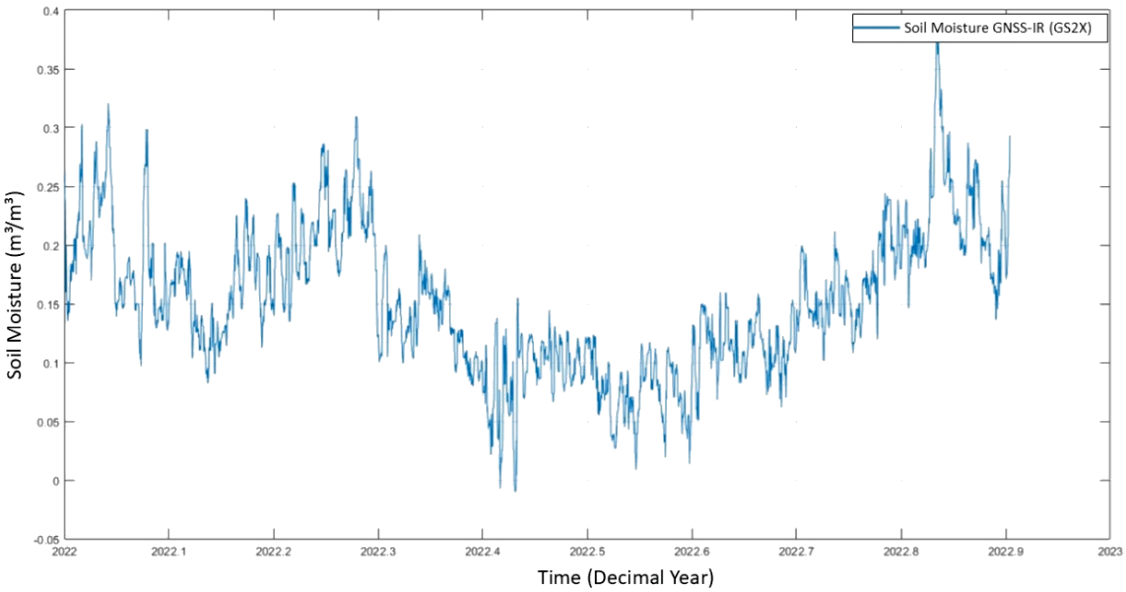

SOURCE: The authors (2024).

The precipitation events were plotted by downloading the data provided by INMET to compare them with the resulting soil moisture series. It was identified that the RS2P signal, specifically the precise signal of the L2 carrier wave from GLONASS, showed the best correspondence with the precipitation events when considering the same processing configurations. In the upper panel of FIGURE 11, the soil moisture series estimated from the RS2P signal is shown. It can be observed that, in this case, the moisture varies approximately between 0 and 0.35 m³/m³. For GLONASS, the series is normally represented throughout the entire year of 2022, even after the transition from IGb14 to IGS20 (2022.9). The precipitation graph (mm/day) for the year is presented in the lower panel.

Soil moisture varies with depth and also horizontally due to several factors. In the more superficial layers, moisture variation is greater due to the direct effects of precipitation, evaporation, and runoff. The reference depth for soil moisture estimates using GNSS-IR is associated with more superficial layers, with depths of up to 5 cm, due to the penetration power of electromagnetic waves related to GNSS frequencies in the soil (Edokossi et al. 2020). Therefore, it is expected that soil moisture estimated

by GNSS-IR will exhibit a highly variable behavior, as evidenced in FIGURE 10, where the moving average configurations resulted in less data smoothing compared to what is seen in FIGURE 11. When comparing with precipitation events, it is advisable to use more restrictive moving average settings to highlight more consistent phenomena, such as the direct contribution of precipitation to soil moisture.

Analyzing FIGURE 11, it is noticeable that the peaks in soil moisture occur simultaneously with precipitation events, as shown in situation 1 in the upper panel. In this regard, it is important to emphasize that the moving average settings, especially in terms of window width, should be carefully configured, as they can excessively smooth out isolated events.

FIGURE 11 - SOIL MOISTURE TIME SERIES X PRECIPITATION EVENTS

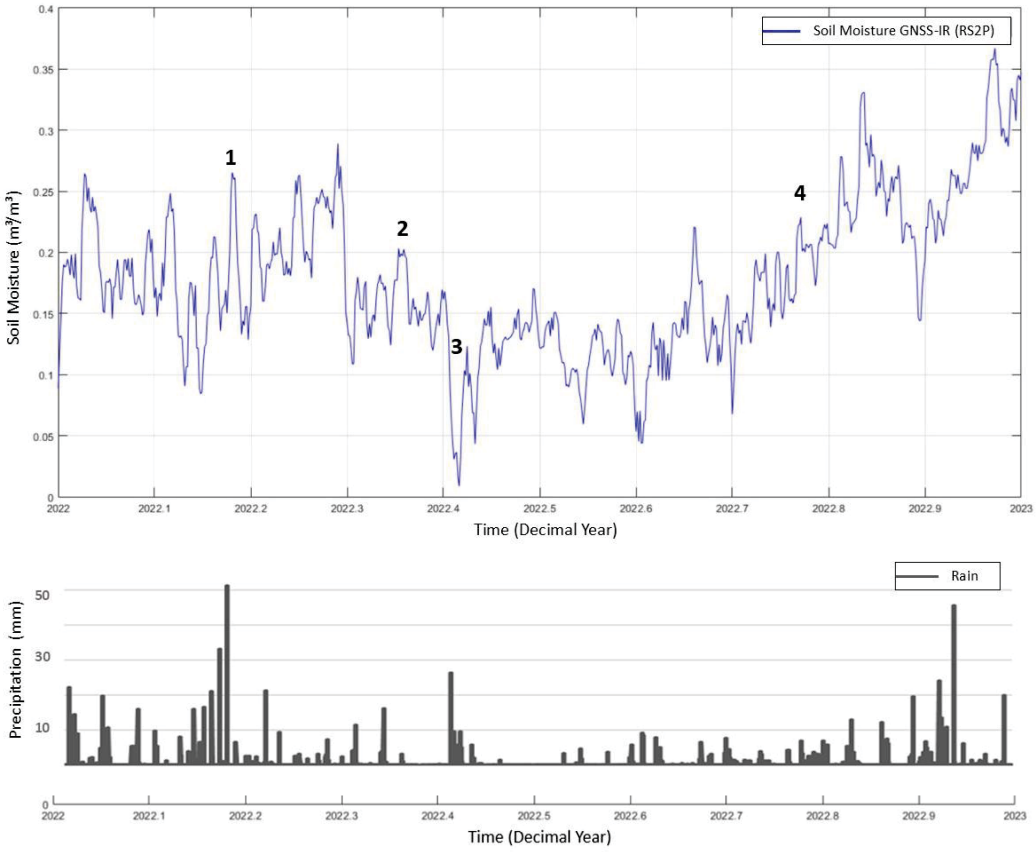

FONTE: The authors (2024).

It is observed that when the soil is relatively dry and precipitation events occur, moisture moves downward more slowly, initially remaining closer to the surface (scenario 2). When the soil is wetter and precipitation events occur, the opposite

process happens: the surface soil loses moisture more quickly (scenario 3), remaining wetter at greater depths. From epoch 2022.7, after a period of relatively regular maximum precipitation peaks, and increasingly higher after 2022.8, a growing trend of increased soil moisture emerges (scenario 4).

4 CONCLUSIONS

Based on the presented results, it is possible to affirm that the continuously recorded data from the UFPR station of the RBMC was successfully used to estimate soil moisture around the station using the GNSS-IR technique. The results show correspondence with precipitation events recorded by a rain gauge from INMET located near the GNSS station.

Investigations were carried out to make a methodology for estimating soil moisture feasible for other RBMC stations that meet the requirements of the GNSS-IR technique. In this regard, the development of a Python algorithm for downloading, converting, standardizing, and filtering GNSS data, based on the data available on the IBGE portal, is highlighted. This algorithm is available on the GitHub platform. It can be used to automate the preparation of GNSS data from any RBMC station to GNSS-IR or positioning applications. An evaluation of the configurations of the employed reflectometric algorithm was carried out, including elevation and azimuth masks defined by a combination of oscillation assessments using RTKLIB software and the GNSS-IR Reflection Zone Mapping tool, as well as a topographic survey.

Additionally, the results were evaluated based on different signals defined by the modulation/frequency combination of GPS and GLONASS. The best results are associated with the L2 carrier wave. Thus, it is considered that opportunistic soil moisture monitoring using GNSS-IR from RBMC stations can be carried out at a low cost, since no modifications to the existing equipment are necessary and the data is distributed free of charge by IBGE. The results can be made available to the public and may improve the modeling of various phenomena. In this way, they can contribute to national institutions such as the Brazilian Agricultural Research Corporation (In Portuguese, Empresa Brasileira de Pesquisa Agropecuária - EMBRAPA), the National Center for Monitoring and Early Warning of Natural Disasters (In Portuguese Centro Nacional de Monitoramento e Alerta de Desastres Naturais - CEMADEN), the National Water Agency (In Portuguese, Agência Nacional das Águas - ANA), and INPE.

In future works, it is recommended to validate the results using data from conventional soil moisture measurement sensors, such as TDR probes, as well as data obtained from satellite missions, which could contribute to direct analyses of soil moisture results.

Acknowledgments

The authors would like to thank colleagues Prof. Paulo Sergio de Oliveira Junior (UFPR), Allan Gomes (IFSC), and Fabiano Freiman (UFBA) for their contributions to the work. The authors would like to thank CNPq (grant number 406486/2023-9) for its support in financing the project *'Métodos geodésicos aplicados à estimação da umidade do solo e do total de água armazenada*,' in which this research is included. The work of J. F. Euriques was supported by, the Brazilian Coordination of Superior Level Staff Improvement (CAPES) process Nº 88882.382285/2019-01.

REFERENCES

ACHARYA, T. D., LEE, D. H. 2019, 'Remote sensing and geospatial technologies for sustainable development: A review of applications', **Sensors and Materials**, vol. 31, n. 11, pp. 3931–45.

ALTAMIMI, Z., REBISCHUNG, PP., MÉTIVIER, L., COLLILIEUX, X. 2016, 'ITRF2014: A new release of the International Terrestrial Reference Frame modeling nonlinear station motions', **Journal of Geophysical Research**: Solid Earth, vol. 121, n. 8, pp. 6109–31.

ALTAMIMI, Z., REBISCHUNG, PP., MÉTIVIER, L., COLLILIEUX, X. 2021, 'ITRF2020: An enhanced realization of the International Terrestrial Reference Frame', **Journal of Geophysical Research: Solid Earth**, vol.126, n.10, e2020JB021490. DOI: 10.1029/2020JB021490

ARROYO, A. A., CAMPS, A., AGUASCA, A., et al. 2014, 'Dual-polarization GNSS-R interference pattern technique for soil moisture mapping', **IEEE Journal of Selected Topics in Applied Earth Observations and Remote Sensing**, vol. 7, n. 5, pp. 1533–44.

AWANGE, J. L., KYALO KIEMA, J. B. 2013, **Environmental Geoinformatics**. Berlin, Heidelberg: Springer Berlin Heidelberg.

BABAEIAN, E., SADEGHI, M., JONES, S. B., et al. 2019, 'Ground, Proximal, and Satellite Remote Sensing of Soil Moisture', **Reviews of Geophysics**, vol. 57, n. 2, pp. 530–616. https://doi.org/10.1029/2018RG000618.

CHEW, C. C., SMALL, E. E., LARSON, K. M., ZAVOROTNY. 2014, 'Effects of near-surface soil moisture on GPS SNR data: Development of a retrieval algorithm for soil moisture', **IEEE Transactions on Geoscience and Remote Sensing**, vol. 52, n. 1, pp. 537–43.

EDOKOSSI, K., CALABIA, A., JIN, S., MOLINA, I. 2020, 'Gnss-reflectometry and remote sensing of soil moisture: A review of measurement techniques, methods, and applications', **Remote Sensing**, vol. 12, n. 4.

ENTEKHABI, D., NJOKU, E. G., O'NEILL, PP. E., et al. 2010, 'The soil moisture active passive (SMAP) mission', **Proceedings of the IEEE**, vol. 98, n. 5, pp. 704–16.

EURIQUES, J. F. 2019, **'Determinação da umidade do solo por meio da técnica de Refletometria GNSS – Primeiros resultados no Brasil'**, Dissertação de mestrado, Universidade Federal do Paraná.https://acervodigital.ufpr.br/bitstream/handle/1884/62323/R - D - JORGE FELIPE EURIQUES.pdf?sequence=1&isAllowed=y

EURIQUES, J. F., KRUEGER, C. PP., MACHADO, W. C., SAPUCCI, L. F., GEREMIA-NIEVINSKI, F. 2021, 'Soil Moisture Estimation with GNSS Reflectometry: A Conceptual Review', **Revista Brasileira de Cartografia**, vol. 73, n. 2, pp. 413–34.

GEORGIADOU, PP. Y., KLEUSBERG, A. 1988, 'On Carrier Signal Multipath Effects in Relative GPS Positioning', **Map Collector,** vol. 13, pp. 172–79.

GEREMIA-NIEVINSKI, F., HOBIGER, T. 2019, '**Site guidelines for multi-purpose GNSS reflectometry stations**'.

HATANAKA, Y. 2008, '**A Compression Format and Tools for GNSS Observation Data', Bulletin of the Geospatioal Information Authority of Japan**, 55, pp. 21-30. https:/www.gsi.go.jp/ENGLISH/Bulletin55.html

HILLEL, D. 1998, **Environmental Soil Physics**. 1st edn, Academic Press, San Diego.

INSTITUTO BRASILEIRO DE GEOGRAFIA E ESTATÍSTICA. RBMC - **'Rede Brasileira de Monitoramento Contínuo dos Sistemas GNSS Relatório de Informação de Estação UFPR - Curitiba**.' Rio de Janeiro, RJ, 2024.

INTERNATIONAL GNSS SERVICE (IGS). **'Adoption of IGS20 Reference Frame,** 2022. https://igs.org

INSTITUTO NACIONAL DE METEOROLOGIA. **Climatologia: Dados e informações climáticas**. INMET, 2023. Disponível em: http://www.inmet.gov.br. Acesso em: 10 jun. 2024.

JIN, S., CARDELLACH, E., XIE, F. 2014, '**Remote Sensing and Digital Image Processing: Theory, Methods and Applications**'. Springer International Publishing, 2014.

LARSON, K.M. 2024, 'Gnssrefl: an open source software package in python for GNSS interferometric reflectometry applications', **GPS Solut**, vol.28, no.165. https://doi.org/10.1007/s10291-024-01694-8

LARSON, K. M., BRAUN, J. J., SMALL, E. E., et al. 2010, 'GPS Multipath and Its Relation to Near-Surface Soil Moisture Content', **IEEE Journal of Selected Topics in Applied Earth Observations and Remote Sensing,** vol. 3, n. 1, pp. 91–99.

LARSON, K. M., NIEVINSKI, F. G. 2013, 'GPS snow sensing: Results from the EarthScope Plate Boundary Observatory', **GPS Solutions**, vol. 17, n. 1, pp. 41–52.

LARSON, K. M., SMALL, E. E., GUTMANN, E., et al. 2008a, 'Using GPS multipath to measure soil moisture fluctuations: Initial results', **GPS Solutions,** vol. 12, n. 3, pp. 173–77.

LARSON, K. M., SMALL, E. E., GUTMANN, E. D., et al. 2008b, 'Use of GPS receivers as a soil moisture network for water cycle studies', **Geophysical Research Letters**, vol. 35, n. 24.

LEICK, A. 1995, **GPS Satellite Surveying**, 2nd edn, John Wiley & Sons, New York, USA.

LI Y, YU K, LI J, JIN T, CHANG X, ZHANG Q, YANG S, 2022, 'Measuring soil moisture with refracted GPS signals', **IEEE Geosci Remote Sens Lett**, vol. 19, pp.1–5. https://oi.org/10.1109/LGRS.2022.3161409

MARTÍN, A., IBÁÑEZ, S., BAIXAULI, C., et al. 2020, '**Multi-constellation GNSS interferometric reflectometry with mass-market sensors as a solution for soil moisture monitoring**' , pp. 3573–82.

NISCHAN, T. 2016, '**GFZRNX - RINEX GNSS Data Conversion and Manipulation Toolbox'. GFZ Data Services**. http://dx.doi.org/10.5880/GFZ.1.1.2016.002

NIEVINSKI, F. G., LARSON, K. M. 2014a, 'Forward modeling of GPS multipath for near-surface reflectometry and positioning applications', **GPS Solutions**, vol. 18, n. 2, pp. 309–22.

NIEVINSKI, F. G., LARSON, K. M. 2014b, 'An open source GPS multipath simulator in Matlab/Octave' **GPS Solutions**, vol. 18, n. 3, pp. 473–81.

NIEVINSKI, F. G., LARSON, K. M. 2014c, 'Inverse modeling of GPS multipath for snow depth estimation - Part I: Formulation and simulations', **IEEE Transactions on Geoscience and Remote Sensing,** vol. 52, n. 10, pp. 6555–63.

NIEVINSKI, F. G., LARSON, K. M. 2014d, 'Inverse modeling of GPS multipath for snow depth estimation - Part II: Application and validation', **IEEE Transactions on Geoscience and Remote Sensing,** vol. 52, n. 10, pp. 6564–73, 2014d.

NIEVINSKI, F. G., SILVA, M. F. E., BONIFACE, K., MONICO, J. F. G. 2016, 'GPS Diffractive Reflectometry: Footprint of a Coherent Radio Reflection Inferred from the Sensitivity Kernel of Multipath SNR', **IEEE Journal of Selected Topics in Applied Earth Observations and Remote Sensing,** vol. 9, n. 10, pp. 4884–91.

OCHSNER, T. E., COSH, M. H., CUENCA, R. H., et al. 2013, 'State of the Art in Large-Scale Soil Moisture Monitoring', **Soil Science Society of America Journal**, vol. 77, n. 6, pp. 1888–1923.

PAGANINI, M., PETITEVILLE, I., WARD, S., et al. 2018, '**Satellite Earth Observations in support of the Sustainable Development Goals**', European Space Agency (ESA).

PLAG, H. PP., PEARLMAN, M. 2009, Geodetic Global System Observing.

ROBINSON, D. A., CAMPBELL, C. S., HOPMANS, J. W., et al. 2008, 'Soil Moisture Measurement for Ecological and Hydrological Watershed-Scale Observatories: A Review', **Vadose Zone Journal**, vol. 7, n. 1, pp. 358–89.

RODRIGUEZ-ALVAREZ, N., BOSCH-LLUIS, X., CAMPS, A., et al. 2009, 'Soil moisture retrieval using GNSS-R techniques: Experimental results over a bare soil field', **IEEE Transactions on Geoscience and Remote Sensing**, vol. 47, n. 11, pp. 3616–24.

ROUSSEL, N., FRAPPART, F., RAMILLIEN, G., et al. 2016, 'Detection of Soil Moisture Variations Using GPS and GLONASS SNR Data for Elevation Angles Ranging from 2° to 70°', **IEEE Journal of Selected Topics in Applied Earth Observations and Remote Sensing**, vol. 9, n. 10, pp. 4781–94.

ROUSSEL, N., RAMILLIEN, G., FRAPPART, F., et al. 2015, 'Sea level monitoring and sea state estimate using a single geodetic receiver', **Remote Sensing of Environment**, vol. 171, pp. 261–77. http://dx.doi.org/10.1016/j.rse.2015.10.011

SEEBER, G. 2003, **Satellite Geodesy: Foundations, Methods, and Applications**. 2nd edn, New York.

SENEVIRATNE, S. I., CORTI, T., DAVIN, E. L., et al. 2010, 'Investigating soil moisture-climate interactions in a changing climate: A review', **Earth-Science Reviews**, vol. 99, n. 3–4, pp. 125–61.

SIMON, P., HOLLINGSWORTH, A., CARLI, B., et al. 2006, '**The Changing Earth : New scientific challenges for ESA's Living Planet Programme**', ESA Publications Division.

TABIBI, S., NIEVINSKI, F. G., VAN DAM, T. 2017, 'Statistical Comparison and Combination of GPS, GLONASS, and Multi-GNSS Multipath Reflectometry Applied to Snow Depth Retrieval', **IEEE Transactions on Geoscience and Remote Sensing**, vol. 55, n. 7, pp. 3773–85, 2017.

TABIBI, S., NIEVINSKI, F. G., VAN DAM, T., MONICO, J. F. G. 2015, 'Assessment of modernized GPS L5 SNR for ground-based multipath reflectometry applications', **Advances in Space Research,** vol. 55, n. 4, pp. 1104–16.

TEUNISSEN, PP. J. G., MONTENBRUCK, O. (Ed) 2017, **Springer Handbook of Global Navigation Satellite Systems**, Springer International Publishing.

VEY, S., GÜNTNER, A., WICKERT, J., BLUME, T., RAMATSCHI, M. 2016, 'Long-term soil moisture dynamics derived from GNSS interferometric reflectometry: a case study for Sutherland, South Africa', **GPS Solutions**, vol. 20, n. 4, pp. 641–54.

WANG Q, ZHENG Y, XU S, ZHOU G, YU J. 2022, 'In situ mesoscale soil moisture content monitoring based on global navigation satellite system interferometric reflectometry and ensemble modeling', **J Appl Remote Sens** vol.16, n. 02, pp.1–17. https://doi.org/10.1117/1.jrs.16.024505

WEI H, YANG X, PAN Y, SHEN F. 2023, 'GNSS-IR Soil Moisture Inversion Derived from Multi-GNSS and Multi-Frequency Data Accounting for Vegetation Effects', **Remote Sensing**, vol.15 n. 22. https://doi.org/10.3390/rs15225381

WU, X., MA, W., XIA, J., et al. 2021, 'Spaceborne GNSS-R soil moisture retrieval: Status, development opportunities, and challenges', **Remote Sensing**, vol. 13, n. 1, pp. 1–24, 2021.

YAN, S. H., ZHANG, N., CHEN, N. C., GONG, J. Y. 2018, 'Feasibility of using signal strength indicator data to estimate soil moisture based on GNSS interference signal analysis', **Remote Sensing Letters,** vol. 9, n. 1, pp. 61–70. https://doi.org/10.1080/2150704X.2017.1384587

YANG, T., WAN, W., CHEN, X., et al. 2019, ' Land surface characterization using BeiDou signal-to-noise ratio observations', **GPS Solutions**, vol. 23, n. 2, pp. 1–12. http://dx.doi.org/10.1007/s10291-019-0824-4

YANG, T., WAN, W., CHEN, X., CHU, T., HONG, Y. 2017, 'Using BDS SNR observations to measure near-surface soil moisture fluctuations: Results from low vegetated surface', **IEEE Geoscience and Remote Sensing Letters,** vol. 14, n. 8, pp. 1308–12.

ZAVOROTNY, VOL. U., Gleason, S., Cardellach, E., Camps, A. 2014, 'Tutorial on remote sensing using GNSS bistatic radar of opportunity', **IEEE Geoscience and Remote Sensing Magazine**, vol. 2, n. 4, pp. 8–45.

ZAVOROTNY, V. U., VORONOVICH, A. G. 2000, 'Scattering of GPS signals from the ocean with wind remote sensing application', **IEEE Transactions on Geoscience and Remote Sensing**, vol. 38, n. 2, pp. 951–64.

ZHANG, S., ROUSSEL, N., BONIFACE, K., et al. 2017, 'Use of reflected GNSS SNR data to retrieve either soil moisture or vegetation height from a wheat crop', **Hydrology and Earth System Sciences**, vol. 21, n. 9, pp. 4767–84.

ZHANG, X., NIE, S., ZHANG, C., ZHANG, J., CAI, H. 2021, 'Soil moisture estimation based on triple-frequency multipath error', **International Journal of Remote Sensing**, vol. 42, n. 15, pp. 5953–68. https://doi.org/10.1080/01431161.2021.1933246

3 CONCLUSIONS AND RECOMMENDATIONS

3.1 CONCLUSIONS

This research presented investigations through specific case studies involving different characteristics of GNSS-IR station setups and processing configurations for soil moisture estimation. The study was organized into stages that enabled the technique to be examined and refined, considering ideal scenarios and adverse conditions, such as rugged topography, vegetation presence, and obstructions near the stations.

In Chapter 1, a literature review article was presented to establish the theoretical framework of the thesis.

In Chapter 2, soil moisture estimation using GNSS-IR under ideal conditions was demonstrated, validating the technique’s effectiveness with data acquisition and processing settings recommended by foundational literature used in this work.

Chapter 3 applied the technique to non-ideal environments with significant vegetation and irregular terrain. In these cases, it became evident that specific configurations in the reflectometric algorithm are required to optimize the accuracy of the results. The configurations analyzed including GNSS signal selection, range of elevation angles of the satellites, azimuthal masks, and the moving average.

The range of elevation angles of the satellites and the azimuthal masks played a key role in mitigating the impact of incoherent signals, particularly those coming from directions with obstructions, complex topography, or substantial vegetation. The moving average, in turn, plays an important role, as it can mask the actual behavior of the phenomenon under evaluation. On one hand, a strict (i.e., overly wide) moving average window width may overly smooth the data, diminishing the phenomenon's signature. On the other hand, a narrow window may preserve a highly noisy signature, with data that may not truly represent the phenomenon itself, but rather reflect instrumental and methodological biases.

These investigations are crucial to broaden the applicability of GNSS-IR, while mitigating the impact of varying geographic contexts and installation conditions. The study confirmed that customizing processing configurations for each station can significantly improve outcomes and can partially mitigate the limitations of the technique. In particular, investigations focused on optimizing these configurations

yielded enhancements of up to 54%. As a result, it was shown that soil moisture estimation via GNSS-IR is feasible even in non-ideal locations. However, the adverse effects of unsuitable environments are only minimized, not eliminated, through station-specific configurations. For example, vegetation remains a challenge in reflectometric estimations.

Finally, in Chapter 4, a methodology was proposed for automating soil moisture estimation using data from RBMC stations. The chosen station represents moderately challenging surroundings, with low vegetation but some GNSS signal obstructions. An algorithm was developed in Python to automate the preparation of input data for the reflectometric algorithm, enabling continuous monitoring of soil moisture near the station. The results were promising at the test station UFPR and confirmed the technique's applicability in a continuously operating RBMC station. The algorithm is available and may be used to automate the download and preparation of GNSS data from other RBMC stations. The process can be replicated across the network, though station-specific evaluations are recommended to properly adjust processing configurations.

Considering all premises presented throughout this work, the results confirm the feasibility of applying the GNSS-IR technique under various installation conditions, land cover configurations, and terrain types. However, the adjustment of processing parameters must be case-specific. While such configurations improve outcomes, they do not eliminate errors, especially those associated with irregular topography and vegetation. Despite the existence of numerous filtering techniques, vegetation's impact on soil moisture estimates cannot be completely removed.

For RBMC stations, low-cost opportunistic soil moisture monitoring using GNSS-IR is possible. Nonetheless, the installation conditions must be assessed to ensure the station meets the minimum requirements for this application. It is also recommended that a conventional soil moisture sensor be installed on-site during an initial period to enable validation and refinement of the reflectometric processing settings.

3.2 RECOMMENDATIONS FOR FUTURE WORK

The following recommendations are proposed for future studies:

a) develop a methodology to enable soil moisture monitoring via GNSS-IR from other RBMC stations with potential for this application. In this pilot project, only one station was evaluated due to the heterogeneity of the RBMC network, for example, in terms of antenna height relative to the ground, equipment used, and surrounding conditions, which makes it necessary to assess each station individually. This line of research represents a direct continuation of the present thesis and is currently underway. Appendix 1 presents a map of stations already assessed and classified according to their potential for GNSS-IR soil moisture estimation.
b) systematize the processing workflow for RBMC stations and make the results of weekly processing available through continuous operations, so that the developed methodology can be adopted by IBGE and replicated at other stations while considering their specific characteristics. This would allow the creation of a national soil moisture monitoring network based on the RBMC. Such initiatives already exist internationally (https://www.unavco.org/data/gps-gnss/derived-products/pbo-h2o/documentation/documentation.html) and can significantly contribute to both national and international sectors.
c) conduct further investigations to minimize the influence of vegetation, since its effects can be mitigated by using Multi-GNSS (Wei et al., 2023). Specific statistical tools can be applied for this purpose. Therefore, it is recommended that future studies focus directly on this topic.

REFERENCES

ARROYO, A. A.; CAMPS, A.; AGUASCA, A.; et al. Dual-polarization GNSS-R interference pattern technique for soil moisture mapping. **IEEE Journal of Selected Topics in Applied Earth Observations and Remote Sensing**, v. 7, n. 5, p. 1533–1544, 2014.

AWANGE, J. L.; KYALO KIEMA, J. B. **Environmental Geoinformatics**. Berlin, Heidelberg: Springer Berlin Heidelberg, 2013.

BABAEIAN, E.; SADEGHI, M.; JONES, S. B.; et al. Ground, Proximal, and Satellite Remote Sensing of Soil Moisture. **Reviews of Geophysics**, v. 57, n. 2, p. 530–616, 19. jun. 2019. [s.l.]. Disponível em: <https://onlinelibrary.wiley.com/doi/abs/10.1029/2018RG000618>.

DI BELLO, R. C. **Análise do Comportamento da Umidade do Solo no Modelo Chuva-Vazão SMAP II – Versão com Suavização Hiperbólica. Estudo de Caso: Região de Barreiras na Bacia do rio Grande - BA**, 2005. Universidade Federal do Rio de Janeiro.

CHANG, X.; JIN, T.; YU, K.; et al. Soil moisture estimation by GNSS multipath signal. **Remote Sensing**, v. 11, n. 21, p. 1–16, 2019.

CHEW, C. C.; SMALL, E. E.; LARSON, K. M.; ZAVOROTNY, V. U. Effects of near-surface soil moisture on GPS SNR data: Development of a retrieval algorithm for soil moisture. **IEEE Transactions on Geoscience and Remote Sensing**, v. 52, n. 1, p. 537–543, 2014.

EDOKOSSI, K.; CALABIA, A.; JIN, S.; MOLINA, I. GNSS-reflectometry and remote sensing of soil moisture: A review of measurement techniques, methods, and applications. **Remote Sensing**, v. 12, n. 4, 2020.

ENTEKHABI, D.; NJOKU, E. G.; O'NEILL, P. E.; et al. The soil moisture active passive (SMAP) mission. **Proceedings of the IEEE**, v. 98, n. 5, p. 704–716, 2010.

EURIQUES, J. F. **Determinação da umidade do solo por meio da técnica de Refletometria GNSS – Primeiros resultados no Brasil**, 2019. Universidade Federal do Paraná. Disponível em: <https://acervodigital.ufpr.br/bitstream/handle/1884/62323/R - D - JORGE FELIPE EURIQUES.pdf?sequence=1&isAllowed=y>. .

EURIQUES, J. F.; KRUEGER, C. P.; MACHADO, W. C.; SAPUCCI, L. F.; GEREMIA-NIEVINSKI, F. Soil Moisture Estimation with GNSS Reflectometry: A Conceptual Review. **Revista Brasileira de Cartografia**, v. 73, n. 2, p. 413–434, 2021.

GEREMIA-NIEVINSKI, F.; HOBIGER, T. **Site guidelines for multi-purpose GNSS reflectometry stations**. 2019.

IBGE. **Rede Brasileira de Monitoramento Contínuo dos Sistemas GNSS em Tempo Real**. Rio de Janeiro, RJ, 2020.

IBGE. **RBMC - Rede Brasileira de Monitoramento Contínuo dos Sistemas GNSS Relatório de Informação de Estação UFPR - Curitiba**. Rio de Janeiro, RJ, 2021.

LARSON, K. M.; BRAUN, J. J.; SMALL, E. E.; et al. GPS Multipath and Its Relation to Near-Surface Soil Moisture Content. **IEEE Journal of Selected Topics in Applied Earth Observations and Remote Sensing**, v. 3, n. 1, p. 91–99, 2010.

LARSON, K. M.; SMALL, E. E.; GUTMANN, E.; et al. Using GPS multipath to measure soil moisture fluctuations: Initial results. **GPS Solutions**, v. 12, n. 3, p. 173–177, 2008.

LARSON, K. M.; SMALL, E. E.; GUTMANN, E. D.; et al. Use of GPS receivers as a soil moisture network for water cycle studies. **Geophysical Research Letters**, v. 35, n. 24, 2008.

NIEVINSKI, F. G.; LARSON, K. M. Forward modeling of GPS multipath for near-surface reflectometry and positioning applications. **GPS Solutions**, v. 18, n. 2, p. 309–322, 2014a. Springer Verlag.

NIEVINSKI, F. G.; LARSON, K. M. An open source GPS multipath simulator in Matlab/Octave. **GPS Solutions**, v. 18, n. 3, p. 473–481, 2014b. Springer Verlag.

NIEVINSKI, F. G.; LARSON, K. M. Inverse modeling of GPS multipath for snow depth estimation - Part I: Formulation and simulations. **IEEE Transactions on Geoscience and Remote Sensing**, v. 52, n. 10, p. 6555–6563, 2014c. Institute of Electrical and Electronics Engineers Inc.

NIEVINSKI, F. G.; LARSON, K. M. Inverse modeling of GPS multipath for snow depth estimation - Part II: Application and validation. **IEEE Transactions on Geoscience and Remote Sensing**, v. 52, n. 10, p. 6564–6573, 2014d. Institute of Electrical and Electronics Engineers Inc.

PLAG, H. P.; PEARLMAN, M. **Geodetic, Global System, Observing**. 2009.

ROUSSEL, N.; FRAPPART, F.; RAMILLIEN, G.; et al. Detection of Soil Moisture Variations Using GPS and GLONASS SNR Data for Elevation Angles Ranging from 2° to 70°. **IEEE Journal of Selected Topics in Applied Earth Observations and Remote Sensing**, v. 9, n. 10, p. 4781–4794, 2016.

SENEVIRATNE, S. I.; CORTI, T.; DAVIN, E. L.; et al. Investigating soil moisture-climate interactions in a changing climate: A review. **Earth-Science Reviews**, v. 99, n. 3–4, p. 125–161, 2010.

SIMON, P.; HOLLINGSWORTH, A.; CARLI, B.; et al. **The Changing Earth : New scientific challnges for ESA's Living Planet Programme.** ESA Publications Division, 2006.

TABIBI, S.; NIEVINSKI, F. G.; VAN DAM, T. Statistical Comparison and Combination of GPS, GLONASS, and Multi-GNSS Multipath Reflectometry Applied to Snow Depth Retrieval. **IEEE Transactions on Geoscience and Remote Sensing**, v. 55, n. 7, p.

3773–3785, 2017. Institute of Electrical and Electronics Engineers Inc.

TABIBI, S.; NIEVINSKI, F. G.; VAN DAM, T.; MONICO, J. F. G. Assessment of modernized GPS L5 SNR for ground-based multipath reflectometry applications. **Advances in Space Research**, v. 55, n. 4, p. 1104–1116, 2015. Elsevier Ltd.

VEY, S.; GÜNTNER, A.; WICKERT, J.; BLUME, T.; RAMATSCHI, M. Long-term soil moisture dynamics derived from GNSS interferometric reflectometry: a case study for Sutherland, South Africa. **GPS Solutions**, v. 20, n. 4, p. 641–654, 2016. Springer Verlag.

WU, X.; MA, W.; XIA, J.; et al. Spaceborne gnss-r soil moisture retrieval: Status, development opportunities, and challenges. **Remote Sensing**, v. 13, n. 1, p. 1–24, 2021.

YAN, S. H.; ZHANG, N.; CHEN, N. C.; GONG, J. Y. Feasibility of using signal strength indicator data to estimate soil moisture based on GNSS interference signal analysis. **Remote Sensing Letters**, v. 9, n. 1, p. 61–70, 2018. Taylor & Francis. Disponível em: <https://doi.org/10.1080/2150704X.2017.1384587>. .

YANG, T.; WAN, W.; CHEN, X.; et al. Land surface characterization using BeiDou signal-to-noise ratio observations. **GPS Solutions**, v. 23, n. 2, p. 1–12, 2019. Springer Berlin Heidelberg. Disponível em: <http://dx.doi.org/10.1007/s10291-019-0824-4>. .

YANG, T.; WAN, W.; CHEN, X.; CHU, T.; HONG, Y. Using BDS SNR observations to measure near-surface soil moisture fluctuations: Results from low vegetated surface. **IEEE Geoscience and Remote Sensing Letters**, v. 14, n. 8, p. 1308–1312, 2017.

ZHANG, S.; ROUSSEL, N.; BONIFACE, K.; et al. Use of reflected GNSS SNR data to retrieve either soil moisture or vegetation height from a wheat crop. **Hydrology and Earth System Sciences**, v. 21, n. 9, p. 4767–4784, 2017. Copernicus GmbH.

ZHANG, X.; NIE, S.; ZHANG, C.; ZHANG, J.; CAI, H. Soil moisture estimation based on triple-frequency multipath error. **International Journal of Remote Sensing**, v. 42, n. 15, p. 5953–5968, 2021. Taylor & Francis. Disponível em: <https://doi.org/10.1080/01431161.2021.1933246>. .

APPENDIX 1

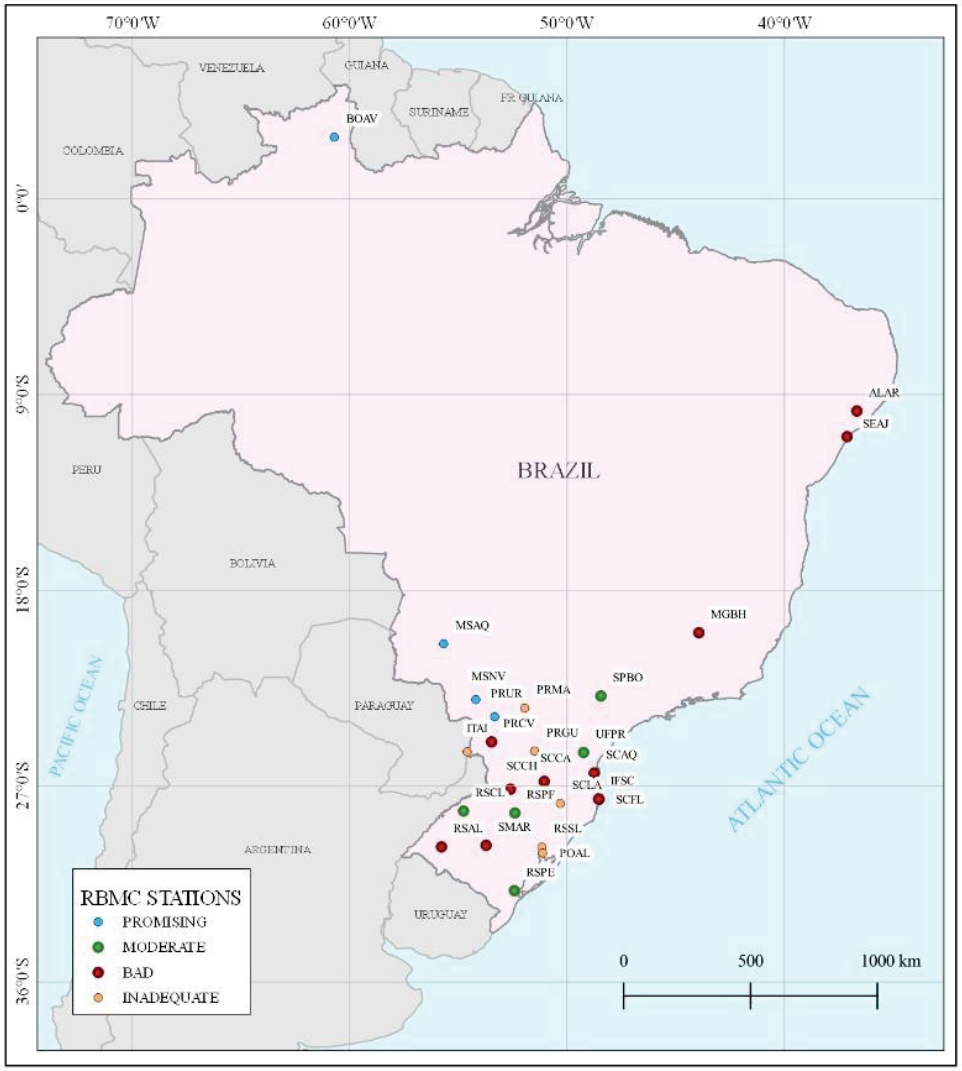

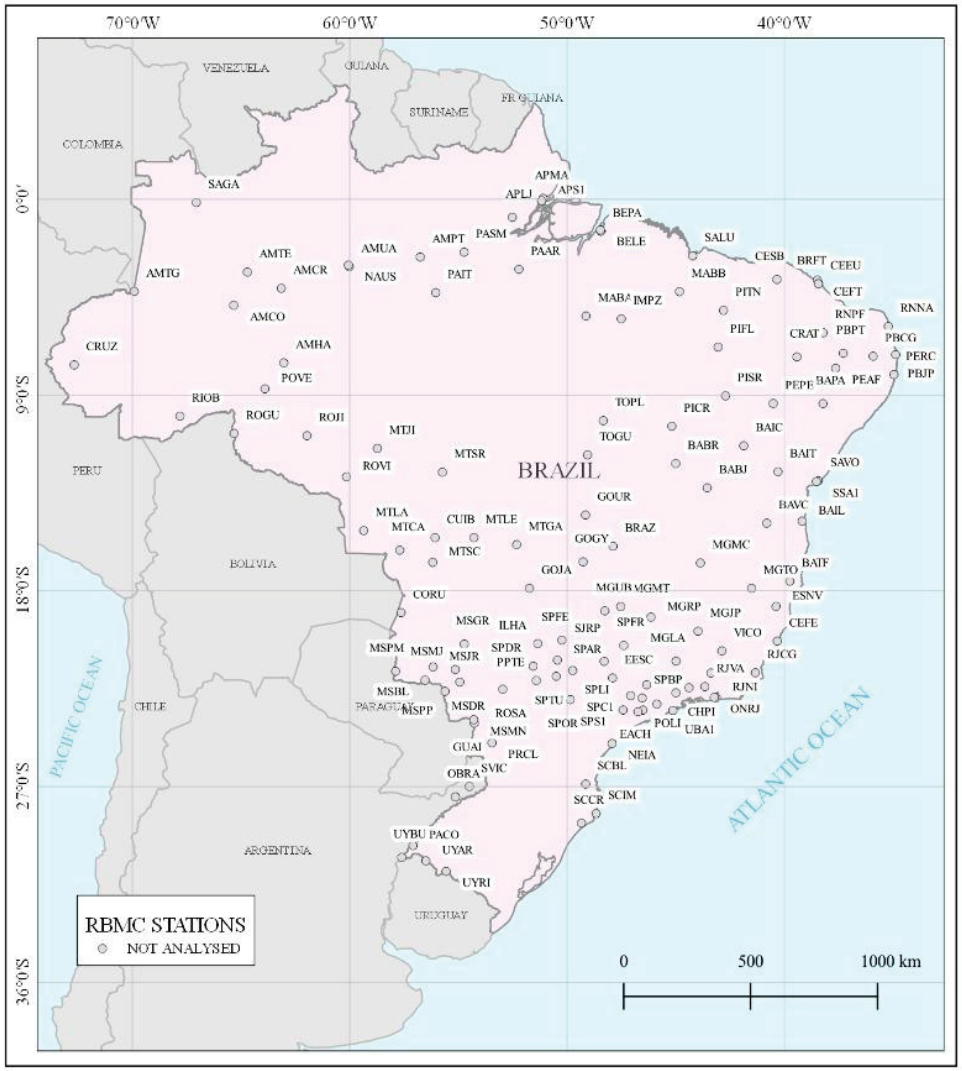

GEODESIC REFERENCE SYSTEM: WGS84